Cape Peninsula
University of Technology

NANOCLAY SILVER PROTEIN HSA ELECTROCHEMICAL SENSOR FOR ZIDOVUDINE

by

Sapokazi Timakwe

Thesis submitted in fulfilment of the requirements for the degree

Master's Degree: Chemistry

in the Faculty of Applied Sciences

at the Cape Peninsula University of Technology

Supervisor: Prof M.C. Matoetoe

Bellville

DECLARATION

I, Sapokazi Timakwe, declare that the contents of this dissertation/thesis represent my own unaided work, and that the dissertation/thesis has not previously been submitted for academic examination towards any qualification. Furthermore, it represents my own opinions and not necessarily those of the Cape Peninsula University of Technology.

24/04/2022

Signed **Date**

ABSTRACT

The synthesis process of AgNPs has attracted a lot in the field of biosensors, diagnostics and therapeutically application. An attempt to understand the effect of different concentrations of reducing agents in the synthetic design process has been investigated. In this study, we gather information on the voltammetry studies and relate it with UV- Vis and SEM analysis. Given the kinetics, LSPR band, and narrow size distribution of these methods, it was possible to compare the obtained measurements and clearly distinguish sizes and aggregation. AgNPs measured by SEM showed a statistically significant reduction of the nanoparticle sizes from 65 to 17.5 nm as the reducing agent was increased. The UV-Vis studies showed SPR bands shifting towards the blue region as the reducing agent concentration was increased, indicating a decrease in the particle sizes. It is worth emphasizing that CV and DPV coincide well with SEM on the aggregation of AgNPs at higher concentrations. 10 mM reducing agent concentration resulted in uniform outcomes for producing AgNPs with the smallest size in terms of FWHM in all the methods used in this study, while UV –Vis band gaps increased with increasing reducing agent concentration.

In agreement with all the methods investigated, the results suggested that the best concentration of the reducing agent is 10 mM trisodium citrate for a target application. Furthermore, three different fractions of nanoclay (0.5, 1 and 1.5 g 1.44P) were functionalised with Ag forming silver nanoclay composites (Ag/1.44P) and the optical and electrochemical properties of nanoclay were studied. Optical, morphology and electrochemical techniques were used for the characterisation of the synthesised Ag/1.44P composites. The presence and the absence of functional groups observed in FTIR spectrum of Ag/1.44P, compared with those found in the spectra of silver and pure 1.44P proves that a reaction took place, thus a successful functionalisation of 1.44P with silver. All X-ray data of the composites showed four diffraction peaks within the silver spectrum range, with intensity of silver decreasing with increasing concentration of 1.44P. SEM represented well dispersed particles of different shapes with average particle sizes of 2.5, 27.5, 5 nm with enhanced concentration of 1.44P.

The decrease in diffusion coefficient (D) values from 4.26×10^{-10}, 2.50×10^{-13}, 1.40×10^{-13} $cm^2.s^{-1}$ and electron transfer rate constant (Ks) 1.50×10^{-5}, 3.94×10^{-7}, 2.86×10^{-7} $cm.s^{-1}$ with proportional 1.44P concentration depicted greater nanocomposites size. These findings suggest the usefulness of voltammetry as a complementary method that can be used as a qualitative guide to identify the size and aggregation of nanoparticles. Subsequently, AgNPs with 10 mM trisodium citrate and 0.5 g Ag/1.44P were used in the fabrication of sensor for zidovudine detection. The redox properties of the sensor (GCE/Ag/1.44P/HSA) were studied with cyclic voltammetry with varied scan rates using Randles-Sevcik equation, where diffusion coefficient was calculated as 1.55×10^{-11} $cm^2.s^{-1}$and Ks which was 3.40×10^{-6} $cm.s^{-1}$, with one electron

transfer process. The developed sensor produced acceptable %RSD for reproducibility and repeatability, with limit of detection of 0.3 μM and 1.0 μM limit of quantification. It was also found to be stable for 10 days and unaffected by the presence of interferences. The sensor can be applied in pharmaceuticals as it was able to successfully detect the target analyte in commercial tablets.

ACKNOWLEDGEMENTS

Firstly, I am grateful to the Lord Almighty and my ancestors (ooDlamini, Zizi, kwaye nooNala, ooNdokose) for giving me the strength and courage to carry out this study successfully. To my supervisor, Professor Mangaka Matoetoe, thank you for your constant guidance, for the knowledge and wisdom that you shared, and for making sure that you contribute on black excellence, woman in academics and in science. Continue with the excellent work that you do and keep passing on that knowledge. To my dearest mother (Nomandla Timakwe), if I were to describe you in words, I would say you are caring, supportive, loving, patient, encouraging and selfless person. You sacrificed your dreams so we can fulfil ours, for that I will forever be indebted to you. The support and love that I received from Akhona Timakwe, Loyiso Mrwebi, Piwokuhle Timakwe, Bekithemba Timakwe, Olona Timakwe, Maqambayi family, Uminathi and Akhulenathi Solora is much appreciated. To Lutho Xakayi, I can never thank you enough for the role that you have played throughout this journey. There were so many adversities encountered, but your endless support and words of encouragement kept me going. I am more grateful to you than you will ever know. To Dr Bongiwe Silwana, whose energy and connection was restorative, and your work ethics made it easy to work with you, I will forever be grateful that our paths crossed. A special thanks to the Dean of Applied Sciences, Professor Joseph Kioko, your understanding on socio economic issues and the struggles of women in science is commendable. To everyone else that I might have omitted who played a role in this journey, I am sincerely thankful.

I would also like to acknowledge the Cape Peninsula University of Technology for admission to carry out the research. The University of São Paulo (Universidade de São Paulo) and International Society of Electrochemistry for the exposure, the financial assistance of the National Research Foundation (NRF) and Centre for Postgraduate Bursary (CPUT) towards this research. Opinions expressed in this thesis and the conclusions arrived at, are those of the author, and are not necessarily to be attributed to the National Research Foundation/ CPUT.

DEDICATION

This is for my mother (Nomandla Timakwe), my late grandparents and uncle (Lungile, Nokwezi and Siyasanga Timakwe).

TABLE OF CONTENTS

DECLARATION ii
ABSTRACT iii
ACKNOWLEDGEMENTS v
DEDICATION vi
TABLE OF CONTENTS vii
LIST OF FIGURES x
LIST OF TABLES xii
LIST OF SCHEMES xiii
LIST OF APPENDICES xiv
GLOSSARY xv
PREFACE xvii
RESEARCH OUTPUTS xix
CHAPTER ONE 1
INTRODUCTION 1
1.1 Problem statement 1
1.2 Background 1
1.3 Assumptions 4
1.4 Research questions 4
1.5 Objectives 4
1.6 Significance and importance of the research 5
1.7 Research methodology 5
1.8 References 5
CHAPTER TWO 7
LITERATURE REVIEW 7
2.1 Introduction 7
2.1.1 Detection methods for zidovudine 9
2.2 Sensors 10
2.2.1 Nanomaterials used in sensors 13
2.2.1.1 Silver nanoparticles 13
2.2.1.1.1 Applications of silver nanoparticles in sensors and biosensors 14
2.2.1.2 Nanoclays as sensing materials 15
2.2.2 Applications of sensors 16
2.3 References 17
CHAPTER THREE 24
SYNTHESIS AND CHARACTERISATION OF SILVER NANOPARTICLES AND THEIR COMPOSITES 24
3.1 Introduction 24
3.2 Experimental 27
3.2.1 Reagents and Materials 27
3.2.2 Synthesis of silver nanoparticles 27

3.2.3 Synthesis of silver nanoclay composites 28
3.2.4 Characterisation 28
3.2.4.1 Ultraviolet visible characterisation 28
3.2.4.2 Fourier transform infra-red characterisation 29
3.2.4.3 X-ray diffraction 29
3.2.4.4 Scanning Electron Microscopy 29
3.2.4.5 Electrochemistry 29
3.3 Results and discussion 30
3.3.1 Ultraviolet visible characterisation of silver nanoparticles 31
3.3.2 FTIR characterisation of silver nanoparticles 32
3.3.3 X-ray diffraction characterisation of silver nanoparticles 33
3.3.4 Scanning Electron Microscopy of silver nanoparticles 33
3.3.5 Electrochemistry 36
3.3.5.1 Cyclic and Differential Pulse voltammetry of silver nanoparticles 36
3.3.6 FTIR characterisation of silver nanoclay composites 40
3.3.7 X-ray diffraction characterisation of silver nanoclay composites 42
3.3.8 Scanning Electron Microscopy of silver nanoclay composites 44
3.3.9 Electrochemistry 45
3.3.9.1 Cyclic and Differential pulse voltammetry of silver nanoclay composites 45
3.4 Conclusion 47
3.5 References 48
CHAPTER 4 52
ELECTROCHEMICAL PARAMETERS 52
4.1 Background 52
4.2 Experimental 54
4.3 Results and discussion 54
4.3.1 Silver nanoparticles 54
4.3.2 Silver nanoclay composites 58
4.4 Conclusion 63
4.5 References 63
CHAPTER 5 65
FABRICATION OF SENSOR FOR DETECTION OF ZIDOVUDINE 65
5.1 Background 65
5.2 Experimental 68
5.2.1 Material and reagents 68
5.2.2 Preparation of phosphate buffer saline (pH 7.04) 68
5.2.3 Synthesis of silver nanoparticles and composites 68
5.2.4 Zidovudine solution preparation 68
5.2.5 Preparation of Human Serum Albumin solution 68
5.2.6 Instrumentation 68
5.2.7 Optimisation of sensor fabrication method 68

5.2.8 Detection of zidovudine at different concentrations of PBS electrolyte 69
5.2.9 Optimisation of procedures for zidovudine detection 69
5.2.10 Validation 69
5.2.10.1 Reproducibility, repeatability, stability 69
5.2.10.2 Interference studies 69
5.2.10.3 Spiked urine samples 69
5.2.11 Application of sensor in real samples 70
5.2.11.1 Preparation of commercial tablet (300 mg) solution 70
5.3 Results and discussion 70
5.3.2 Optimisation of fabrication method 70
5.3.3 Detection of zidovudine at different concentrations of PBS electrolyte 71
5.3.4 Effect of HSA drying time 73
5.3.5 Effect of stirring 73
5.3.6 Optimisation of procedures for zidovudine detection 74
5.3.7 Determination of electrochemical parameters of zidovudine 76
5.3.8 Calibration 79
5.3.9 Validation 81
5.3.9.1 Reproducibility, repeatability, stability 81
5.3.9.2 Interference studies 82
5.3.9.3 Detection of zidovudine in spiked urine samples 85
5.3.10 Application of the sensor in real samples 86
5.3.10.1 Detection of zidovudine in commercial tablets 86
5.4 Conclusion 87
5.5 References 88
CHAPTER SIX 90
CONCLUSION AND RECOMMENDATIONS 90
6.1 Conclusion 90
6.2 Recommendations 90
APPENDICES 92

LIST OF FIGURES

Figure 1.1: Chemical structure of zidovudine ($C_{10}H_{13}N_5O_4$). 2
Figure 2.1: Types of electrochemical sensors. 12
Figure 2.2: Applications of silver. 14
Figure 2.3: Nanoclay structure. 15
Figure 2.4: Types of clay minerals. 15
Figure 2.5: Processes taking place during functionalisation of nanoclay. 16
Figure 3.1: AgNPs formation by chemical reduction of $AgNO_3$ using different concentrations of reducing agent tri-sodium citrate and changes in the colour during formation of AgNPs. 28
Figure 3.2: Silver nanoparticles with different reducing agent concentrations. 31
Figure 3.3: FTIR spectra of trisodium citrate dihydrate and silver nanoparticles. 32
Figure 3.4: XRD spectrum of silver nanoparticles with (a) 5 (b) 10 (c) 50 & (d) 100 mM TSC. 33
Figure 3.5: SEM images of AgNPs in Ag: TSC ratio of (A) 1:5, (B) 1:10, (C) 1:50, (D) 1:100 mM and corresponding diameter histograms. 35
Figure 3.6: (A) Cyclic voltammograms of AgNPs at scan rate 0.1 V/s; (B) Differential pulse voltammograms with parameters: potential step 8 mV, (5 s waiting time and 20 s for current sampling time), pulse amplitude 50 mV, without accumulation step for different TSC. 36
Figure 3.7: The proposed pathway for new nanoparticle formation from parent AgNPs on a GCE. 38
Figure 3.8: The full width at half maximum (FWHM) and particle sizes as a function of the reducing agent concentration. 39
Figure 3.9: FTIR spectra of A (PGV nanoclay, AgNPs, PGV/Ag); B (1.44 nanoclay, AgNPs, 1.44P/Ag). Insert: A (Silver nanoclay composites (Ag/0.5g, Ag/1g, Ag/1.5g PGV). 41
Figure 3.10:XRD spectrum of 1.44P nanoclay (a) Ag/1.44P composites with (b) 0.5 (c) 1 & (d) 1.5 g nanoclay. 43
Figure 3.11: SEM images of Ag/1.44P composites with (A) 0.5 (B) 1 & (C) 1.5 g 1.44P and corresponding diameter histograms. 44
Figure 3.12: (A) Cyclic voltammograms of 1.44P nanoclay, Ag/1g 1.44P, Ag/1.5g 1.44P composites at 0.08 V/s. Insert: Ag/0.5g 1.44P, AgNPs. (B) Differential pulse voltammograms of Ag/ 1.44P composites at potential step 8 mV at GCE in 0.1 M HCl. Insert: AgNPs. 46
Figure 4.1: Cyclic voltammograms of AgNPs with (A) 5 (B) 10 (C) 50 & (D) 100 mM TSC at bare, (a) 20 (b) 40 (c) 80 (d) 100 (e) 120 (f) 160 mV/s at GCE in 0.1 M HCl. 56
Figure 4.2: Plots of anodic peak current against (A) scan rates and (B) square root of scan rates for (a) 5 (b) 10 (c) 50 (d) 100 mM TSC AgNPs. 57
Figure 4.3: Cyclic voltammograms of silver nanoclay composites of (A) 0.5 (B) 1 (C) 1.5 g 1.44 P nanoclay at bare, (a) 20 (b) 60 (c) 80 (d) 100 (e) 120 mV/s at GCE in 0.1 M HCl. 60

Figure 4.4: Plots of anodic peak current against (A) scan rates and (B) square root of scan rates for (b) Ag/1g 1.44P (c) Ag/1.5 g 1.44P, inserts: Ag/0.5g 1.44P. 61
Figure 5.1: Electrochemical sensor performance criteria. 65
Figure 5. 2: Fabrication methods of a sensor 66
Figure 5.3: DPV of 2.5 μM ZDV detection at (a) blank (b) HSA immersed (c) HSA dropcoated in 0.1 M PBS, pH 7.04 at GCE. 70
Figure 5. 4: DPV of 2.5 μM ZDV at (a) blank (b) bare (c) Ag (d) Ag/1.44P (e) Ag/1.44P/HSA in (A) 0.01 (B) 0.1 (C) 1 M PBS, pH 7.04 at GCE. 72
Figure 5.5: Effect of HSA drying time on 2.5 μM ZDV detection at 1 M PBS, pH 7.04 at GCE/Ag/1.44P/HSA. 73
Figure 5. 6: Effect of stirring time for 2.5 μM ZDV detection in 1 M PBS, pH 7.04 at GCE/Ag/1.44P/HSA. 74
Figure 5. 7: Optimisation of (a) step potential (b) modulation amplitude (c) modulation time (d) interval time for 2.5 μM ZDV in 1 M PBS, pH 7.04 at GCE/Ag/1.44P/HSA. 76
Figure 5.8: CVs of reduction of 0.03 mM ZDV at different scan rates in 1 M PBS at GCE/Ag/1.44P/HSA. 77
Figure 5.9: Plots of cathodic peak current of 0.03 mM ZDV versus (A) scan rates and (B) square root of scan rates. 79
Figure 5.10: Calibration curve from addition of 0.12 to 6.98 μM ZDV. Insert: DPV at (a) blank (b) 0.12 (c) 0.44 (d) 1.06 (e) 3.24 (f) 4.49 (g) 5.73 (h) 6.98 (I) 8.22 μM ZDV at 1 M PBS at GCE/Ag/1.44P/HSA (parameters: 0.0405 V step potential, 0.075 V modulation amplitude, 0.01 second modulation time, 0.25 second interval time). 80
Figure 5.11: Developed sensor stability over 10 days. 82
Figure 5.12: DPV of 0.24 μM ZDV in the presence of ascorbic acid (A), citric acid (B), D-glucose (C). 84
Figure 5.13: DPV of (a) blank and 0.12 μM ZDV at different ratios of Urine:1 M PBS (b) 1:4 (c) 1:9 (d) 1:14 at GCE (parameters: 0.0405 V step potential, 0.075 V modulation amplitude, 0.01 second modulation time, 0.25 second interval time). 86
Figure 5.14: DPV of (a) blank, (b) tablet 1, (c) tablet 2 in 1 M PBS, pH 7.04 at GCE (parameters: 0.0405 V step potential, 0.075 V modulation amplitude, 0.01 second modulation time, 0.25 second interval time). 87

LIST OF TABLES

Table 3. 1: Characterisation techniques for silver nanoparticles and their composites. 27
Table 3.2: Silver nanoparticle potentials with changes in concentration of sodium citrate using anodic peak data. 37
Table 3.3: The experimental particle sizes of AgNP analysed by electrochemical methods and UV-Vis spectra of different concentration of TSC (n = 3). 40
Table 3.4: Interpretation of FTIR spectra of the synthesised material. 42
Table 3.5: Silver nanoclay composites potential with changes in concentration of nanoclay using anodic peak data. 47
Table 4.1: Electrochemical parameters of the modified GCE with AgNPs calculated using equation 4.2 to 4.6. 58
Table 4.2: Electrochemical parameters of the modified GCE with Ag/1.44P composites calculated using equation 4.2 to 4.6. 62
Table 5.1: The effect of working electrode and electrolyte on the zidovudine potential. 71
Table 5.2: Electrochemical parameters of ZDV from Randles plot. 79
Table 5.3: Parameters of the sensor of ZDV from the calibration measured at GCE. 80
Table 5.4: Detection methods for zidovudine. 81
Table 5.5: Zidovudine drug recovery in the presence of interferences (%recovery in brackets). 84
Table 5.6: Zidovudine drug spiking/recovery studies. 85

LIST OF SCHEMES

Scheme 2.1: Synthesis of zidovudine. 7
Scheme 2.2: Zidovudine mechanism of action. 8
Scheme 2.3: Structure of the sensor. 11
Scheme 3.1: Primary and secondary growth step of AgNPs formation. 26
Scheme 3.2: The formation of colloidal AgNPs using silver nitrate precursor. 30
Scheme 5.1: Glassy carbon electrode modification for the detection of ZDV. 67
Scheme 5.2: Zidovudine reduction reaction. 77

LIST OF APPENDICES

Appendix A 1: Antiretroviral drugs from each drug class (AIDSinfo, 2019). 92
Appendix B 1: Antiretroviral drugs combination (AIDSinfo, 2019). 93

GLOSSARY

Terms/Acronyms/Abbreviations	Definition/Explanation
AdSV	Adsorptive stripping voltammetry
AIDS	Acquired immunodeficiency syndrome
ARV	Antiretrovirus
AZT	Azidothymidine
CV	Cyclic voltammetry
DMTA	Dynamic mechanical thermal analysis
DNA	Deoxyribonucleic acid
DPV	Differential Pulse Voltammetry
DTA	Differential thermal analysis
EDXR	Energy-dispersive x-ray
EIS	Electrochemical impedance spectroscopy
FTIR	Fourier transform infrared
FWHM	Full-width height maximum
GCE	Glassy Carbon Electrode
GFP	Green Florescence Protein
HCl	Hydrochloric acid
HLB	Hydrophilic-lipophilic balance
HIV	Human immunodeficiency virus
HMDE	Hanging Mercury Drop Electrode
HPLC	High Performance liquid chromatography
HAS	Human Serum Albumin
IgY	Immunoglobulin Y
LC-MS	Liquid chromatography- Mass spectrometry
LLOQ	Lower limit of quantification
LSPR	Local surface plasmon resonance
MEF	Metal-enhanced fluorescence
MWCNT	Multi-walled carbon nanotubes
NRTI	Nucleoside reverse transcriptase inhibitor
PBS	Phosphate buffer saline
PVP	Polyvinyl pyrrolidone
RP-LC	Reverse Phase liquid chromatography
RSD	Relative standard deviation
RNA	Ribonucleic acid
SEM	Scanning electron microscopy
SERS	Surface-enhanced Raman Scattering
SWV	Square Wave Voltammetry

TEM	Transmission electron microscopy
TGA	Thermogravimetric analysis
TSC	Trisodium citrate dihydrate
UV	Ultraviolet Visible
XRD	X-ray diffraction spectroscopy
ZDV	Zidovudine

PREFACE

Thesis overview

The following thesis outline gives a brief description of what will be discussed in the chapters.

Chapter one

The chapter highlights the background of the research study including the reasons for the study. The work purpose is also included as well as the significance and importance of the study. A brief discussion on various methods commonly adopted in the analysis of antiretroviral drugs will be highlighted as well as how the study will be carried out which will be further detailed in chapter three.

Chapter two

This work elaborates on zidovudine as mentioned in chapter one. This will further include information on the synthesis of zidovudine, its chemistry as well as mechanism of action. In addition, various analytical techniques commonly adopted in the analysis of antiretroviral drugs as well as the importance of the study will be further elaborated. A discussion will extend to electrochemical techniques, especially sensors and nanomaterials of choice in the study. The description on sensor components and the role of the nanomaterials in fabrication of sensors will also be highlighted.

Chapter three

An introduction on the synthesis and characterisation of silver nanoparticles and nanoclay composites is included in this chapter, followed by the detailed experimental procedure of silver nanoparticles with different concentrations of reducing agent and silver nanoclay composites with different concentration of nanoclays such as surface modified nanoclay (1.44P) and hydrophylic bentonite (PGV). Furthermore, discusses the characterisation of the synthesized material with spectroscopic and electrochemical techniques. The data interpretation and discussion of spectra and voltammogram is comparison of the data on the literature. The choice of silver nanoparticles and nanoclay composite will be made which will be further used in sensor fabrication that will be elaborated in chapter five. The conclusion on the materials optical and electrochemical properties is made based on the data obtained.

Chapter four

The brief background on kinetics with appropriate equations and their importance are found in the chapter. This elaborates on kinetics of silver nanoparticles and their nanoclay composites which were synthesised in chapter three, as well as their electrochemical behaviour on the surface modified glassy carbon electrode. The discussion will extend to the summary of the

most important findings, to obtain a general picture of the redox behaviour and changes in cyclic voltammogram at lower and higher scan rates.

Chapter five

This chapter is about the application of the selected material previously discussed for sensor fabrication, including the application of human serum albumin for the detection of zidovudine. The modification methods of the electrode will be discussed as well as the techniques used for detection. This discussion elaborates on the methods of fabrication including the criteria for sensor performance. The data on the validation of the sensor developed and its implementation in real samples will also be provided with discussion, as well as the summary on the data accumulated.

Chapter six

The conclusion of the research study as well as the recommendations will be highlighted in the chapter.

RESEARCH OUTPUTS

1. Publications

i. **Sapokazi Timakwe**, Bongiwe Silwana, Mangaka C. Matoetoe. Electrochemistry as a complimentary technique for revealing the influence of reducing agent concentration in AgNPs. *Journal of American Chemical Society.* (**Paper published**).

ii. **Sapokazi Timakwe**, Bongiwe Silwana, Mangaka C. Matoetoe. The impact of silver nanoclay functionalisation on optical and electrochemical properties. *RSC Advances*. (**Paper Accepted**).

2. Conference presentations

i. 70th International Society of Electrochemistry conference. International Convention Centre (ICC), Durban, 4-9 August 2019. (**Poster prize winner**).

Sapokazi Timakwe, Nomasoldier Mngcwengi, Mangaka C. Matoetoe. Title: Analysis of Lead and Cadmium in fruit juices by Anodic Stripping Voltammetry using Bismuth Modified Glassy Carbon electrodes.

ii. 10th South African Nanotechnology Initiative-Nanosciences Young Researcher's symposium (SANI-NYRS): National. 7-8 October 2021. (Poster).

Sapokazi Timakwe, Bongiwe Silwana, Mangaka C. Matoetoe. Title: The impact of silver nanoclay functionalisation on optical and electrochemical properties.

3. Schools attended

14th PTA School of Electrochemistry. Universidade de São Paulo, Instituto de Química, São Paulo - Brazil, 2-6 December 2019.

CHAPTER ONE
INTRODUCTION

1.1 Problem statement

The interest in monitoring ARV drugs pharmacokinetics in the field of HIV infection has been in the past years (Marchei *et al.*, 2002). Their demand is of outmost and thus being a threat in the environment due to large number of consumptions, with zidovudine having little therapeutic interval that is, becoming ineffective to many patients causing metabolic diseases. Therefore, that has brought attention in the investigation and monitoring of the drug quality. To assist, monitoring of the drug was done with techniques such as chromatographic (Dolci *et al*., 2011; Marchei *et al.*, 2002), voltammetric (Castro *et al*., 2011; Kominkova *et al*., 2014) and spectroscopic (Kominkova *et al*., 2014; Matta *et al*., 2012) methods. However, due to the expensive instruments, large amounts of sample preparation, longer analysis time that the spectroscopic and chromatographic methods require, as well as large number of foreign substances that is affecting the accuracy of the results, possible loss of analyte during the re-extraction process limits the application of these techniques. This has brought attention in the development of electrochemical methods which are great in sensitivity, good stability, fast detection of analytes and low-cost were developed as alternatives. In this work, nanoclays were applied because they are less costly, ever available, and due to their poor conductivity, silver was used to increase their conductivity. The functionalised nanoclay was used to modify the glassy carbon electrode to detect zidovudine. Moreover, the developed sensor was validated and applied in commercial tablets and artificial biological fluids.

1.2 Background

Zidovudine (also called ZDV, azidothymidine or AZT), structural represented in figure 1.1, is a type of nucleoside reverse transcriptase inhibitor (NRTI) antiretroviral drug that is used for the treatment of Human immunodeficiency virus/acquired immunodeficiency syndrome (HIV/AIDS) and now widely used as the generic drug (Dolci *et al*., 2011; Patil *et al*., 2015). It belongs under thymide analog and is said that it does not demolish the HIV infection but rather slows down the disease from progressing (Castro *et al.*, 2011). It prevents HIV from spreading through the healthy cells but cannot help the cells that are infected already. It was first developed as an anti-neoplastic agent which was said to control the growth of the human cancer cells (Fang *et al*., 2009). However, in 1987 zidovudine was declared as the first anti-HIV agent (Hoetelmans *et a*l., 1997). It is an odourless, crystalline solid drug, white to beige in colour and is soluble in 95% ethanol but partially soluble in water (Shetti *et al.*, 2017).

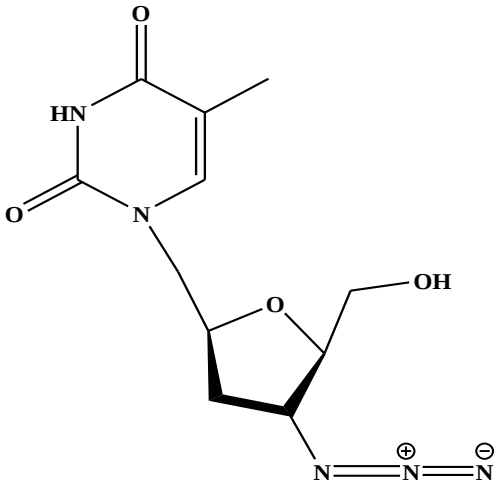

Figure 1.1: Chemical structure of zidovudine ($C_{10}H_{13}N_5O_4$).

Zidovudine may cause nausea, vomiting, gastric pain, anaemia, and headache. However, these effects can be reversible if one stops using the drug. Fluorescent labelling with a Green Florescence Protein (GFP) can be used to monitor the effects of zidovudine at the cellular level (Komnikova *et al.*, 2014). ZDV affects the growth of the normal liver cell and might slow down the cell cycle progression which could lead to apoptotic cell death if the damage is not repaired (Fang *et al*., 2009). Zidovudine is used in combination with other antiretroviral drugs such as lamudivine, nevirapine, efavirenz and abacavir (Komnikova *et al.*, 2014; Patil *et al*., 2015). In combination with other chemotherapeutic agents, ZDV has also been used to treat patients having colorectal cancer (Fang *et al*., 2009).

Several methods have been developed for the analysis of zidovudine. These methods include chromatographic (Dolci *et al.*, 2011), voltammetric (Castro *et al.*, 2011; Komnikova *et al.*, 2014) and spectroscopic (Komnikova *et al.*, 2014; Matta *et al.*, 2012) methods. The first synthesis of zidovudine was prepared in 19960s by mesylation of 1'-(2'- deoxy-5'-O-trityl-β-D-lyxosyl) thymine added to the sulfonate which was then treated with lithium azide in N,N-dimethyl formamide forming 3'- azido-3'- deoxythymide (Sethi *et al.*, 1991).

In chromatography, High Performance liquid chromatography (HPLC) is the mostly used method for the determination of zidovudine. Liquid chromatography- Mass spectrometry (LC-MS/MS) method was developed to quantify zidovudine simultaneously in human plasma (Matta *et al.*, 2012). Reverse Phase liquid chromatography (RP-LC) method was used in the analysis of zidovudine at 275 nm UV detection and for the determination of zidovudine in human plasma from the HIV infected human (Dolci *et al.*, 2011; Marchei *et al*., 2002). In spectroscopy, the interaction of Green Florescence Protein-Azidothymidine (GFP-AZT) was investigated using fluorescence spectroscopy (Komnikova *et al.*, 2014). GFP was found to be the best fluorescent label to AZT due to the AZT linked to GFP which does not influence the fluorescence of GFP significantly. In the synthesis of nanocomposites, Fourier transform

infrared (FTIR) (Nazir *et al.*, 2016; Zhang *et al.*, 2003), X-ray diffraction spectroscopy (XRD) (Kim *et al*., 2006; Shetti *et al.*, 2017; Zhang *et al.*, 2003), Energy-dispersive x-ray (EDXR) (Bui *et al*., 2015), Ultraviolet visible (UV) (Kim *et al*., 2006) were used to characterize the synthesised material. XRD was also used in the study of drug-clay interactions (Suresh *et al.*, 2010).

However, the developed methods use expensive instruments, require large amounts of sample preparation, the analysis takes long, there is also a large number of foreign substances affecting the accuracy of the results and loss of analyte during the re-extraction process. Therefore, they could not be considered in this study. Recently, voltammetric methods were proposed as alternatives due to their great sensitivity, good stability, fast detection of analytes and low-cost.

In electrochemical studies, the nano level voltammetric sensing method was developed for the determination of acyclovir using carbon paste electrode modified with nanoclay, employing cyclic voltammetry (CV) and square-wave voltammetry (SWV) in pH 5 (Shetti *et al.*, 2017). The differential pulse voltammetry (DPV) and CV techniques were also used to detect parathion-ethyl pesticide using glassy carbon electrode (GCE) modified with mixture of laponite clay and zirconium oxide gel nanocomposites (Bui *et al*., 2015) and in the detection of paracetamol using GCE organoclay modified (Gomdje *et al.*, 2017). The determination of zidovudine using adsorptive stripping method was conducted at the thin-film mercury electrode using 0.10 ppm ZDV in $2.0X10^{-3}$ M NaOH (with 1%v/v of ethylic alcohol) as the supporting electrolyte, an accumulation potential of -0.30 V and a scan rate 100 mVs^{-1} (Castro *et al*., 2011). Voltammetric methods such and SWV and DPV were considered in the investigation of the interaction of GFP-AZT (Komnikova *et al*., 2014). The method uses phosphate buffer as the supporting electrolyte in SWV and Brdicka buffer in DPV with the use of hanging mercury drop electrode (HMDE) as the working electrode.

However, due to the high toxicity levels of mercury, nanosensors have been developed for the detection of antiretroviral drugs. A nanosensor is a sensor that consists of sensitive layer (chemical, biological) which is built on the atomic scale for the nanometer measurements (Agrawal *et al*., 2012). An antibody, enzyme, protein, or nucleic acid can be used as biological sensing elements and the chemical sensing elements can be nanoparticles (Agrawal *et al*., 2012). The nanomaterials chosen for the study are nanoclays also known as nanofillers which are phyllosilicates dominant and may be isolated from clay fraction by energetic stirring, centrifugation, freeze-drying, crossflow filtration and ultracentrifugation (Nazir *et al.*, 2016). Nanoclays are ever-available, cheap, and environmentally friendly hence there have been studies on nanoclays and their development for various applications (Feng *et al.*, 2018; Nazir

et al., 2016). A new electrochemical method which uses glassy carbon electrode modified with nanoclay was developed. This method is fast, high in sensitivity and is not affected by the presence of other antiretroviral drugs (Barry *et al*., 2016; Shetti *et al.*, 2017). Development of an electrochemical sensor from the nanoclay metal composites and their conjugates for the detection of zidovudine. The application of nanomaterials in the development of electrochemical nanosensors has led to a great interest in the past years (Barry *et al*., 2016. The modification of electrodes with nanomaterials provides increased chemical and physical properties hence the improvement of current electroanalytical applications (Barry *et al*., 2016). Nanoclays have been applied in pharmaceutical for the detection of paracetamol and acyclovir (Gomdje *et al*., 2017; Shetti *et al.*, 2017).

1.3 Assumptions

A cheap electrochemical sensor which will be rapid and with lower detection limit will be developed. This will be done through the synthesis of silver nanoparticles which will be used to functionalize the nanoclay. The sensor will be applied in spiked urine samples and commercial tablets.

1.4 Research questions

- What is the difference in structural and properties of the synthesised nanoparticles?
- Which nanoparticles suitable for the functionalisation of nanoclays?
- What is the best nanoclay for detection of zidovudine?
- What are the best methods of detection of zidovudine?
- How does the current developed method vary from the previously developed methods?
- How can the modified electrode be applied in the detection of zidovudine?
- How will the developed method be applied in the detection of zidovudine in various matrices?

1.5 Objectives

The aim of the study is to develop an electrochemical sensor fabricated with silver nanoclay composites and their conjugates for the detection of zidovudine. To achieve this, the following objectives were followed:

- Synthesis and characterisation of silver nanoparticles.
- Functionalisation of nanoclay to form composites and conjugates.
- Characterisation of the functionalised material using spectroscopic techniques (FTIR, XRD, SEM) and electrochemical (CV, DPV).

- Fabrication of the sensor by modification of the glassy carbon working electrode and optimisation sensor fabrication (drop coating, electrodeposition).
- Optimisation of the sensor and detection of the AZT (method optimisation: Concentration of supporting electrolyte, Electrochemical technique, scan rate and pulse amplitude).
- Validation of the developed sensor through reference standard analysis, interference detection, repeatability, sensor stability, and spiked biological fluids.
- Use of the sensor in real samples: tablets

1.6 Significance and importance of the research

An electrochemical sensor that will be developed will be cheap, rapid and with lower limit of detection.

1.7 Research methodology

The detailed methodology is found in chapter 3 and 5.

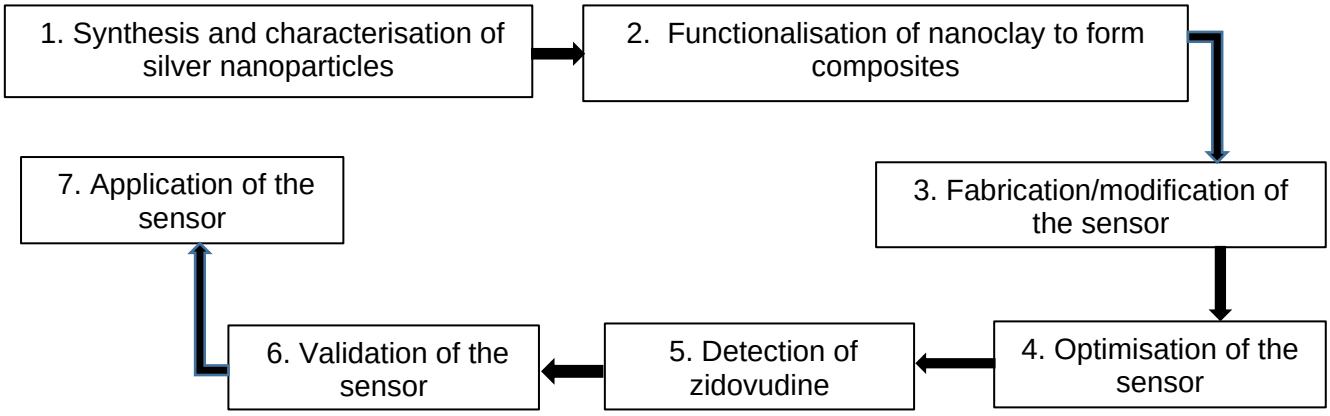

1.8 References

Aidsinfo. 2019. Drug resistance. *Understanding human immune virus/Acquired immunodeficiency syndrome (HIV/AIDS)*. U.S. Department of Health and Human Services Online [https://aidsinfo.nih.gov/understanding-hiv- aids/fact - sheets/21/56/drug-resistance].

Aluja, M.I., Ruisanchez, I. & Larrechi, M.S. 2013. Quantitative analysis of the effect of zidovudine, efavirenz, and ritonavir on insulin aggregation by multivariate curve resolution alternating least squares of infrared spectra. *Analytica Chimica Acta*. Vol.16(24). Elsevier B.V. Online [http://dx.doi.org/10.1016/j.aca.2012.10.057].

Castro, A.A, Aucelio, Q.R, Rey, A.N., Miguel, M.E. & Farias, A.P. 2011. Determination of the antiretroviral drug zidovudine in diluted alkaline electrolyte by adsorption stripping voltammetry at the mercury film electrode. *American journal of analytical chemistry*. Scientific research. Online [http://www.SciRP.org/journal/ajac].

Dolci, M. & Gartland, J. 2011. Analysis of zidovudine using a core enhanced technology accucore HPLC column. *Thermo fisher scientific.* Online [ANCCSCETZIDOV_0611.pdf].

Kominkova, M., Kensova, R., Zikta, O., Kynicky, J., Guran, R., Trnkova, L., Adam, V. & Kizek, R. 2014. Electrochemical and spectrometric study of GFP-AZT Interaction. *International journal of electrochemical science.* Vol.9. Online [www.electrochemsci.org].

Marchei, E., Valvo, L., Pacifici, R., Pellegrini, M., Tossini, G. & Zuccaro, P. 2002. Simultaneous determination of zidovudine and neverapin in human plasma by RP-LC. *Journal of pharmaceutical and biomedical analysis.* Elsevier science B.V. Vol.29. Online [www.Elsevier.com/locate/jpba].

Matta, M.K., Pilli, N.R., Inamadugu, J.K., Burugula, L. & Seshagiri, R. 2012. Simultaneous quantification of lamivudine, zidovudine & nevirapine in human plasma by liquid chromatography-tandem mass spectrometry and application to pharmacokinetic study. *Acta pharmaceutica Sinica B*. Institute of materia Medica: Elsevier. Vol.2(5). Online [http://dx.doi.org/10.1016/japsb.2012.07.003].

Mayoclinic. 2018. HIV/AID Diagnosis and treatment. Online [Mayoclinic.org/disease-conditions/hiv-aids/diagnosis-treatment/drc-z0373531].

Pietrangelo, A & Cherney, K. 2017. Effects of HIV on your body. Online [health line.com/health/hiv-aids-on-body#1].

CHAPTER TWO

LITERATURE REVIEW

This work elaborates on zidovudine as mentioned in chapter one. This will further include information on the synthesis of zidovudine, its chemistry as well as mechanism of action. In addition, various analytical techniques commonly adopted in the analysis of antiretroviral drugs as well as the importance of the study will be further elaborated. A discussion will extend to electrochemical techniques, especially sensors and nanomaterials of choice in the study. The description on sensor components and the role of the nanomaterials in fabrication of sensors will also be highlighted.

2.1 Introduction

Zidovudine as a nucleoside reverse transcriptase inhibitor (NRTI) or 2',3'-dideoxynucleoside (ddN) analogue, prevents HIV from making copies of itself by blocking the reverse transcriptase (Mayoclinic, 2018; AIDSinfo, 2019). The synthesis of zidovudine is represented in scheme 2.1, where methansulfonyl chloride in pyridine is added to 1-(2'- deoxy-5'-O-trityl-β-D-lyxosyl) thymine to form a similar mesylate which is then treated with lithium azide in N,N-dimethyl formamide and heated in 80% acetic acid to remove trityl protection, producing 3'-azido-2',3'- dideoxythymidine (Vardanyan *et al.*, 2006).

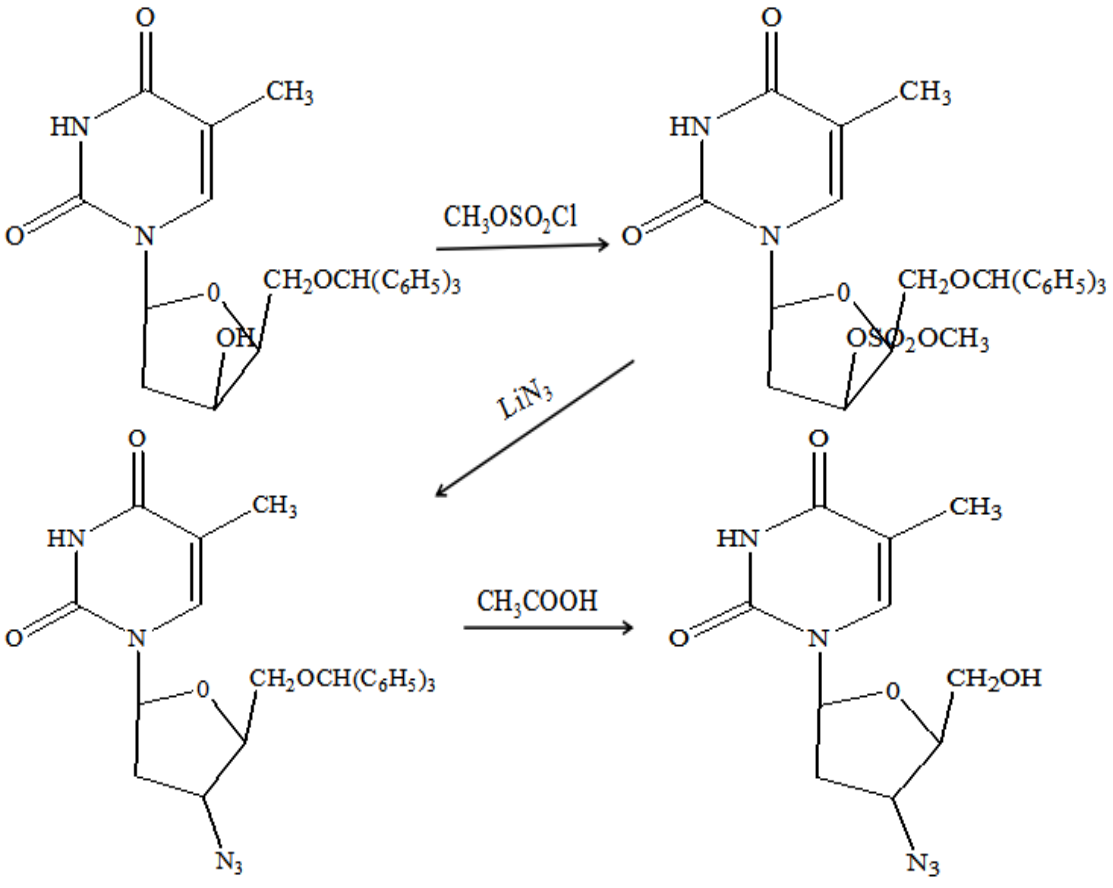

Scheme 2.1: Synthesis of zidovudine.

The NRTI drugs necessitates activation by phosphorylation, followed by end of termination and inhibition of nucleotide-binding site for HIV reverse transcriptate (Kominkova *et al.*, 2014). The mechanism of ZDV is shown in Scheme 2.2, where cellular enzymes such as 2'-deoxynucleoside (dThd) kinase, 2'-deoxynucleotide (dTMP) kinase and 2'-deoxynucleoside-5'-diphosphate (NDP) kinase carry the phosphorylations of ddNs, followed by the shut off synthesis of RNA-dependent DNA as chain eradicators after conversion of ddN to their 5'-triphosphate (TP) form which is ddN-TP (e.g ZDV-TP) (De Clercq *et al.*, 2009).

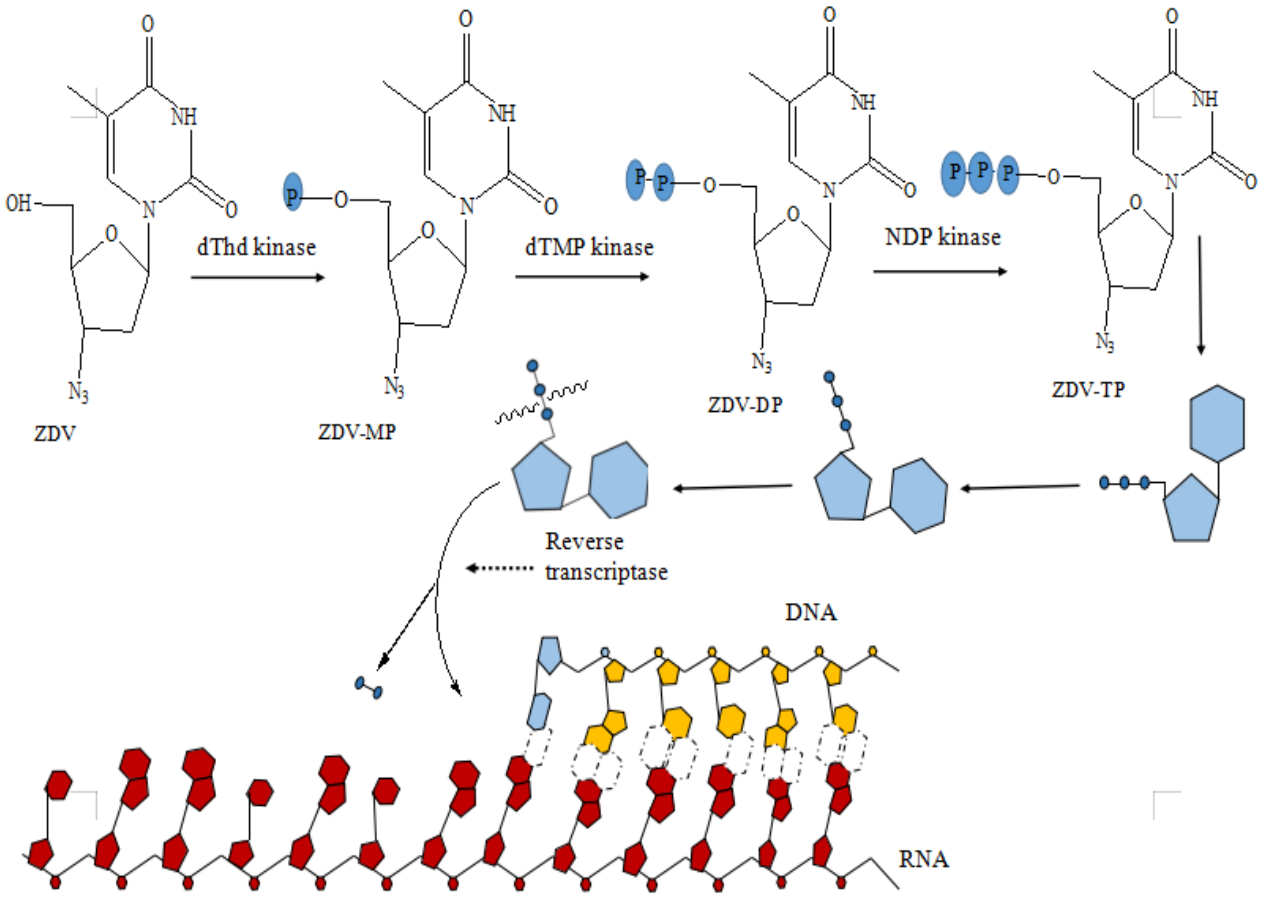

Scheme 2.2: Zidovudine mechanism of action.

The activity of ZDV depends on the formation of ZDV-TP which is a weak mammalian DNA polymerases α, β and γ that catalyze replication of DNA in vivo and also blocks HIV reverse transcriptase efficiently by acting as normal nucleotides competitive inhibitor, leading to termination of proviral DNA (Fang *et al.*, 2009). The use of treatment result in decline in the occurence of mitochondrial deoxyribonucleic acid (mtDNA) due to the inhibition of gamma-polymerase (Kominkova *et al.*, 2014). ZDV is intracellularly anabolized to its potent inhibitor of HIV reverse transcriptase such as 5'-triphosphate and destroys the proviral DNA growth (Marchei *et al.*, 2002). A decrease in the binding affinity of ddN-TP to the HIV reverse trancriptase causes resistance to NRTIs (De Clercq *et al.*, 2009). The mechanisms contributing to enhanced sensitivity of cancer cells to the growth-inhibitory effects of ZDV was examined

and was achieved by incubation of hepatoma cell line and a normal liver cell line with ZDV in continuous culture (Fang *et al.*, 2009). The mechanisms of action of these drugs can also be explained with the possibility of in vivo imaging of the interaction of the drug in an organism (Kominkova *et al.*, 2014). The in vivo monitoring of events in real time was carried out using green fluorescence protein (GFP) for labelling of target molecule due to its fluorescent properties (Kominkova *et al.*, 2014).

2.1.1 Detection methods for zidovudine

In the last 25 years, there has been a significant change in extension of the lives of infected people which currently live up to thirty-five years and longer compared to when cART was not introduced (Komnikova *et al.*, 2014). The body of an infected person with HIV becomes resistant to drugs due to some HIV mutations formed while a person is using the medicines. These mutations are due to the accumulation of the HIV in the body (AIDSinfo, 2019). Therefore, it is advised to combine three drugs from two classes of anti-HIV drugs to prevent drug-resistant strains of HIV (Mayoclinic, 2018). In the presence of ZDV, it has been reported that insulin remains stable for a short time in its native state, but the quantitative effect of ZDV on aggregation could not be determined (Aluja *et al.*, 2013). Quantifying the effects of the drugs and understanding the underlying mechanism of these effects could help decrease effects of antiretroviral therapy.

Several methods have been developed for the analysis of zidovudine. These methods include chromatographic (Dolci *et al*., 2011; Marchei *et al.*, 2002), voltammetric (Castro *et al*., 2011; Kominkova *et al*., 2014) and spectroscopic (Kominkova *et al*., 2014; Matta *et al*., 2012) methods. In chromatography, high performance liquid chromatography (HPLC) is the mostly used method for the determination of zidovudine (Dolci *et al*., 2011). Liquid chromatography-mass spectrometry (LC-MS/MS) method was developed to quantify zidovudine simultaneously in human plasma (Matta *et al.*, 2012). Reverse Phase liquid chromatography (RP-LC) method was used in the analysis of zidovudine at 275 nm UV detection and for the determination of zidovudine in human plasma from the HIV infected human (Dolci *et al*., 2011; Marchei *et al*., 2002). In spectroscopic studies, fluorescence spectroscopy was used to analyse the azidothymidine interaction with green florescence protein (GFP), which is the best fluorescent label due to its connection to AZT which does not significantly affect the fluorescence of GFP (Kominkova *et al.*, 2014). However, due to the expensive instruments that the spectroscopic methods require, large amounts of sample preparation, longer analysis time, as well as large number of foreign substances that is affecting the accuracy of the results. There is also possible loss of analyte during the re-extraction process which also limit the application of the techniques. Hence, why electrochemical methods which are great in sensitivity, good stability, fast detection of analytes and low-cost were developed as alternatives.

Electrochemical methods are widely applied in pharmaceutical fields for the analysis of drugs in their dosage forms as well as in biological fluids (Farghaly *et al.*, 2014). One of these electrochemical methods include adsorptive stripping which has been used to determine zidovudine at thin-film mercury electrode with NaOH as the supporting electrolyte (Castro *et al*., 2011). Square-wave voltammetry (SWV) and differential-pulse voltammetry (DPV) have also been considered in the investigation of GFP-AZT interaction at hanging mercury drop electrode (HMDE) using phosphate buffer in SWV and Brdicka buffer in DPV as supporting electrolytes (Kominkova *et al.,* 2014). However, due to the high toxicity levels of mercury, nanosensors have been developed for the detection of antiretroviral drugs. A new electrochemical method which uses glassy carbon electrode modified with nanoclay was developed. This method is fast, high in sensitivity and is not affected by the presence of other antiretroviral drugs including nevirapine (Barry *et al.*, 2016; Shetti *et al.*, 2017). In electrochemical studies, the nano level voltammetric sensing method was developed for the determination of acyclovir using carbon paste electrode modified with nanoclay, employing clyclic voltammetry (CV) and square-wave voltammetry (SWV) in pH 5 (Shetti *et al*., 2017). The differential pulse voltammetry (DPV) and CV techniques were also used to detect parathion-ethyl pesticide using glassy carbon electrode (GCE) modified with mixture of laponite clay and zirconium oxide gel nanocomposites (Bui *et al*., 2015) and in the detection of paracetamol using GCE organoclay modified (Gomdje *et al.*, 2017). The amperometry technique was implemented in nevarapine determination with carboxylate multi-walled carbon nanotubes and synthesized 11-mercaptoundecanol hydrazine carbothioamide coated silver nanoparticles modified at GCE (Ahmadi *et al.*, 2019). The surface modified electrode can be characterized with techniques including CV, SEM, electrochemical impedance spectroscopy (EIS) (Ahmadi *et al.*, 2019). The electrochemical methods in biosensors are used as readout techniques and the electrode is used as the transduction element (Farghaly *et al.*, 2014).

2.2 Sensors

Sensors are chemical or physical devices built at microscopic or submicroscopic scale (Agrawal *et al.*, 2012). They are also known as energy converters (Fraden, 2004). A chemical sensor is known as a device that gives information about its environment continuously and gives a response which is directly related to the amount of a particular chemical species (Fraden, 2004; Stradiotto *et al.*, 2003). It can also be defined as a device that gives electric signal of a chemical reaction and is used for quantitative or qualitatively determination of a chemical liquid or gaseous phase species (Fraden, 2004; Farghaly *et al.*, 2014). It is highly sensitive, detecting a single chemical or biological molecule (Agrawal *et al.*, 2012). They have biosensitive layer that is made of biological elements attached to the transducer covalently, see scheme 2.3 (Maleh *et al.*, 2020; Agrawal *et al.*, 2012).

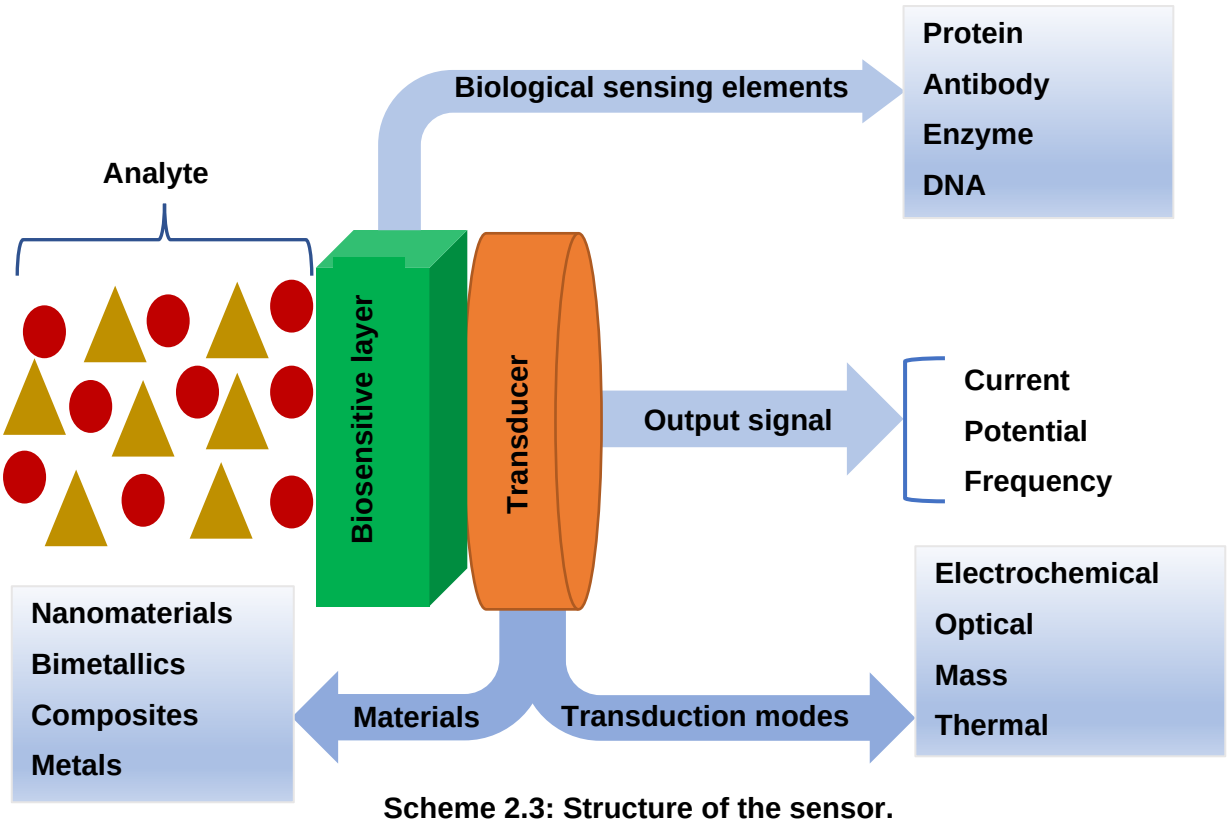

Scheme 2.3: Structure of the sensor.

Silicon, plastic, glass, ceramics, and metals can be used as sensing materials (Fraden, 2004). The chemical sensing element can be nanoparticles while enzyme, protein, antibody, aptamer, or nucleic acid can be used as biological sensing elements, including living biological system such as cells, tissue or an entire organism using biochemical mechanisms for recognition (Agrawal *et al.*, 2012). Enzymes have also been used as biorecognition elements in the development of enzyme-based biosensors due to their high sensitivity (Barry *et al.*, 2016). The combined selectivity of enzymes with recent development in nano electrochemistry resulted in more sensitive and specific biosensors. However, free enzymes have thermal instability, susceptibility to attack from proteins, high sensitivity to denaturing agents (Barry *et al.*, 2016). The main purpose of the sensor is to convert data obtained on atomic scale into the data that can be analysed easily. The two major groups of chemical sensors include direct sensor which directly converts energy into electrical signal modification or generation; and complex sensor which uses one or more transducers of energy before employing a direct sensor for electric output generation (Fraden, 2004). Chemical sensor is one of the major groups of sensors followed by physical sensor which determines physical quantities and biosensors whose transducer is connected to the biological sensing element (Farghaly *et al.*, 2014). A transducer is one of the sensor components which generates the response resulting from the interaction of the analyte with the biomolecule and convert it into a detectable signal, followed by a chemically selective layer which separates the analyte response from its instant environment (Khanmohammadi *et al.*, 2020; Stradiotto *et al.*, 2003).

Other types of sensors are shown in figure 2.1, including electrochemical sensors which are widely applied in industrial, environmental, agricultural, and clinical analyses due to their

remarkable detectability, experimental simplicity and are cheap compared to other sensors (Stradiotto *et al.*, 2003). Their output signal can be expressed as voltage, current or charge (Fraden, 2004).

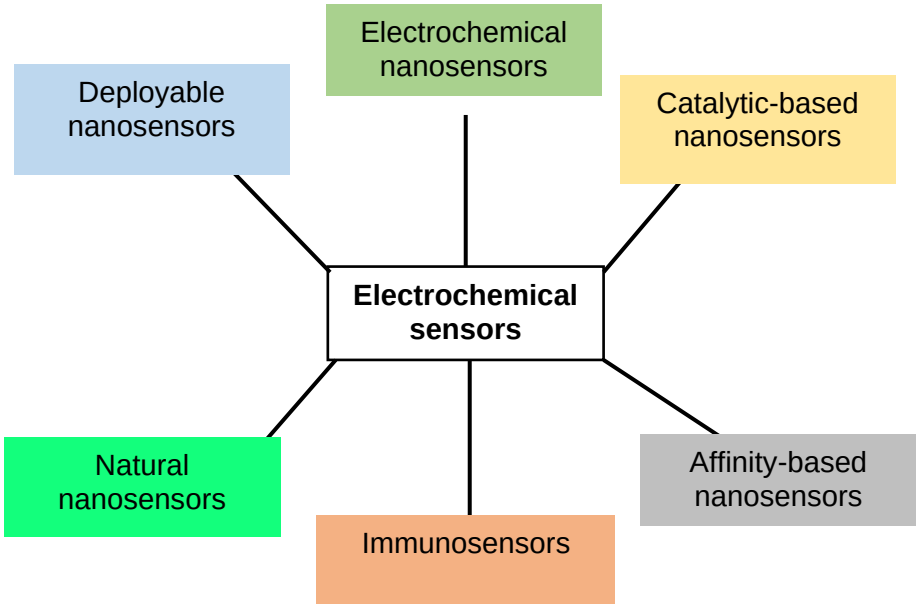

Figure 2.1: Types of electrochemical sensors.

The main difficulty in fabricating a highly sensitive electrochemical sensor is high overpotential and low oxidation signal of compounds in pharmaceutical, food and environmental. Improving its selectivity makes it possible to analyse drugs and food additives with low concentration in real samples (Maleh *et al.*, 2020). Fabrication of voltammetric and amperometric sensors considers selectivity and sensitivity as main important factors. The selectivity of sensors can be improved by applying DNA, protein, enzymes, RNA, aptamer, organic & inorganic mediator for determination of compounds in environmental, pharmaceutical and food, with biological molecules specifically interacting with the analyte. Modified electrochemical sensor has an advantage of determining drugs or food additives with a single electrochemical sensor simultaneously with mostly used electroanalytical sensor electrodes such as gold, platinum, pencil graphite, carbon paste, silver, glassy carbon, carbon paper and boron-doped diamond (Maleh *et al.*, 2020). Nanoelectrodes have small footprint, high sensitivity and cell time constants which allows them to respond quicker to changes in the potential applied. They exhibit low ohmic drop due to their reduced surface area compared to larger electrodes (Barry *et al.*, 2016). The trace levels of compounds in food, pharmaceutical and environmental can be analysed with carbon-based electrodes including glassy carbon, which have been applied in extremely selective & sensitive fabrication of electroanalytical sensors due to their simple modification process which involves the use of conducting materials to increase the sensors sensitivity and decreasing the value of the charge transfer resistance of the biosensor fabricated (Maleh *et al.*, 2020).

2.2.1 Nanomaterials used in sensors

The application of nanomaterials in the development of electrochemical nanosensors has led to a great interest in the past years (Barry *et al.*, 2016). They have been applied especially in potentiometric sensors to enhance the rate of electron transfer and electrochemical reactions catalytic properties, providing advantage in analysis of food quality, chemicals of cancer, pharmaceutical and environmental compounds (Maleh *et al.*, 2020; Gupta *et al.*, 2013; Ahmadi *et al.*, 2019). Nanomaterials have been used as electrode modifiers materials to improve the properties of the sensor. These include nanoparticles (metallic, polymeric), nanoclays, quantum dots, carbon-based nanomaterials including graphene, carbon nanopowder, fullerene, nanoribbons, and carbon nanotubes (Kempahanumakkagari *et al.*, 2017; Pramanik *et al.*, 2013; Shetti *et al.*, 2019). They can be incorporated into electrochemical sensing system and into procedures to remove or detect the number of compounds ensuring safety in surface and ground water levels, thus improving current sensor technologies (Barry *et al.*, 2016; Rashid *et al*., 2013). Nanoparticles have the ability to strongly bind to biomolecules, allowing them to immobilise electrostatically and covalently on the electrode surface (Sharma *et al.*, 2015). Nanoparticles together with other nanomaterials have been implemented in the development of electrochemical impendence spectroscopy (EIS) based immunosensors and in wide range of aptamer-based cocaine sensors to increase the signal in the law enforcement area (Barry *et al.*, 2016). They can be used as electrodes independently, and as biolabelling combating microbes in cancer treatment (Gurunathan *et al.*, 2009; Barry *et al.*, 2016). The use of nanomaterials in sensors reduces the limit of detection of various biomolecules from nano to pico level (Shetti *et al.*, 2019). Carbon-based nanomaterials provide excellent electronic and catalytic activity characteristics and have been investigated in electrosensing applications. A sensor functionalised with carbon nanotubes has been implemented in pharmaceuticals, specifically for the detection of paracetamol and hesperidin (Shetti *et al.*, 2019). The synthetic molecular imprinted polymers have been applied in electrochemical sensors for isolation of different analytes in matrices at GCE modified with silicon carbide nanoparticles (Roushani *et al.*, 2016).

2.2.1.1 Silver nanoparticles

Silver nanoparticles (AgNPs) are antimicrobial materials, which makes them non-toxic to human cells at low concentrations (Sileikaite *et al.*, 2006). They are cheap with high specific surface area, excellent electrical conductivity, rapid charge and mass transport, good availability and biocompatibility compared to other metals (Ahmadi *et al.*, 2019; Chelly *et al.*, 2021). Silver ions break the proton-motive force across the cytoplasmic membrane or disconnects the respiratory chain from oxidative phosphorylation (Gurunathan *et al.*, 2009).

2.2.1.1.1 Applications of silver nanoparticles in sensors and biosensors

A sensor modified with silver nanoparticles result to increased signal provided by surface area, reduced overvoltage, fast electrode, thus resulting to low detection limit and rapid response (Gupta *et al.*, 2013). Silver nanoparticles are applied in biosensors as biological tags for biorecognition of an antibody because of their high fluorescence, detecting quantitatively antibacterial or antifungal agents in biotechnology and bioengineering, textile engineering and silver-based consumer products (Rashid *et al*., 2013; Agrawal *et al.*, 2012). They are used to improve the macro electrodes response, and in oxidation or reduction of hydrogen peroxide due to their electrocatalytic properties. Metal nanoparticles can also be applied in the detection of nitroaromatic explosives and plastic explosives, and in development of highly sensitive aptasensor where they were incorporated with multi-walled carbon nanotubes (MWCNT) at glassy carbon electrode (Barry *et al.*, 2016).

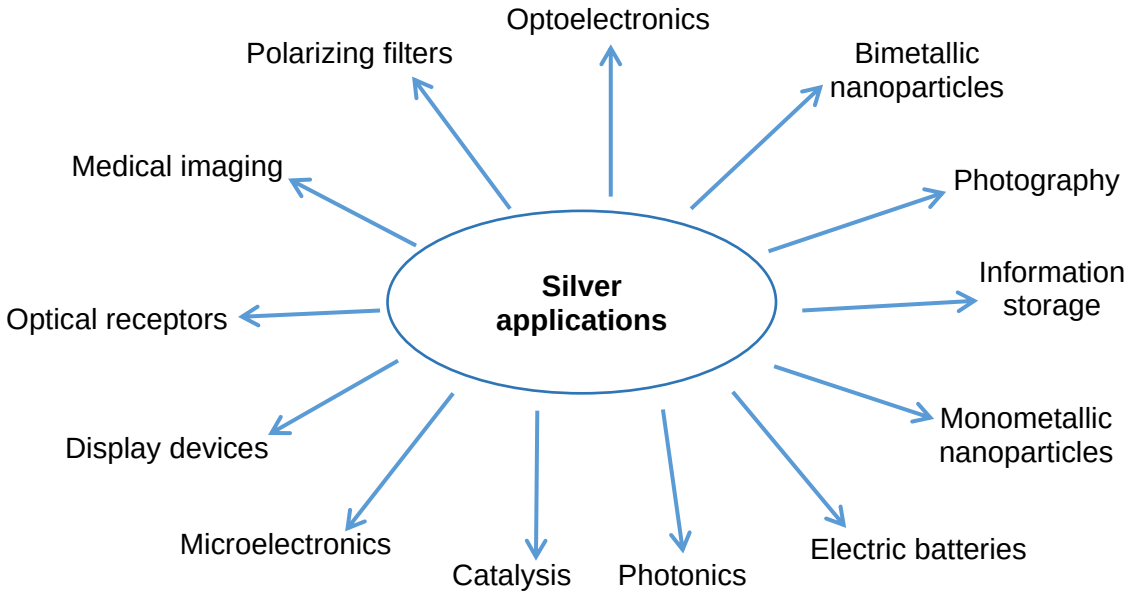

Figure 2.2: Applications of silver.

Silver nanoparticles have proven to be a good choice for metal-enhanced fluorescence (MEF) and surface-enhanced Raman Scattering (SERS) measurements due to the SPR and large effective cross section of single AgNPs (Sileikaite *et al.*, 2006; Kim *et al.*, 2006; Pillai *et al.*, 2004; Rashid *et al.*, 2013; Narasimha *et al.*, 2013; Manivel *et al.*, 2012). Chemically synthesized AgNPs have also been used quantitatively in the analysis of ascorbic acid in tablets containing Vitamin C (Rashid *et al.*, 2013). More information on the synthesis of silver nanoparticles will be detailed in chapter three.

2.2.1.2 Nanoclays as sensing materials

Nanoclays are nanofillers which are phyllosilicates dominant made of SiO_4 tetrahedra polymeric layers attached to (Mg, Fe, Al) $(O,OH)_6$ octahedra thin sheets as shown in figure 2.3 (Shetti *et al.*, 2019).

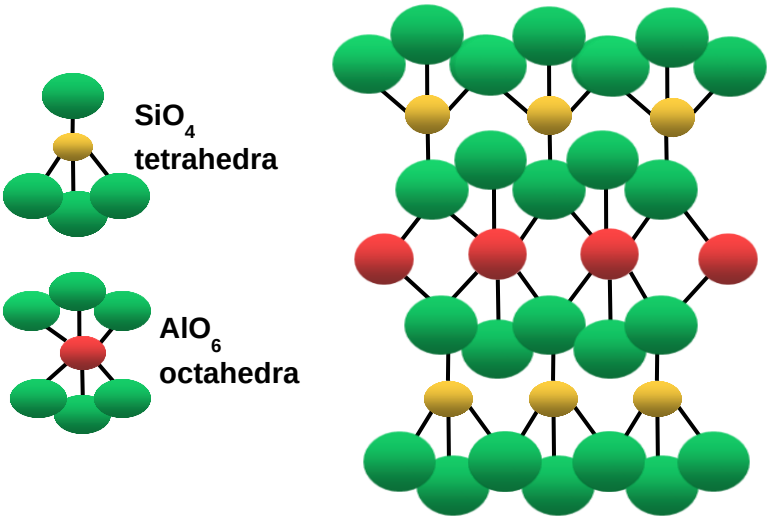

Figure 2.3: Nanoclay structure.

They may be isolated from clay fraction by energetic stirring, centrifugation, freeze-drying, crossflow filtration and ultracentrifugation (Nazir *et al.*, 2016). Nanoclays have platy structure with thickness approximately 1 nm or less and size ranging from 1 to 100 nm (Vipulanandan *et al.*, 2015). They are ever-available, cheap, high surface area, increased stability, resistant to extreme temperature, excellent intercalation properties and environmentally friendly hence there have been studies on nanoclays and their development for various applications (Feng *et al.*, 2018; Nazir *et al.*, 2016, Vahedia *et al*., 2018; Shetti *et al*., 2019). Clay materials were first applied in ceramics and pottery, and over four thousand clay minerals were discovered (Shetti *et al.*, 2019). The most popular clay minerals are shown in figure 2.4.

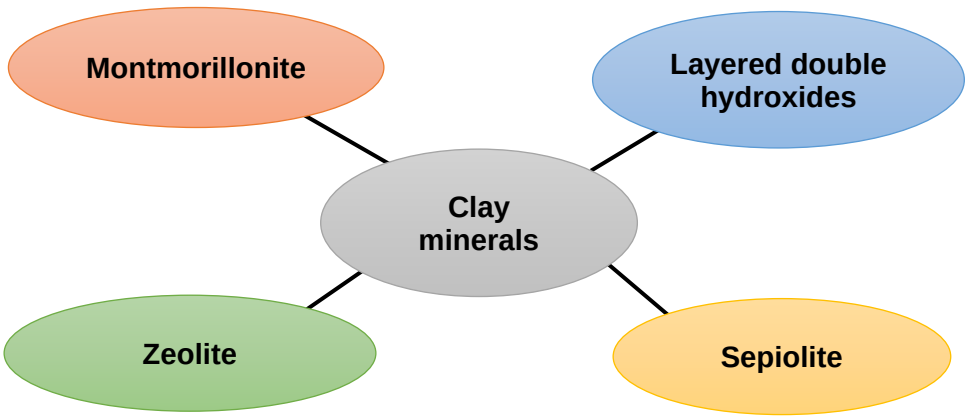

Figure 2.4: Types of clay minerals.

They have been applied in pharmaceutical for the detection of paracetamol and acyclovir (Gomdje *et al.*, 2017; Shetti *et al.*, 2017), and in polymer matrices forming nanocomposites which is a new class of materials (Colunga *et al.*, 2014). Clay modified electrodes provide high chemical stability, good biocompatibility, increased analyte mobility, good ion exchange and adsorption capacity, and increased product mobility (Shetti *et al.*, 2019). The particles of clay have activated sites for assembling of electrochemical species but only few possess redox properties. The clay matrix can be used as a device or as redox intermediator to capture biomolecules at the surface of the electrode (Shetti *et al.*, 2019). The sensing elements can be adsorbed on the clay in various sites (figure 2.5). The detailed information on this will be elaborated in chapter three.

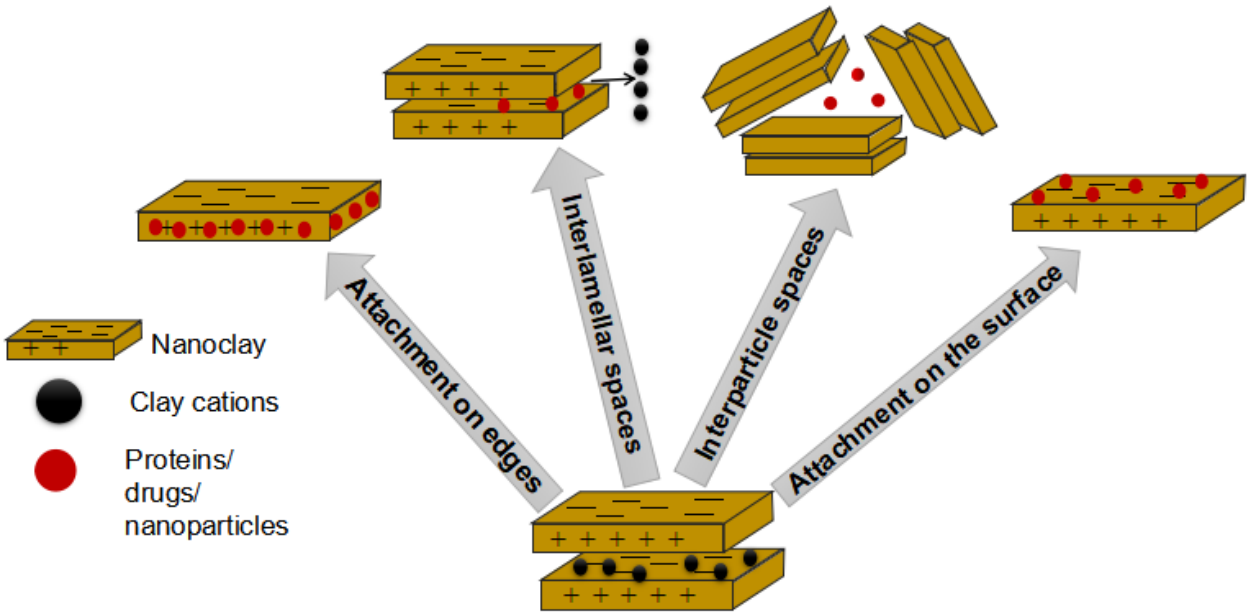

Figure 2.5: Processes taking place during functionalisation of nanoclay.

2.2.2 Applications of sensors

Sensors are applied in medical field, security, aerospace, integrated circuits, law enforcement, food safety and environment (Agrawal *et al.*, 2012; Barry *et al.*, 2016). In health, they have been used to detect large range of medically relevant analytes which ranges from small to more complex molecules such as bacteria or pharmaceutical drugs. Electrochemical nanosensors have been applied in food safety to detect a potential source of food poisoning known as staphylococcal enterotoxin B, sulfite in sugar, grapes, water and wine, aflatoxin, durabolin and animal growth stimulants (Barry *et al.*, 2016). Sensors can be used to detect hypoglycemia with type 1 diabetes people, asthma attack approximately three weeks before they take place, organophosphorus compounds detection, pH sensing, detection of DNA and protein, drug delivery, detection of microorganisms, diagnosis of cancer, cell monitoring, detection, and quantification of variety of gases present in real time. They can also be applied

in the detection of damage or viruses in astronauts by sensing signs (Agrawal *et al.*, 2012). Nanoelectrochemical sensors are versatile, and therefore applied in more areas of research such as in detection of Immunoglubulin Y (IgY) to identify egg yolk as pigment in tempera paintings using nanoelectrode ensembles (Barry *et al.*, 2016). In this study, the developed sensor modified with conducting material will be applied in the analysis of zidovudine, which will be detailed in chapter four.

2.3 References

Agrawal, S. & Prajapati, R. 2012. Nanosensors and their pharmaceutical applications. *International journal of pharmaceutical sciences and nanotechnology*. Vol.4(4).

Ahmadi, E., Eyvani, M.R., Riahifar, V., Momeneh, H. & Karami, C. 2019. Amperometric determination of nevirapine by GCE modified with c-MWCNTs and synthesized 11-mercaptundecanoyl hydrazinecarbothioamide coated silver nanoparticles. *Microchemical Journal*. Elsevier B.V. Online [https://doi.org/10.1016/j.microc.2019.02.054].

Aidsinfo. 2019. Drug resistance. *Understanding human immune virus/Acquired immunodeficiency syndrome (HIV/AIDS)*. U.S. Department of Health and Human Services Online [https://aidsinfo.nih.gov/understanding-hiv- aids/fact - sheets/21/56/drug-resistance].

Ali, M.S., Al-Lohedan, H.A., Atta, M.A., Ezzat, A.O. & Al-Hussain, S.A.A. 2015. Interaction of human serum albumin with silver nanoparticles functionalized with polyvinylthiol. *Journal of Molecular Lipids*. Elsevier B.V. Online [www.elsevier.com/locate/molliq].

Aluja, M.I., Ruisanchez, I. & Larrechi, M.S. 2013. Quantitative analysis of the effect of zidovudine, efavirenz, and ritonavir on insulin aggregation by multivariate curve resolution alternating least squares of infrared spectra. *Analytica Chimica Acta*. Vol.16(24). Elsevier B.V. Online [http://dx.doi.org/10.1016/j.aca.2012.10.057].

Aziz, B.S., Abdullah, O.G., Saber, D.R., Rasheed, M.A. & Ahmed, H.M. 2017. Investigation of metallic siver nanoparticles through UV-Vis and optical micrograph techniques. *International journal of electrochemical science*. Vol.12. Online [doi:10.20964/2017.01.22].

Barry, S. & O'Riordan, A. 2016. Electrochemical nanosensors, advances and applications. *Reports in electrochemistry*. Dove press. Vol.6. Online [https://www.dovepress.com/].

Bui, N.M. & Seo, S.S. 2015. Electrochemical analysis of parathion-ethyl using zirconium oxide-laponite nanocomposites modified glassy carborn electrode. *Journal of applied electrochem*. Springer science & business media. Vol.45. Online [DOI 10.1007/s10800-0015-0789-0].

Casademont, J., Barrientos, A., Grau, J.M., Pedrol, E., Estivill, X., Marquez, A. & Nunes, V. 1996. The effect of zidovudine on skeletal muscle mtDNA in HIV-1 infected patients with mild or no muscle dysfunction. *Brain article*. Oxford UniversityPress.Online[https://doi.org/10.1093/brain/119.4.1357].

Castro, A.A, Aucelio, Q.R, Rey, A.N., Miguel, M.E. & Farias, A.P. 2011. Determination of the antiretroviral drug zidovudine in diluted alkaline electrolyte by adsorption stripping voltammetry at the mercury film electrode. *American journal of analytical chemistry*. Scientific research. Online [http://www.SciRP.org/journal/ajac].

Chelly, M., Chelly, S., Zribi, R., Bouaziz-Ketata, H., Gdoura, R., Lavanya, N., Veerapandi, G., Sekar, C. & Neri, G., 2021. Synthesis of Silver and Gold Nanoparticles from Rumex roseus Plant Extract and Their Application in Electrochemical Sensors. *Nanomaterials.* Vol.11(3). Online [https://doi.org/10.3390/nano11030739].

Colunga, J.G.M., Valdes, S.S., Ramos-deValle, L.F., Jimenez, M. L., Vargas, E.R., Alonso, I. M.C., Ramirez, T.L. & Lafleur, P.G. 2014. Simultaneous polypropylene Functionalization and Nanoclay dispersion in PP/Clay nanocomposites using ultrasound. *Journal of applied polymer science*. Wiley Periodicals. Online [DOI: 10.1002/APP.40631].

De Clercq, E. & Neyts, J. 2009. Antiviral agents acting as DNA or RNA chain terminators. *Article in Handbook of experimental pharmacology*. Springer-Verlag: Berlin Hiedelberg. Online [DOI:10.1007/978-3-540-79086-0-3].

Djurdjevic, P., Laban, A., Markovic, S. & Stankov, J.M. 2004. Chemometric optimization of a RP-HPLC method for the simultaneous analysis of abacavir, lamivudine and zidovudine in tablets. *Analytical Letters*. Vol.37(13). Marcel Dekker. Online [DOI:10.1081/AI.200031946].

Dolci, M. & Gartland, J. 2011. Analysis of zidovudine using a core enhanced technology accucore HPLC column. *Thermo fisher scientific.* Online [ANCCSCETZIDOV_0611.pdf].

Duy, S.V., Tournier, L.I., Pichon, V., Chapuis, H.F., Puy, J.Y. & Perigaud, C. 2009. Molecularly imprinted polymer for analysis of zidovudine and stavudine in human serum by liquid chromatography-mass spectrometry. *Journal of chromatography B*. Elesivier B.V. Online [doi: 10.1016/j.jchromb.2009.02.068].

Fang, L. J. & Beland, F.A. 2009. Long-term exposure to zidovudine delays cell cycle progression, induces apoptosis and decreases telemerase activity in human hepatocytes. *Toxicological sciences*. Oxford University Press. Online [doi:10.1093/toxsci/kfp 136].

Farghaly, O.A., Hameed, A.S.R. & Abu, N.H. 2014. Analytical application using modern electrochemical techniques. *International journal of electrochemical science*. Vol.9. Online [www.electrochem.sci.org].

Feng, G., Saman, A., Yinghui, H. & Yunpeng, J. 2018. A review of synthesis and applications of polymer-nanoclay composites. *Journal of applied sciences*. Vol.8. Online [applsci-08-01696.pdf].

Fraden, J. 2004. Physics, designs, and applications. *Handbook of mordern sensors*. 3rd edition. Springer-Verlag: New York.

Gomdje, H.V., Rahman, N.A., Wahabou, A., Laura, B. & Chtaini, A. 2017. Synthesis of organoclay and its applications in electrochemical detection of paracetamol. *Palagia research library*. Der Chemica Sinica: USA. Vol.8(1). Online [www.pelagiaresearchlibrary.com].

Gupta, K.V., Sadeghi, R. & Karimi, F. 2013. A novel elec trochemical sensor based on zinc-oxide nanoparticles and ionic liquid binder for square-wave voltammetric determination of droxidopa in pharmaceutical and urine samples. *Sensors and actuators B.* Elsevier B.V. Online[http://dx.doi.org/10.1016/j.snb.2013.06.048].

Habte, G., Hymete, A. & Mohamed, A.M.I. 2009. Simultaneous determination of lamivudine and zidovudine in pharmaceutical formulations using the HPTLC method. *Analytical Letters*. Taylor & Francis Group. Vol.42. Online [DOI:10.1080/00032710902993852].

Hoetelmans, R.M., Kraaijeveld, C.L., Meenhorst, P.L., Mulder, J.W., Burger, D.M., Koks, C.H.W. & Beijnen, J.H. 1997. Penetration of 3′-amino-3-deoxythymidine, a cytotoxic metabolite of zidovudine into the cerebrospinal fluid of HIV-1-infected patients. *Journal of acquired Immune Deficiency Syndrome in human Retrovirol.* Vol.15(2).

Huang, M., Du, L. & Feng, J. 2016. Photochemical synthesis of silver nanoparticles/ eggshell membrane composite, its characterization and antibaterial activity. *Science of advanced materials*. Vol.8(8). American Scientific Publishers: USA. Online [www.aspbs.com/sam].

Kabra, V., Agrahari, V., Karthikeyam, C. & Trivedi, P. 2009. Simultaneous quantitative determination of zidovudine and nevirapine in human plasma using isocratic reverse phase liquid chromatography. Tropical Journal of Pharmaceutical Research. Vol.18(1). Pharmacotherapy Group: Nigeria. Online [https://www.tjpr.org].

Kempahanumakkagari, S., Deep, A., Kim, K., Kailasa, S.K. & Yoon, H. 2017. Nanomaterial-based electrochemical sensors for arsenic. *Biosensors and Bioelectronics.* Vol. 95. Elsevier B.V. Online [http://dx.doi.org/10.1016/j.bios.2017.04.013].

Khanmohammadi, A., Ghazizadeh, A.J., Hashemi, P., Afkhami, A., Arduini, F. & Bagheri, H. 2020. An overview to electrochemical biosensors and sensors for the detection of the environmental contaminants. *Journal of Iranian Chemical Society*. Springer. Online [https://doi.org/10.1007/s13738-020-01940-z].

Kim, D., Jeong, S. & Moon, J. 2006. Synthesis of silver nanoparticles using the polyol process and the influence of precursor injection. *Journal of nanotechnology*. Institute of physics publishing: Korea. Vol.17. Online [stacks.10p.org/Nano/17/4019].

Kominkova, M., Kensova, R., Zikta, O., Kynicky, J., Guran, R., Trnkova, L., Adam, V. & Kizek, R. 2014. Electrochemical and spectrometric study of GFP-AZT Interaction. *International journal of electrochemical science.* Vol.9. Online [www.electrochemsci.org].

Leandro, K.C., Moreira, C.J. & Farias, M.A.P. 2010. Determination of zidovudine in pharmaceuticals by differential pulse voltammetry. *Analytical Letters*. Vol.43. Taylor & Francis Group. Online [DOI:10.1080/00032711003687021].

Maleh, K.H., Karimi, F., Alizadeh, M. & Sanati, L.A. 2020. Electrochemical sensors, a bright future in the fabrication of portable kits in analytical systems. *The Chemical Record.* The Chemical Society of Japan & Wiley-VCH, GmbH & Co. KGaA: Weinheim. Online [DOI:10.1002/tcr.201900092].

Manivel, A. & Anandan, S. 2012. Spectral interaction between silica coated silver nanoparticles and serum albumins. *Colloids and Surfaces A:Physicochemical and Engineering Aspects*. Elsevier B.V. Online [doi: 10.1016/j.colsurfa.2011.12.001].

Marchei, E., Valvo, L., Pacifici, R., Pellegrini, M., Tossini, G. & Zuccaro, P. 2002. Simultaneous determination of zidovudine and neverapin in human plasma by RP-LC. *Journal of pharmaceutical and biomedical analysis.* Elsevier science B.V. Vol.29. Online [www.Elsevier.com/locate/jpba].

Matta, M.K., Pilli, N.R., Inamadugu, J.K., Burugula, L. & Seshagiri, R. 2012. Simultaneous quantification of lamivudine, zidovudine & nevirapine in human plasma by liquid chromatography-tandem mass spectrometry and application to pharmacokinetic study. *Acta pharmaceutica Sinica B*. Institute of materia Medica: Elsevier. Vol.2(5). Online [http://dx.doi.org/10.1016/japsb.2012.07.003].

Mayoclinic. 2018. HIV/AID Diagnosis and treatment. Online [Mayoclinic.org/disease - conditions/hiv-aids/diagnosis-treatment/drc-z0373531].

Narasimha, G., Alzohairy, M., Khadri, H. & Mallikarjuna, K. 2013. Extracellular synthesis, characterization, and antibacterial activity of silver nanoparticles by Actinomycetes isolative. International journal of Nano Dimension. Vol. 4(1). Online [www.IJND.ir].

Nazir, M.S., Haafiz, M., Kassim, M., Mohapatra, L., Gilani, M.A., Raza, M.R. & Majeed, K. 2016. Characteristic properties of nanoclays and characterization of nanoparticulates and nanocomposites. Springer Science & Business Media. Singapore. Pg 36-52.

Ngumba, E., Kosunen, P., Gachanja, A. & Tuhkanen, T. 2016. A multiresidue analytical method for trace level determination of antibiotics and antiretroviral drugs in wastewater and surface water using SPE-LC-MS/MS and matrix-matched standards. *Analytical Methods*. Vol.8. The Royal Society of Chemistry. Online [DOI:10.1039/c6ay01695b].

Patil, S. A. & Patil, G. 2015. Zidovudine, a review of analytical methods. *Asian journal of pharmaceutical technology and innovation.* Patel institute of pharmaceutical education and research: India. Online [www.asian pharmtech. Com].

Pramanik, S., Murphy, B.P. & Osman, N.A.A. 2013. Developments of immobilized surface modified piezoelectric crystal biosensors for advanced applications. *International Journal of Electrochemical Science*. Vol.8. Elsevier B.V. Online [www.electrochesci.org].

Rashid, M.U., Buiyan, K.H. & Quayum, M.E. 2013. Synthesis of silver nanoparticles and their uses for quantitative analysis of vitamin C tablets. *Journal of pharmaceautical sciences*. Vol.12(1).

Roushani, M., Nezhadali, A. Jalilian, Z. & Azadbakht, A. 2016. Development of novel electrochemical sensor on the base of molecular imprinted polymer decorated on SiC nanoparticles modifified glassy carbon electrode for selective determination of loratadine. *Materials Science and Engineering C.* Vol. 71. Elsevier B.V. Online [http://dx.doi.org/10.1016/j.msec.2016.11.079].

Sharma, V.K., Jelen, F. & Trnkova, L. 2015. Functionalized solid electrodes for electrochemical biosensing of purine nucleobases and their analogues. *Sensors*. Vol.15. Online [doi:10.3390/s150101564].

Shetti, N.P., Nayak, D.S., Malode, S.J. & Kulkarni, R.M. 2017. nano molar detection of acyclovir, an antiretroviral drug at nanoclay modified carbon paste electrode. *Journal of sensing and biosensing research*. Elsevier B.V. Vol.14. Online [http://dx.doi.org/10.1016/j.sbsr.2017.04.004].

Soliwoda, R.K., Tomaszewska, E., Socha, E., Krzyczmonik, P., Ignaczak, A., Orlowsk, P., Krzyzowska, M., Celichowski, G. & Grobelny, J. 2017. The role of tannic acid and sodium citrate in the synthesis of silver nanoparticles. *Journal of nanoparticles research*. Vol.19. Springer. Online [doi:10.1007/s11051-017-3973-9].

Stradiotto, N.R., Yamanaka, H. & Zanoni, M.V. 2003. Electrochemical sensors, a powerful tool in analytical chemistry. *Journal of the Brazillian Chemical Society*. Brazil. Vol.14 (2). Online [DOI: 10.1590/S0103-50532003000200003].

Suresh, R., Brkar, S.N., Sawant, V.A., Shende, V.S. & Dimble, S.K. 2010. Nanoclay drug delivery system. *International journal of pharmaceutical sciences and nanotechnology*. Vol.3 (2). Online [e15fa022025df833f6a876e5b50f89fdd0af].

Tajmir, R.H.A. 2007. An overview of drung binding to human serum albumin: Protein folding and unfolding. *Scientia Iranica*. Vol.14 (2). Sharif University of Technology.
Thaczuk, D. 2019. Drug resistance. *nam aidsmap.*NAM Publication. Online [www.aidsmap.com/resources/treamentsdirectory].

Vahedia, S., Siadatia, S.M.H., Khosravib, H. & Farahani, A.S. 2018. Flexural behavior of fiber–metal laminates reinforced with surface-functionalized Nanoclay. *Mechanics and advanced composite structures.*Vol.5. Semnan University Press. Online [http://MACS.journals.semnan.ac.ir].

Vardanyan, R.S. & Hruby, V.J. 2006. Antiviral drugs. *Synthesis of essential drugs*. Elsevier B.V. Online[https://dOi.org/1.1016/B978-044452166-8/50036-4].

Vipulanandan, C. & Mohammed, A. 2015. Effect of nanoclay on the electrical resistivity and rheological properties of smart and sensing bentonite drilling muds. *Journal of Petroleum Science and Engineering*. Elsevier B.V. Online [http://dx.doi.org/10.1016/j.petrol.2015.03.020].

Wang, H., Qiao, X., Chen, J. & Ding, S. 2005. Preparation of silver nanoparticles by chemical reduction method. *Colloids & Surfaces A*. Elsevier B.V. Online [www.elsevier.com/locate/colsurfa].

Yin, H., Yamamoto, T., Wada, Y. & Yanagida, S. 2003. Large-scale and size-controlled synthesis of silver nanoparticles under microwave irradiation. *Materials chemistry and physics*. Elsevier B.V. Online [www.elsevier.com/locate/matchemphys].

Zang, L., Qiu, J., Yang, C. & Sakai E. 2016. Preparation and application of conducting polymer/ Ag/Clay composite nanoparticles formed by in situ UV-induced dispersion polymerization. *Scientific reports article*. Online [www.nature.com/scientific reports].

Zhang, X., Xu, R., Wu, Z. & Zhou, C. 2003. The synthesis and characterization of polyurethane/clay nanocomposites. *Journal of polymer international society if chemical industry*. Online [DOI: 10.1002/pi.1152].

Zhang, W., Liu, Q. and Chen, P., 2018. Flexible strain sensor based on carbon black/silver nanoparticles composite for human motion detection. *Materials*. Vol.11(10). Online [https://doi.org/10.3390/ma11101836].

CHAPTER THREE

SYNTHESIS AND CHARACTERISATION OF SILVER NANOPARTICLES AND THEIR COMPOSITES

An introduction on the synthesis and characterisation of silver nanoparticles and nanoclay composites is included in this chapter, followed by the detailed experimental procedure of silver nanoparticles with different concentrations of reducing agent and silver nanoclay composites with different concentration of nanoclays such as surface modified nanoclay (1.44P) and hydrophylic bentonite (PGV). Furthermore, discusses the characterisation of the synthesized material with spectroscopic and electrochemical techniques. The data interpretation and discussion of spectra and voltammogram is comparison of the data on the literature. The choice of silver nanoparticles and nanoclay composite will be made which will be further used in sensor fabrication that will be elaborated in chapter five. The conclusion on the materials optical and electrochemical properties is made based on the data obtained.

3.1 Introduction

Silver nanoparticles have been widely used due to their enhanced physical and chemical properties compared to other metals (Aziz *et al*., 2017; Huang *et al.*, 2016; Rashid *et al.*, 2013; Ali *et al.*, 2015). The size, shape, composition, crystallinity, and structure determine intrinsic properties of metal nanoparticles, with size and shape providing an important control in physical and chemical properties of nanoscale material such as luminescence, conductivity, and catalytic activity (Gurunathan *et al.*, 2009; Kim *et al.*, 2006; Sileikaite *et al.*, 2006; Pillai *et al.*, 2004; Rashid *et al.*, 2013). The electrochemical properties of the nanoparticles could be improved by metal nanoparticles such as silver, copper, nickel, iron, gold, platinum and zinc nanoparticles, decorated with organic or inorganic nanocomposites, exhibiting interactive effects towards target analysis (Ahmadi *et al.*, 2019). One of the unique properties of silver nanoparticles is that when interacting with photon of visible light, they exhibit a surface plasmonic resonance (SPR) peak which is sensitive together with line width to the size and shape of metal nanoparticles, with height giving information about metal nanoparticles concentration (Aziz *et al*., 2017). Silver nano material which involves silver nanoparticles on the surface of household appliances was created and marketed by Sumsung (Rashid *et al*., 2013). The main advantage of metal nanoparticles is that its dimension can be controlled by modified optical, structural, and electronic properties without changing the chemical composition (Aziz *et al*., 2017).

Silver nanoparticles synthesis have become a leading part of many technological and scientific developments. Several methods including use of microorganisms and plants have been applied in the reduction of silver precursor forming silver nanoparticles, whose reaction time is long (Huang *et al.*, 2016). The processing regimes for silver nanoparticles include classical Turkevich preparation of metal colloids, reversed micelle process, photo-reduction, ultrasonic

radiation, microwave irradiation (Yin *et al.*, 2003). The photochemical, electrochemical, laser ablation, laser irradiation, γ-radiation (Sileikaite *et al*., 2006; Pillai *et al.*, 2004; Soliwoda *et al.*, 2017), chemical reduction of silver ions with or without stabilizing agent (Kim *et al.*, 2006; Sileikaite *et al*., 2006) are other synthesis methods for silver nanoparticles. The use of these methods leads to various shapes such as spherical, hexagonal, octahedral, cubic, tetrahedral, wire, disc, coaxial cable, triangular mark, triangular prism, and belt shapes of silver nanoparticles (Kim *et al.*, 2006). Polyol method which involves the dissolution of the stabilizer or protecting agent in a polyol medium, produces high monodispersity spherical silver nanoparticles (Kim *et al.*, 2006). However, the chemical method which involves reduction of silver nitrate by trisodium citrate dihydrate is the most popular method which is also chosen in this study due to its simplicity and availability of apparatus required. This method requires use of purified apparatus and reagents such as glassware, water, to remove any foreign substances that might interfere during the synthesis. The two major steps of chemical reduction method include reduction step and stabilization step (Soliwoda *et al.*, 2017). Sodium borohydride and alcohols are other widely used reducing agents for metal nanoparticle synthesis (Pillai *et al.*, 2004). Polymer and organic molecules serve a stabilizing role by binding to the surface of a particle (Pillai *et al.*, 2004), while citrate serve both as a reductant and stabilizer in the chemical reduction of silver (Pillai *et al.*, 2004; Soliwoda *et al.*, 2017). Citrate, which is a weak reducing agent, but strong complexing stabilizer does not allow the control of silver nanoparticles morphology (Soliwoda *et al.*, 2017). It is used as a reducing agent because it's easier to remove it from synthesized silver nanoparticles by washing compared to other stabilizers such as surfactants and ionic polymers which then affect physiochemical properties of the produced nanoparticles (Yin *et al.*, 2003). The growth process can be controlled by the choice of stabilizer, thus making it possible to manipulate the size and shape of the metal nanoparticles. The reduction of silver nitrate with sodium citrate leads to broad sized silver crystallites with variety of shapes compared to other methods (Pillai *et al.*, 2004; Soliwoda *et al.*, 2017). The affinity of citrate ion is greater for silver nanoparticles. Citrate also facilitates photoconversion of silver nanospheres into triangular nanoprism. The exact role of sodium citrate towards the growth of particle can be investigated using pulse radiolysis, γ-radiolysis (Pillai *et al.*, 2004). In pulse radiolytic studies, citrate ions complexes with positively charged Ag_2^+ dimers thus influence the particle growth. The citrate reduction method is unique due to the slow growth of crystal because of silver surface interacting with citrate ion compared to other synthetic methods (Pillai *et al.*, 2004).

The reaction conditions that the morphology and size distribution of metallic particles synthesized by reduction of metallic salts in solution depends on are the time, temperature, concentration, homogeneous and heterogeneous nucleation, molar ratio of metallic salt and reducing agent, type and presence of protective agents, mode and order of reagents addition, degree, and type of agitation (Kim *et al.*, 2006). An increase in temperature leads to an

increase in particle size and rapid nucleation in a short period of time resulting to monodisperse metal particles (Kim *et al.*, 2006). The shape and size control of silver nanoparticles is still a challenge (Sileikaite *et al*., 2006). However, Soliwoda *et al.* was able to control the size and shape of silver nanoparticles using citrate and tannic acid in one synthesis of chemical reduction. Bacterial and fungal strains can be employed in the synthesis of silver nanoparticles to decrease the toxic metal ions into stable metals. AgNPs can also be synthesised intracellular or etracellularly by fungi and with the use of Actinomyecete isolate from the soil (Narasimha *et al.*, 2013). The preparation of silver nanoparticles may involve reduction of silver nitrate in polyvinyl pyrrolidone (PVP) aqueous solution using glucose as the reducer and sodium hydroxide as a catalyst (Wang *et al.*, 2005).

Nanoparticles may be stabilised electrostatically by the presence of free electron pairs in the carbonyl group and with metallic atoms that have free acting as a coordination agent (Soliwoda *et al.*, 2017). The main advantage of using citrate in chemical reduction method is the nanoparticle functionalisation possibility which is due to the weak interaction of citrate molecules with metal surfaces which can then be easily exchanged with other compounds (Soliwoda *et al.*, 2017).

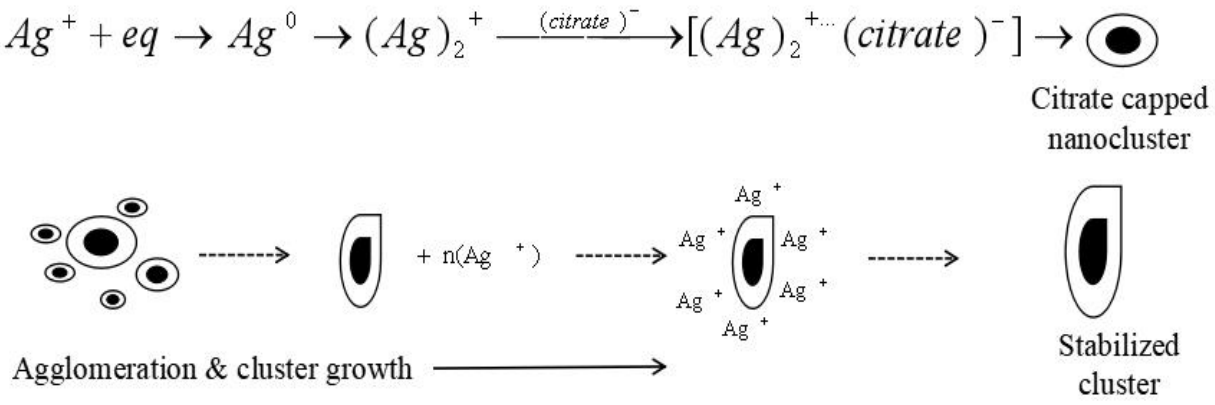

Scheme 3.1: Primary and secondary growth step of AgNPs formation.

Metal nanoparticles such as silver and platinum have been widely used to functionalise nanoclays forming nanocomposite with improved properties (Nazir *et al.*, 2016). Nanocomposites can be classified as ceramic matrix, metal matrix and polymer matrix nanocomposites. The mostly applied nanocomposites are polymer which have good physical and chemical properties, which could be due to the shape, size, concentration, and interaction of the incorporated nanoparticles with the polymer matrix (Saba *et al.*, 2016). Methods such as extrusion, in-situ, melt-intercalation, direct mixing, and casting have been implemented in the production of nanocomposites (Nazir *et al.*, 2016). Others include rapid solidification process, microwave synthesis, complex polymerized, chemical vapour deposition, hydrothermal, template, sol-gel, and high energy ball milling process (Saba *et al.*, 2016). Silver nanoparticles and nanocomposites can be characterised with techniques listed in table 3.1.

This is done to define the properties of the substance or material, and to eliminate some variables from the investigation before conducting a more intensive study of a particular substance.

Table 3. 1: Characterisation techniques for silver nanoparticles and their composites.

Method	Technique	Nature of sample for analysis
Spectroscopic	FTIR	Solid/liquid
	UV-Vis	Liquid
	XRD	Solid/Liquid
Microscopic	TEM	Solid/Liquid
	SEM	Solids
Electrochemical	CV	Liquid
	DPV	Liquid
	SWV	Liquid

***See glossary for abbreviations**

3.2 Experimental

3.2.1 Reagents and Materials

Silver nitrate, $AgNO_3$, trisodium citrate dihydrate (TSC), $Na_3C_6H_5O_7.2H_2O$, the nanoclay hydrophilic bentonite (PGV) and surface modified nanoclay (1.44P) were bought from Sigma Aldrich, UK and used without purifying further. Milli-Q water from the Millipore system was used throughout the experiment.

3.2.2 Synthesis of silver nanoparticles

A solution of 10 mM silver nitrate was heated to boil in a beaker for 15 minutes with constant stirring at 240 ℃, 265 rpm, followed by the dropwise addition of 5 mM trisodium citrate dihydrate. The solution was stirred continuously for another 15 minutes with magnetic stirrer while boiling until the solution turned greyish yellow. The solution was then removed from the hot plate and cooled at room temperature and the nanoparticles were separated by centrifugation using Milli-Q water for purification. The same procedure was followed for the preparation of silver nanoparticles with 10, 50, and 100 mM sodium citrate dihydrate.

$$4Ag^{+} + C_6H_5O_7Na_3 + 2H_2O \rightarrow 4Ag^{0} + C_6H_5O_7H_3 + 3Na^{+} + H^{+} + O_2 \uparrow .....eq\ 1$$

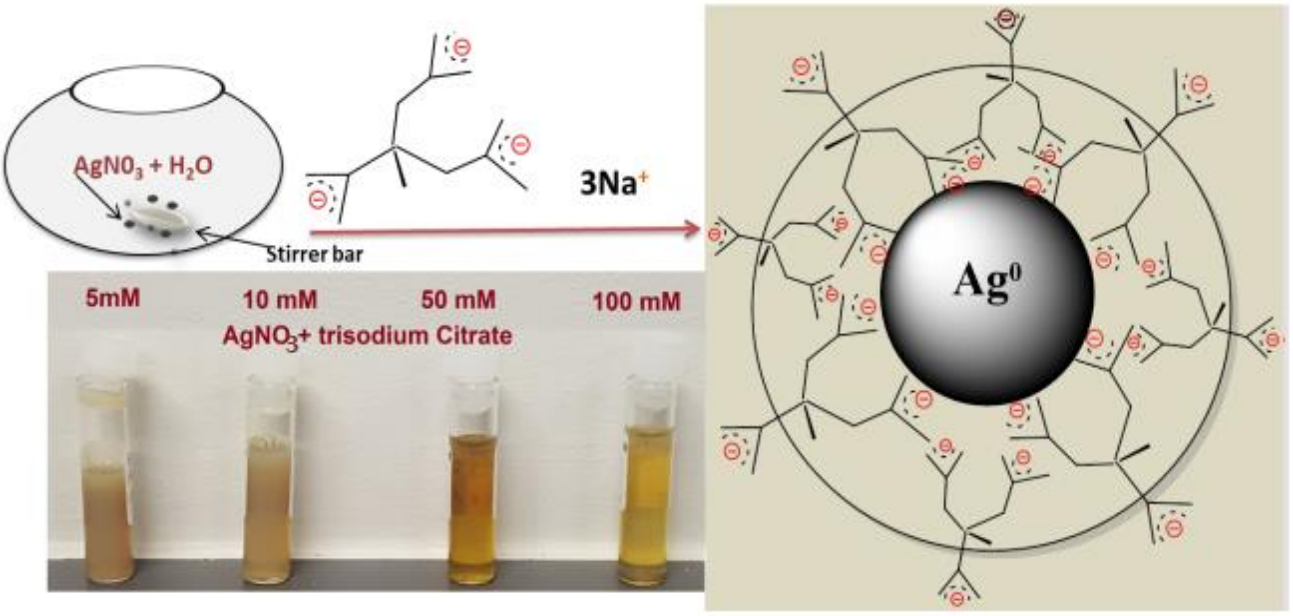

Figure 3.1: AgNPs formation by chemical reduction of $AgNO_3$ using different concentrations of reducing agent tri-sodium citrate and changes in the colour during formation of AgNPs.

3.2.3 Synthesis of silver nanoclay composites

The PGV nanoclay silver composites were prepared by adding fractions 0.5 g, 1 g, and 1.5 g of PGV in different solutions of equal volumes of 10 mM silver nitrate solution. The mixtures were heated to boil while stirring for 20 minutes at 240 ℃, 265 rpm, followed by the dropwise addition of 0.1 M solution of trisodium citrate dihydrate. The mixtures were heated for another 15 minutes and cooled at room temperature. The products were cleaned several times with Milli-Q water through centrifugation. The same procedure was followed for the preparation of 1.44P nanoclay silver composites.

3.2.4 Characterisation

3.2.4.1 Ultraviolet visible characterisation

The absorbance of silver nanoparticles was determined using ultraviolet visible (UV-Vis) SPECTROSstar Nano (BMG LabTech) at a wavelength ranging from 200 nm to 800 nm. The UV analysis for silver nanoclay composites could not be performed due to the UV technique which only measures liquids. However, there are other techniques implemented in the study for further evaluation of the interaction of AgNPs with nanoclay.

3.2.4.2 Fourier transform infra-red characterisation

FTIR was used to confirm the complex formation between trisodium citrate dihydrate and silver nitrate. The characterisation of silver nanoparticles was done using Perkin Elmer spectrometer (USA) between the wavenumber 3700 cm^{-1} to 700 cm^{-1}. Firstly, the sample holder and the presser were cleaned with acetone and the background noise was measured to eliminate interfering substances. The samples, depending on their nature (solid or liquid), were scanned by compressing them onto the sample holder and the spectrums were recorded.

3.2.4.3 X-ray diffraction

Measurements were performed using a multipurpose X-ray diffractometer D8-Advance from BRUKER AXS (Germany), operated in a continuous scan in locked coupled mode with Cu-Kα radiation. The samples were mounted in the centre of the sample holder on a glass slide and levelled up to the correct height. The measurements scanned within a range in 2-theta, with a typical step size of 0.034° in 2. A position sensitive detector, Lyn-Eye, was used to record diffraction data at a typical speed of 0.5 sec/step which is equivalent to an effective time of 92 sec/step for a scintillation counter.

3.2.4.4 Scanning Electron Microscopy

The size distribution and morphology of silver nanoparticles and silver nanoclay composites were analysed with FEI Nova NanoSEM (Netherlands) using an Oxford X-Max detector and INCA software (UK). SEM images were taken with the Tescan MiraGMU SEM (Czech Republic) and analysed by image J, java-based image processing program. The size distribution was investigated statistically by measuring the diameter of random nanoparticles.

3.2.4.5 Electrochemistry

The Autolab PGSTAT 101 (Metrohm, South Africa) was implemented for electrochemical measurements in software NOVA 2.1. The measurements were carried out at room temperature (25 °C) using a three-electrode system that consists of glassy carbon electrode (GCE) as a working electrode (A = 0.071 cm^2), platinum wire (3 mm diameter) as counter electrode and Ag/AgCl (3 M KCl) as the reference electrode. The cleaning of the working electrode was done with alumina slurry of 1.0, 0.3 and 0.05 µm on a polishing pad, followed by 5 min sonication of GCE in water and ethanol between polishing steps. The modification of GCE was prepared by dropcoating the silver nanoparticles or silver nanoclay composite on the working electrode and left to dry for 2 hours, forming GCE/Ag and GCE/Ag/1.44P. Electrochemical measurements were achieved in 3 mℓ solution of 0.1 M HCl supporting electrolyte which was degassed for one minute before measuring.

3.3 Results and discussion

The silver nanoparticles produced by chemical reduction method were greyish yellow as represented above in figure 3.1, which agrees with the previous literature (Goulart *et al.*, 2018). Scheme 3.2 shows a proposed mechanism for the formation of yellowish AgNPs, implying that the presence of van der Waals forces between the positive charge of Ag+ and the oxygen of the citrate increase the reducing and stabilizing efficiency of citrate for the surface of the AgNPs. These were further investigated by different spectroscopic and electrochemical techniques, together with their corresponding nanoclay composites.

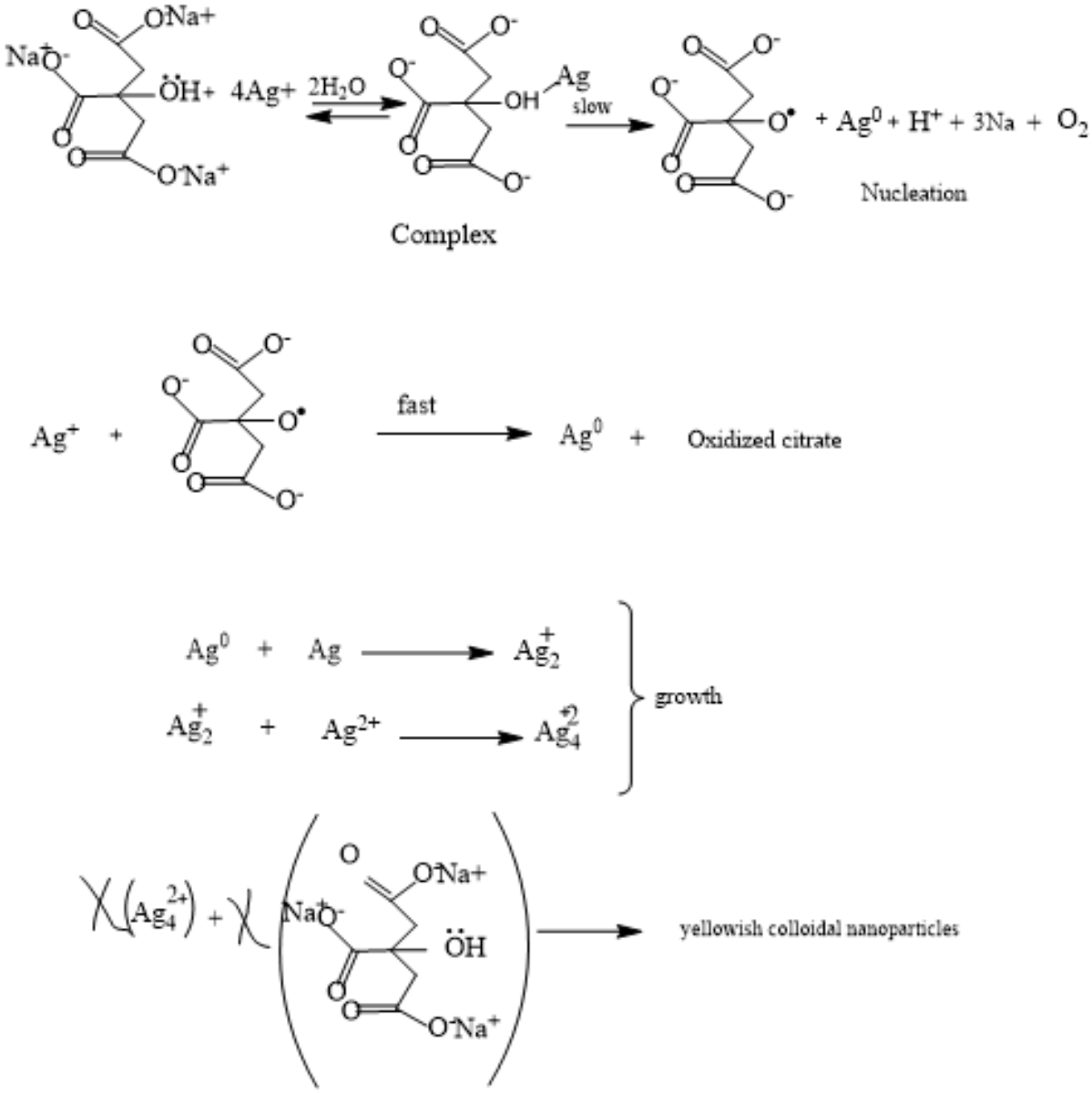

Scheme 3.2: The formation of colloidal AgNPs using silver nitrate precursor.

3.3.1 Ultraviolet visible characterisation of silver nanoparticles

A synthesis of four silver nanoparticles with different concentrations (5, 10, 50, and 100 mM) of trisodium citrate was successfully conducted and the UV spectra obtained is shown in figure 3.2.

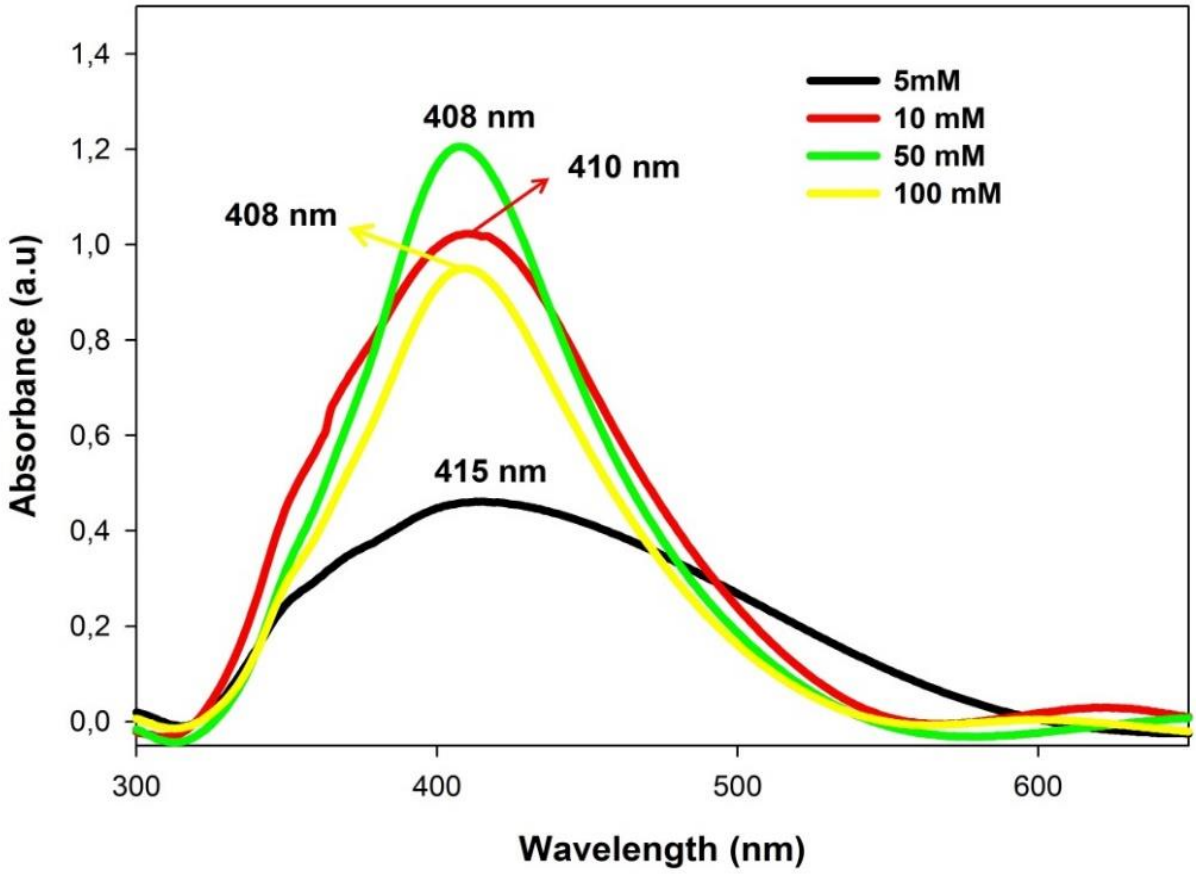

Figure 3.2: Silver nanoparticles with different reducing agent concentrations.

The greyish yellow colour change of the solution observed indicated the reduction of silver ions as the concentration of the citrate ions increased in the solution (Goulart *et al.*, 2018). AgNPs exhibited broad surface plasmon bands of 404, 410, 408 and 408 nm, which comply with the literature where they are expected to form between 400 nm and 450 nm, indicating the AgNPs formation of local surface plasmon resonance (LSPR) (Rashid *et al*., 2013; Soliwoda *et al.*, 2017; Viani *et al*., 2021). This is due to the wide dispersity of particle size and shape (Pillai *et al.*, 2004), and as a result of surface plasmon-oscillation modes of conducting electrons coupled to external electromagnetic fields through the surface (Sileikaite *et al*., 2006). The LSPR absorption bands are also due to the free metal nanoparticle electrons in which their vibration is combined in resonance with the light wave (Soliwoda *et al.*, 2017). AgNPs with 5 and 10 mM citrate showed single unsymmetrical broad SPR bands while 50 and 100 mM showed only single symmetrical band which is an indication of spherical nanoparticles. This is supported by Mie's theory which states that only a single band is expected in the absorption spectra of spherical nanoparticles that indicate electrons oscillate, only on one main axis

(Acharya *et al*., 2018). The broadening of the SPR bands at 5 and 10 mM towards longer wavelength which is known as red shift, is an indication of various shaped and sized nanoparticles (Narisimha *et al.*, 2013; Sohrabnezhad *et al*., 2015). The LSPR band blue-shifted from 410 nm to 408 nm for 50 and 100 mM due to the decrease in size when the concentration of the reducing agents was increased, which agrees with the SEM statistical analysis that will be discussed in the chapter. Nonetheless, 50 mM produced AgNPs with absorbance greater than 1 a.u, thus 100 mM AgNPs were used further in the study to functionalise the nanoclays forming composites.

3.3.2 FTIR characterisation of silver nanoparticles

The data in figure 3.3 represents the spectra of silver nanoparticles and trisodium citrate dihydrate which was used as the reducing agent. When the two spectrums were compared, silver nanoparticle spectrum displayed the stretching vibration of the hydroxyl (OH) group at 3251 cm^{-1}. However, the small absorption in the region of O-H for trisodium citrate dihydrate might have been due to the impurities. The carbonyl group (C=O) for silver nanoparticles was observed at 1627 cm^{-1} which slightly shifted towards a greater wavenumber from the carbonyl group of trisodium citrate dihydrate observed at 1582 cm^{-1}, which indicates that a chemical reaction has taken place.

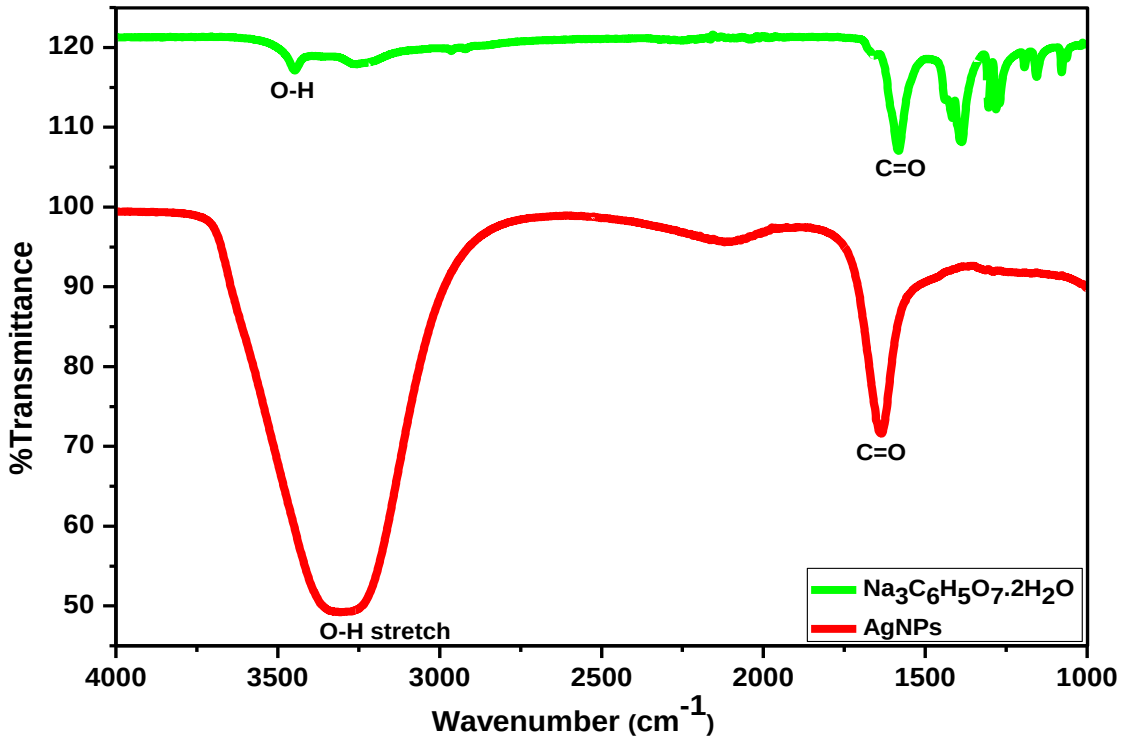

Figure 3.3: FTIR spectra of trisodium citrate dihydrate and silver nanoparticles.

3.3.3 X-ray diffraction characterisation of silver nanoparticles

The crystalline nature of AgNPs was confirmed with XRD spectroscopy. Silver nanoparticle XRD spectrum falls within the 2θ range of 20° to 80° and four diffraction peaks at 38°, 44°, 64° and 78° which corresponds with 111, 200, 220 and 311 were observed in figure 3.4 which complies with the literature (Zhao *et al.*, 2019; Hassan *et al.*, 2021). The high intense peaks are evident when 5 mM (a) TSC reducing agent is used compared to when the concentration of reducing agent is increased. However, the XRD pattern for 100 mM (d) TSC show better diffraction peaks compared to 10 mM (b) and 50 mM (c) TSC silver nanoparticles. The enhanced peak intensity suggests smaller sized crystal that supports the role of citrate as a capping agent for AgNPs (Chen *et al*., 2020).

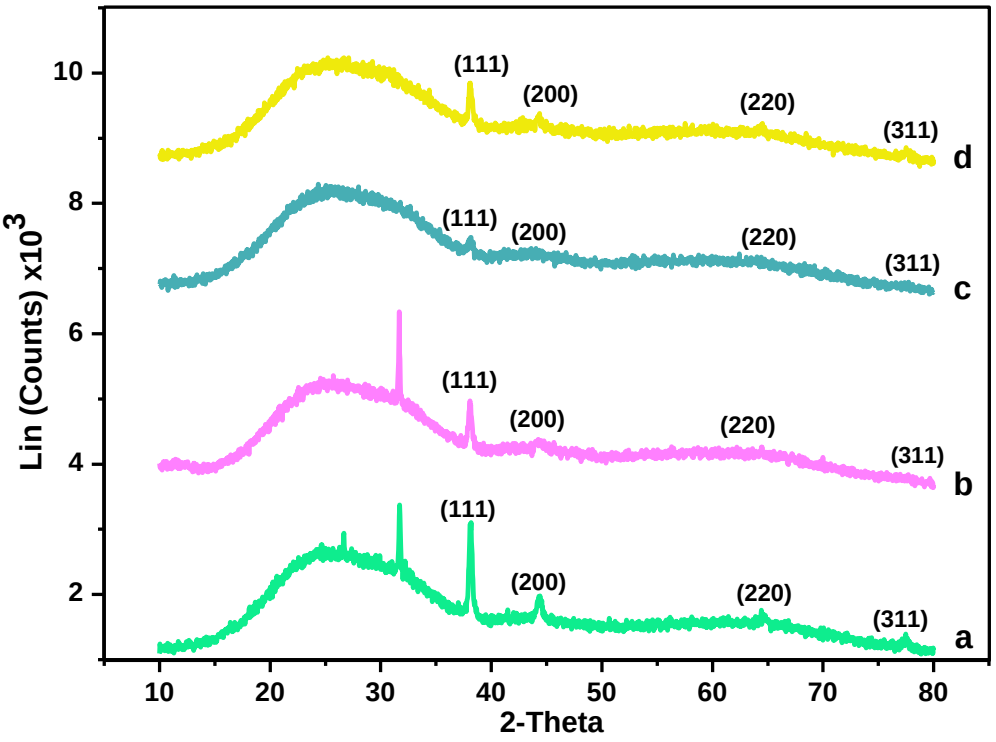

Figure 3.4: XRD spectrum of silver nanoparticles with (a) 5 (b) 10 (c) 50 & (d) 100 mM TSC.

3.3.4 Scanning Electron Microscopy of silver nanoparticles

The SEM images of AgNPs produced by varying TSC reducing agent concentrations are represented in figure 3.5. AgNPs with 5 and 10 mM TSC (figure 3.5 A & B) showed a mixture of well-dispersed AgNPs of different shapes (spherical and nanorods) distributed over the entire surfaces of the sample holder without any substantial aggregation, with an estimated average diameter of 65 nm and 37.5 nm, respectively. The large variety of particle shapes produced at 5 and 10 mM visualized by SEM is also justified by its broader LSPR bands in UV-Vis as previously discussed. An Increased TSC concentration from 50 to 100 mM (figure 3.5 C & D) leads to a decrease in particle size with an average diameter of 22.5 – 17.5 nm.

Although adding more TSC concentration produced smaller AgNPs which is an indication of good sensitivity in comparison to 5 and 10 mM, some evidence of aggregation has been seen, where smaller nanoparticles merged with each other resulting to bigger sized AgNPs which are less distributed, forming clusters and bunches that do not cover the entire surface of the holder (Pillei *et al.*, 2017). The reason might be due to a decrease in the interaction of nanoparticles. These aggregates can have an effect in the homogeneity of the film which is an important issue in the construction of the electrochemical sensors and biosensor. Thus, 10 mM AgNPs were considered as alternative in the fabrication of sensor which will be elaborated in chapter five. Based on figure 3.5, the use of different concentrations of reducing agents leads to different particle sizes, with high concentrations leading to aggregation of AgNPs. The sizes are in order 5>10>50>100 nm which agrees with UV-Vis plasmon bands.

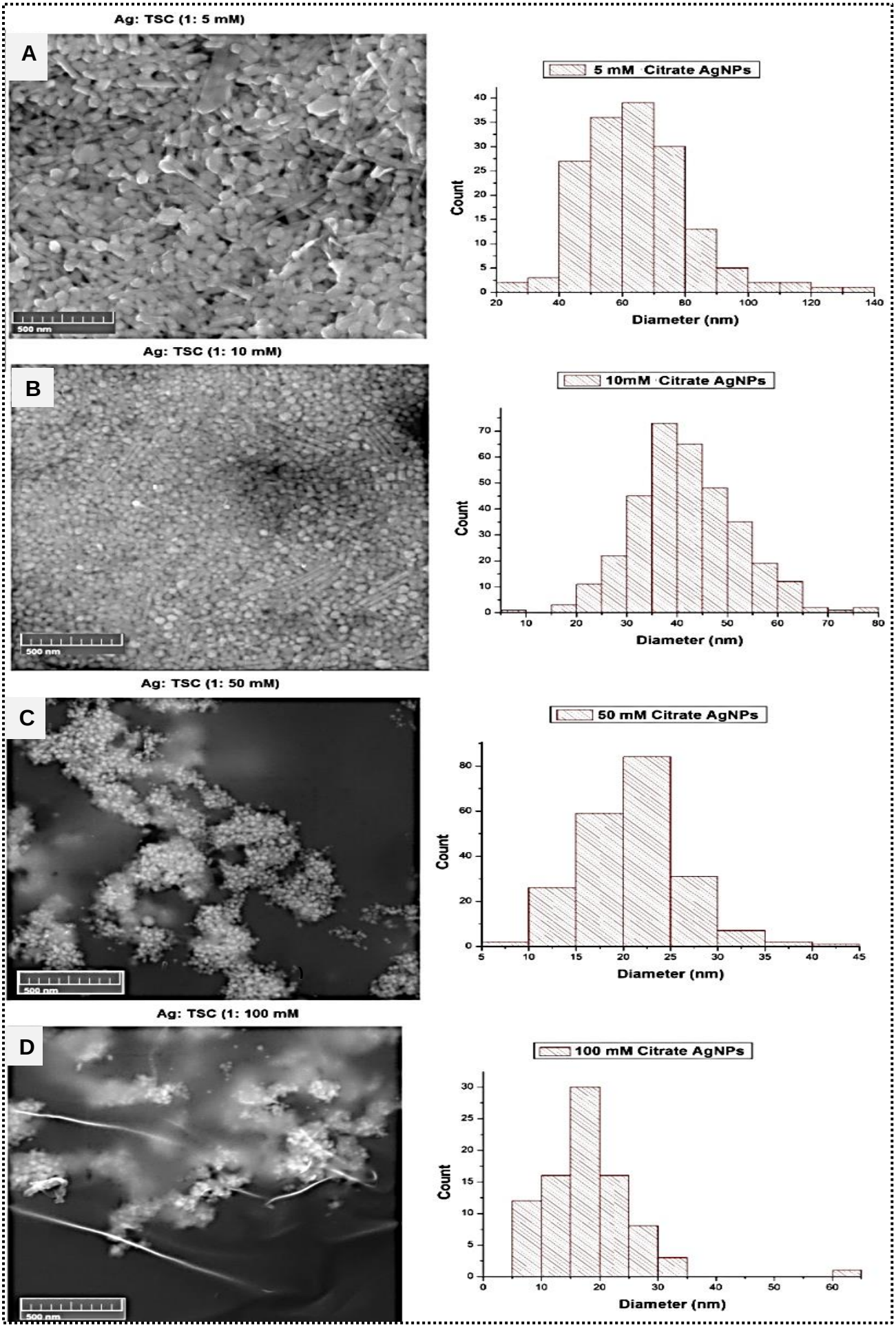

Figure 3.5: SEM images of AgNPs in Ag: TSC ratio of (A) 1:5, (B) 1:10, (C) 1:50, (D) 1:100 mM and corresponding diameter histograms.

3.3.5 Electrochemistry

3.3.5.1 Cyclic and Differential Pulse voltammetry of silver nanoparticles

Figure 3.6 shows the redox potential of CV and oxidation potentials of DPV in comparison of the behaviour of different concentrations of TSC.

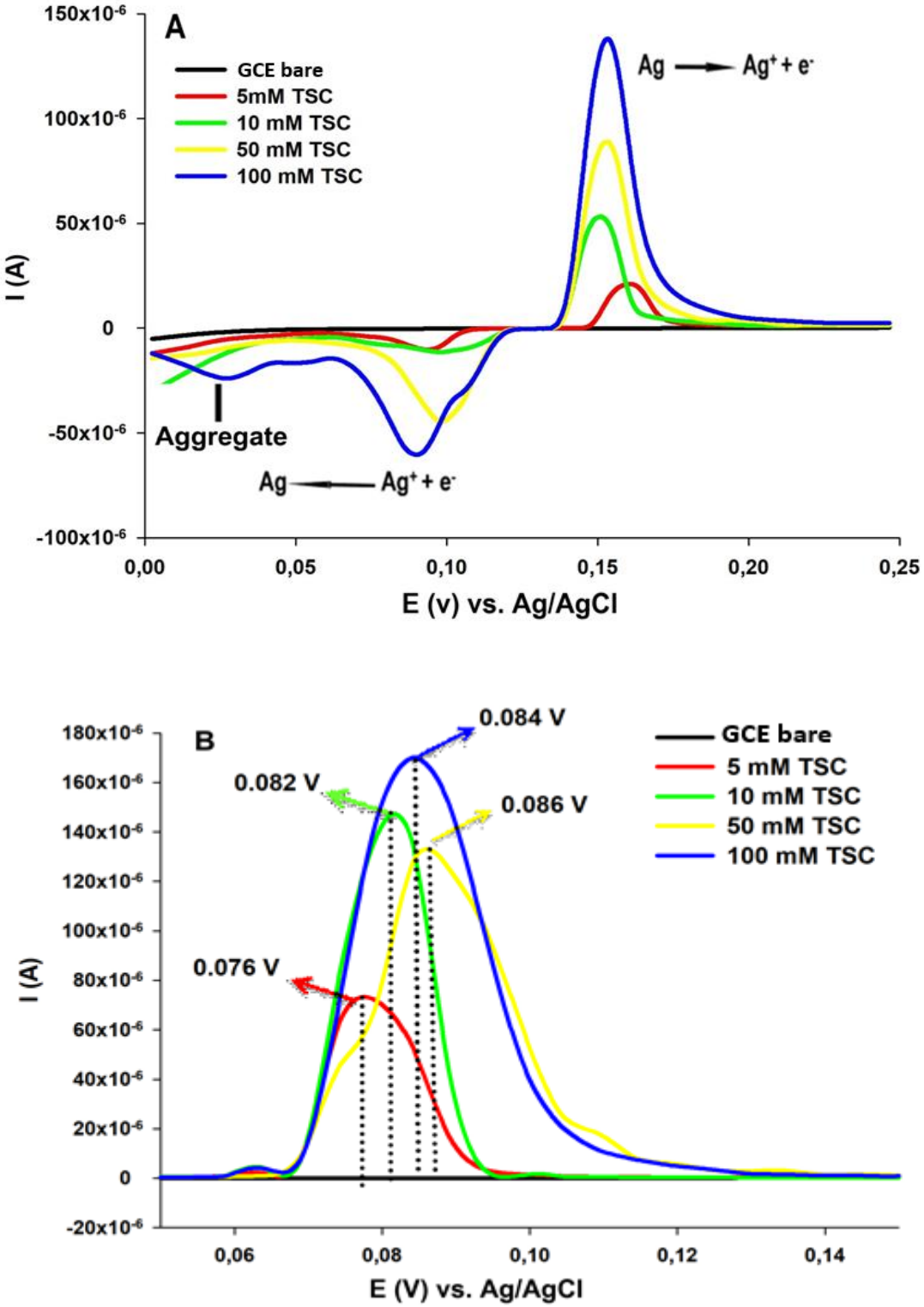

Figure 3.6: (A) Cyclic voltammograms of AgNPs at scan rate 0.1 V/s; (B) Differential pulse voltammograms with parameters: potential step 8 mV, (5 s waiting time and 20 s for current sampling time), pulse amplitude 50 mV, without accumulation step for different TSC.

The oxidation and cathodic peak potentials of AgNPs were observed in the range 0.05 V to 0.2 V, which complies with the literature showing oxidation peak response of silver nanoparticles within that range (Goulart *et al.*, 2018; Eksin *et al.*, 2019). The concentration of TSC affected the recorded redox peak current, as can been seen by shift in peaks in CV especially in 5 and 10 mM concentrations (figure 3.6 A). Stable and prominent oxidation signals were observed in CV at TSC concentration 50 and 100 mM, and their reduction products shifted cathodically. Theoretical and the most experimental studies proved that the radius of metal nanoparticles decreases with its oxidation potential (Brainina *et al.*, 2011; Mainali *et al.,* 2021). That is, oxidation potential shifting cathodically depicting smaller nanoparticle sizes, due to greater exposed surface area compared to larger ones. However, a quite different situation from DPV (figure 3.6 B) was encountered when the positive shift appeared in all the concentrations of the reducing agent.

It is apparent that the oxidation peaks in all concentrations are attributed to Ag^+ ions and the reduction peaks are associated with a reduction of Ag^+ to Ag^0. Based on oxidation potentials, the size of the nanoparticle or if aggregates have occurred was determined. According to the literature, as the nanoparticle sizes decrease, peak potentials move to more negative potentials (Mainali *et al.,* 2021). The differences between anodic and cathodic peak potentials, ΔE_p for each cyclic scan is determined and shown in table 3.2.

Table 3.2: Silver nanoparticle potentials with changes in concentration of sodium citrate using anodic peak data.

[TSC] mM	E_{pa} (V) $x10^{-1}$	E_{pc} (V) $x10^{-2}$	ΔE_p (V) $x10^{-2}$	n	I_{pa} (A) $x10^{-5}$	I_{pc} (A) $x10^{-6}$
5	1.59	9.00	6.90	0.71	2.10	-9.50
10	1.49	9.00	5.90	0.76	5.20	-9.80
50	1.51	9.50	5.60	0.75	8.70	-41.50
100	1.51	8.50	6.60	0.75	13.40	-55.70

The values acquired indicate quasi-reversible one-electron redox process for all the synthesised AgNPs, where the peak-to-peak separation (ΔEp) is equal or close to 0.059 V (Van der Horst *et al.*, 2015; Elgrishi *et al.*, 2018; Okumu *et al.*, 2020). A shift in the anodic peak from 0.149 V (10 mM TSC) towards more positive potential 0.151 V (50 & 100 mM TSC), indicates larger sized molecule (Zhao *et al.*, 2019), that might be possibly related to aggregation as indicated in the voltammogram (figure 3.6 A), confirmed by varying the scan rates, which are detailed in chapter 4. These agrees with the UV and SEM results as discussed previously, where AgNPs aggregates in 50 and 100 mM TSC concentration.

Based on the information obtained in voltammetry measurement, the presence of higher concentration (50 and 100 mM) of the reducing agent formed aggregates with large AgNPs sizes compared to smaller concentrations. The aggregation processes rarely occur alone and always concurrently take place with oxidation and dissolution (Piella *et al.*, 2017; Li *et al.*, 2010). The first scenario of aggregation could be caused by oxygenated conditions during the drying process, which leads to AgNPs liberating Ag^+ ions as represented in figure 3.7 (Piella *et al.*, 2017). This could be due to Ag-citrate bonds losing stability and the nanoparticles interact with each other to form aggregates.

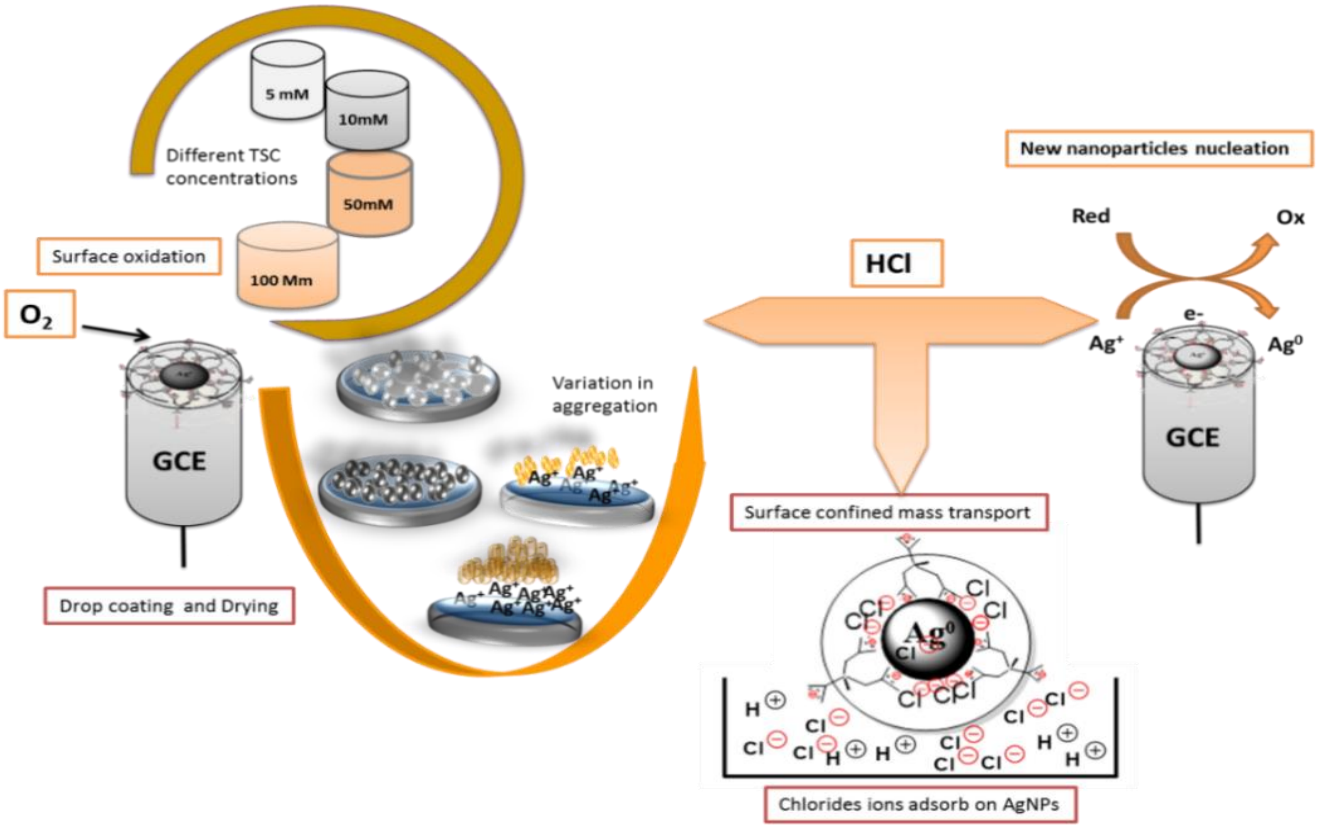

Figure 3.7: The proposed pathway for new nanoparticle formation from parent AgNPs on a GCE.

The second scenario was introducing HCl as an electrolyte solution; this might also be responsible for the formation of aggregates and AgCl layer according to the following reaction:

$$4Ag^+ + 4Cl^- + O_2 \rightarrow 2AgCl + 4OH^- \quad \ldots\ldots eq\ 3.1$$

$$AgCl + e \rightarrow AgNPs + Cl^- \quad \ldots\ldots eq\ 3.2$$

According to the mechanism, HCl ions displace citrate from the surface, thus disrupt the charge layer of the AgNPs allowing the AgNPs to aggregate. When Ag^+ that are liberated to the bulk and Cl^- ions interact, AgCl spontaneously formed which accelerate the oxidation of Ag (Li *et*

al., 2010). As the Ag^+ ions dissolve in electrolytes solution, the rest of aggregated nanoparticles lose electrical contact with the electrode, and the remaining nanoparticles inside the aggregates are not oxidized (Piella *et al.*, 2017).

In addition to the spectra and voltammograms, the half full-width height maximum (FWHM) was plotted in correlation to the SEM particle sizes response over the reducing agent concentration. The graph is represented in figure 3.8, the particle sizes are displayed in black.

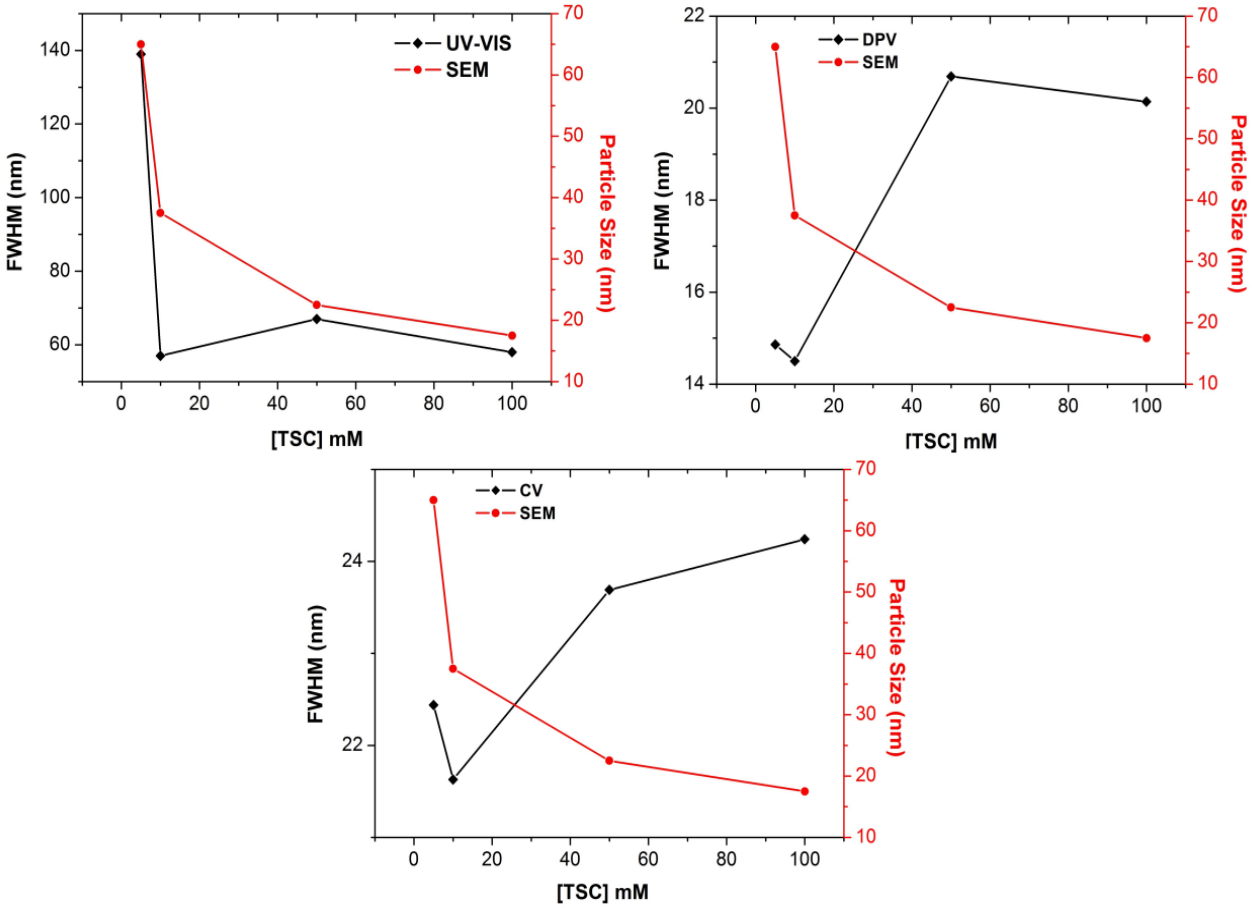

Figure 3.8: The full width at half maximum (FWHM) and particle sizes as a function of the reducing agent concentration.

Generally, the larger molecules would result in bigger red shift and broader FWHM. It is evident that in all the methods used in this study, FWHM follow the same trend with the exception of CV results at 100 mM. If 100 mM in CV can be neglect, a correlation in all these results can be observed. Notable in all these methods, 10 mM reducing agent has shown a minimum value of FWHM indicating the narrowest size distribution. By analysing the FWHM of the UV- VIS, the values show polydispersity and have a large size distribution. The size dependence of the band gap is the most identified aspect of quantum confinement (Movlarooy, 2018). In semiconductors the band gap increases as the size of the particles decreases (Edvinsson, 2018; Movlarooy, 2018). Band gaps also increased with increasing reducing agent concentration as shown in table 3.3.

Table 3.3: The experimental particle sizes of AgNP analysed by electrochemical methods and UV-Vis spectra of different concentration of TSC (n = 3).

Ag: TSC Molar ratio	λ (nm)	Band gap (eV)	FWHM (UV-VIS) (nm)	FWHM (DPV) (mV)	FWHM (CV) (mV)	Particle size (SEM) (nm)
1:5	415	2.99	139	14.90	22.40	65.0 ± 0.75
1:10	410	3.03	57	14.50	21.60	37.5 ± 0.56
1:50	408	3.04	67	20.70	23.70	22.5 ± 1.85
1:100	408	3.04	58	20.10	24.20	17.5 ± 2.12

This increase in the band gap may be due to a decrease in the size of the nanoparticles which is expected since the surface to volume ratio increases for smaller particle sizes. Based on these results, it can be concluded that different concentration of the reducing agent strongly affects the particle sizes, high concentrations resultants to smaller nanoparticle that aggregates to form clusters and bunches at a later stage while small concentrations produced larger nanoparticles. It is confirmed that small nanoparticles are sensitive towards aggregation of the reducing agent strongly affect the particle sizes.

3.3.6 FTIR characterisation of silver nanoclay composites

The comparison between the spectrum of pure nanoclay hydrophylic bentonite (PGV), nanoclay surface modified (1.44P) and that of silver nanoparticles (AgNPs) was done to see the difference in peaks which confirmed successful formation of silver nanoclay composites as shown in figure 3.9.

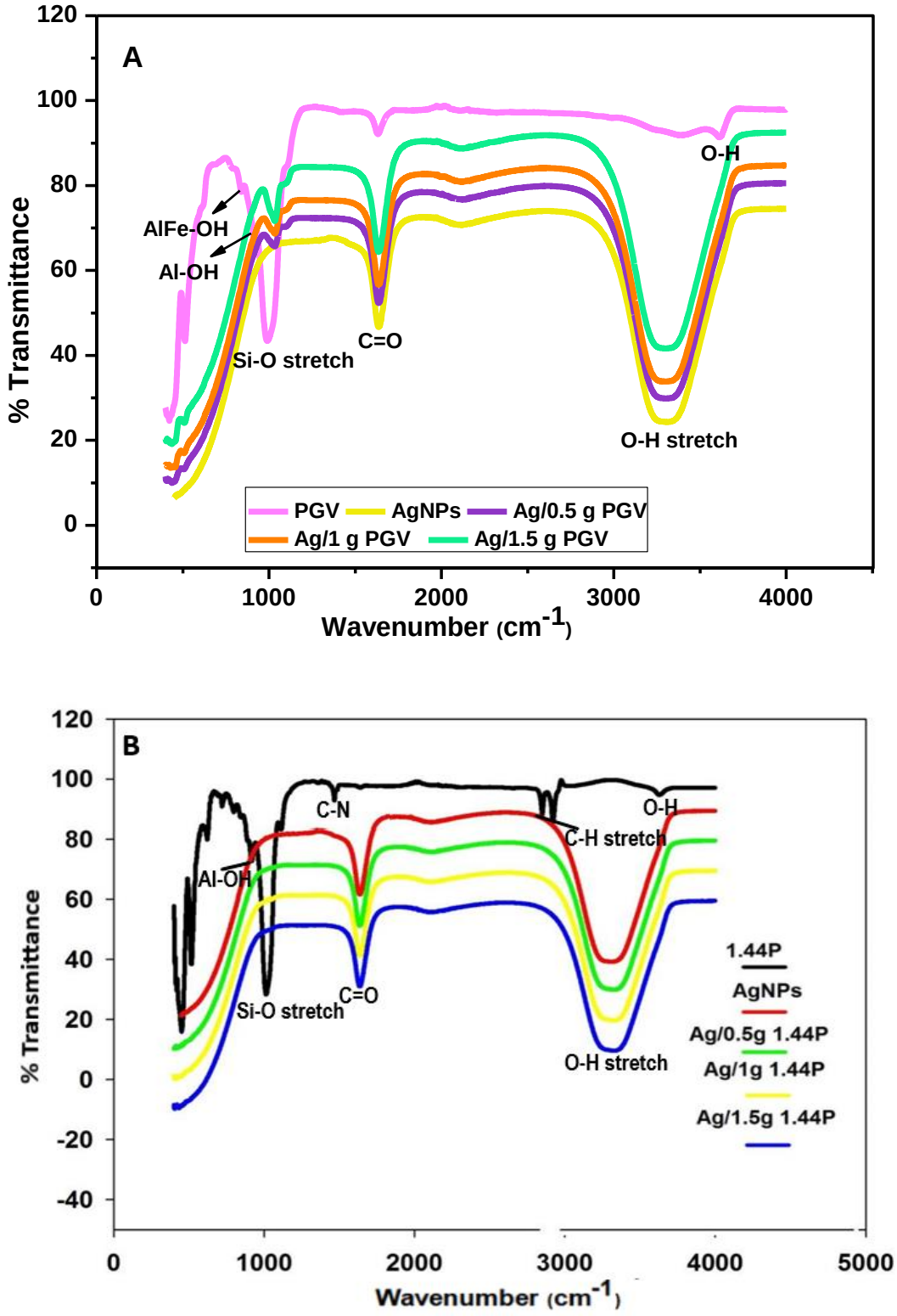

Figure 3.9: FTIR spectra of A (PGV nanoclay, AgNPs, PGV/Ag); B (1.44 nanoclay, AgNPs, 1.44P/Ag). Insert: A (Silver nanoclay composites (Ag/0.5g, Ag/1g, Ag/1.5g PGV).

The fractions 0.5 g, 1 g, and 1.5 g of both PGV and 1.44P were functionalised with silver to form composites Ag/0.5 g, Ag/1 g and Ag/1.5 g PGV and 1.44P. The FTIR spectra shows Al-OH and Si-O functional groups for both clays. The pure 1.44P nanoclay in figure 3.9 (B) shows absorption bands at 2800 cm^{-1} and 2900 cm^{-1} which is due to the C-H group that is not present

in PGV clay spectrum in figure 3.9 (A). The O-H stretch in both clays and the absence of C-H group in the spectra of composites for 1.44P is proof that there is a reaction that took place. The OH molecule involves hydrogen bonding between different molecules having instantaneous arrangements which leads to broad O-H stretching absorption for both spectra (A & B) (Wade, 2006). The small absorption band beyond 3000 cm^{-1} for both 1.44P and PGV pure nanoclays might have been confused with O-H absorption band which is said to appear as broad always (Wade, 2006). Therefore, these small absorption bands could be due to impurities of the nanoclays. The C=O intense infra-red stretching absorptions observed around 1600 cm^{-1} in both spectra (A & B) is due to the large dipole moment (Wade, 2006). The strong Si-O stretching absorption in 1000 cm^{-1} for pure 1.44P and PGV nanoclays can be observed, which is then found in silver nanoclay composites for both clays indicating successful functionalisation of nanoclays with silver. It is evident in figure 3.9 (A) that PGV nanocomposites produced better absorption bands for Si-O which becomes more visible as the concentration of the PGV nanoclay was enhanced due to its hydrophilic nature, compared to 1.44P nanocomposites (B). The poor Si-O absorption band for 1.44P nanocomposites could be due to the hydrophobic behaviour of 1.44P nanoclay which prevented it from dissolving well in silver nitrate solution. Table 3.4 summarises the functional groups present in the spectrums.

Table 3.4: Interpretation of FTIR spectra of the synthesised material.

Functional group	**AgNPs** cm^{-1}	**Type of nanoclay** cm^{-1}		**All silver nanoclay Composites** cm^{-1}	
		PGV	**1.44P**	**Ag/1.44P**	**Ag/PGV**
OH	3400	3600	3600	3400	3400
CH	–	–	2800 & 2900	–	–
C=O	1600	1600	1600	1600	1600
C-N	–	–	1400	–	–
Si-O	–	1000	1000	_	1000
Al-OH	–	800	800	–	–
AlFe-OH	–	700	–	–	–

3.3.7 X-ray diffraction characterisation of silver nanoclay composites

The XRD spectrum of silver nanoclay composites in figure 3.10 shows diffraction patterns within the 2θ range of 20° to 80°.

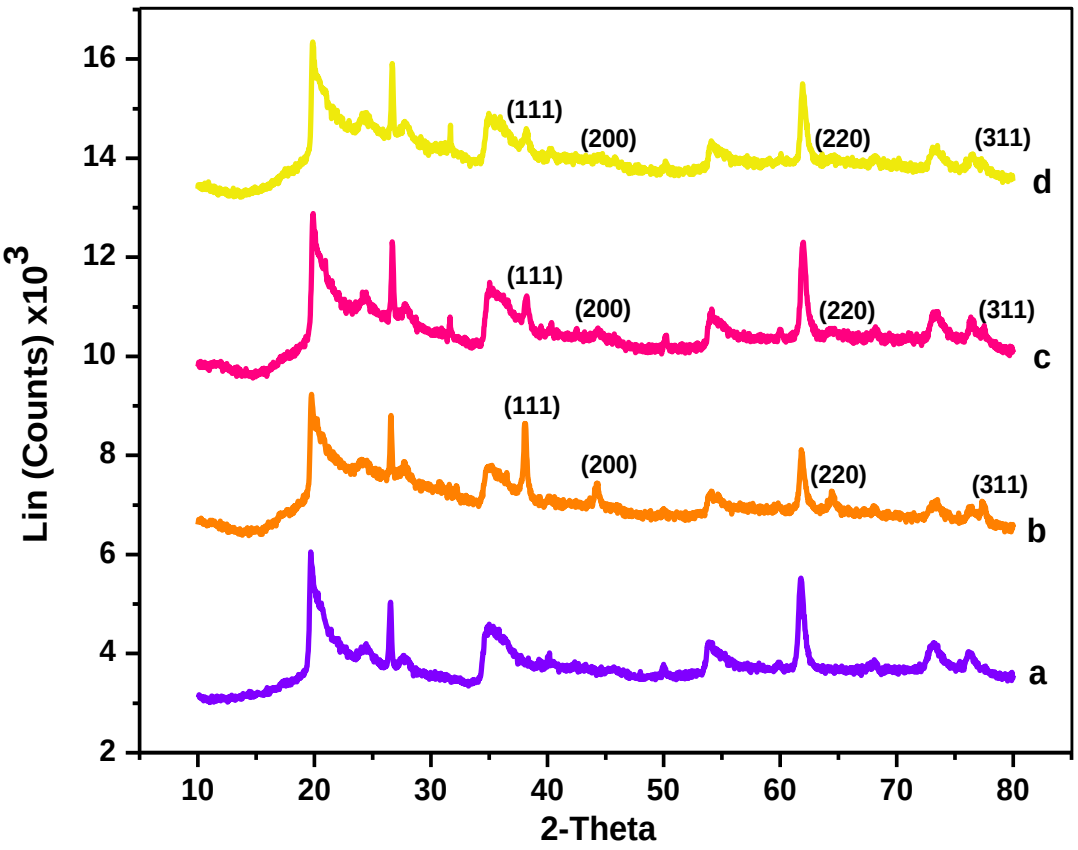

Figure 3.10:XRD spectrum of 1.44P nanoclay (a) Ag/1.44P composites with (b) 0.5 (c) 1 & (d) 1.5 g nanoclay.

Four of these found at 38°, 44°, 64° and 78° which corresponds with 111, 200, 220 and 311 are associated with silver as supported by the literature (Hassan *et al.*, 2021), which decreases with enhanced nanoclay concentration from 0.5 g (b), 1 g (c) and 1.5 g (d) 1.44P nanoclay. In comparison with XRD spectrum of silver nanoparticles with 100 mM TSC that was used to functionalise the nanoclay, there has been an incredible increase in the intensity of diffraction patterns of silver in Ag/0.5 g 1.44P composites. The improved peak intensity suggests smaller sized crystal (Chen *et al*., 2020). However, there are also diffraction patterns observed which could not be observed in the XRD spectrum of silver as previously discussed but are found in the sprectrum of 1.44P nanoclay (a). These include peaks at 22°, 24° and 26° which seem to be stable with improved nanoclay concentration. However, at 32° and 50°, there are diffraction peaks which becomes more visible with increasing nanoclay concentration. There are also peaks at 36°, 55°, 62° and 74° which may be due to increased nanoclay concentration. All these serve as proof that there was an interaction of nanoclay with silver that took place, thus confirming successful functionalisation of nanoclay with silver.

3.3.8 Scanning Electron Microscopy of silver nanoclay composites

The SEM images of Ag/1.44P composites formed by changing nanoclay concentration are represented in figure 3.11.

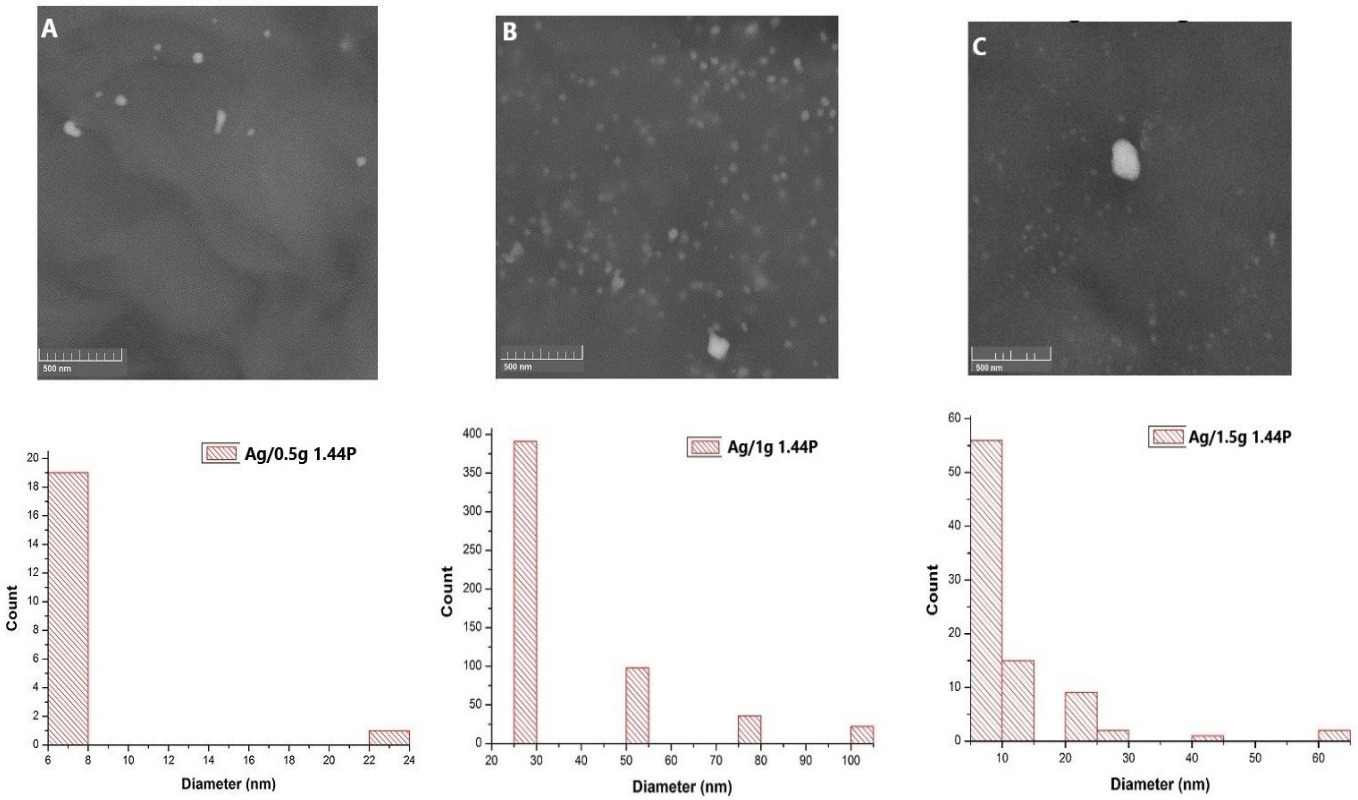

Figure 3.11: SEM images of Ag/1.44P composites with (A) 0.5 (B) 1 & (C) 1.5 g 1.44P and corresponding diameter histograms.

The effect of functionalising nanoclay with AgNPs having 100 mM TSC whose initial average size was 17.5 nm as stated earlier, has led to Ag/1.44P composites of different particle sizes and shapes. The average nanoparticle sizes decreased from that of silver alone. However, Ag/1g 1.44P in figure 3.11 (B) nanoparticles with average size of 27.5 nm which is greater than the size of the silver nanoparticles alone. From the SEM images in figure 3.11, the sizes for Ag/1g and Ag/1.5g 1.44P seem small and well-dispersed. This could be due to the decrease in the concentration of silver as the nanoclay concentration was increased resulting more distribution and good coverage of the sample holder. The same trend was observed in the XRD spectrum discussed previously, where the intensity of silver was reduced with increasing nanoclay concentration. SEM supports the XRD results whose intensity was of Ag/0.5g1.44P was greater suggesting smaller nanoparticle size with good sensitivity compared to other composites. Although Ag/0.5g 1.44P produced smaller nanoparticles of 2.5 nm Ag/0.5g 1.44P in figure 3.11 (A) which suggests good sensitivity, there is high concentration of silver nanoparticles present which had evidence of aggregates as discussed previously, resulting in Ag/0.5g 1.44P having larger molecules due to the smaller sized nanoparticles which combined

causing less distribution and poor coverage of the surface of the sample holder. The sizes are in order Ag/0.5g < Ag/1.5g < Ag/1g 1.44P which can be graphically observed in histograms represented in figure 3.11.

3.3.9 Electrochemistry

3.3.9.1 Cyclic and Differential pulse voltammetry of silver nanoclay composites

The surface modified and bentonite nanoclays were successfully functionalised with silver forming silver nanoclay composites, with varied concentration of nanoclays. However, bentonite nanoclay was found to be unsuitable for the study due to its inability to stick on the electrode surface, hence surface modified nanoclay was considered going forward. The cyclic voltammograms of silver modified nanoclay composites (Ag/1.44P) with fractions of nanoclay 0.5, 1 and 1.5 g were recorded and represented in figure 3.12.

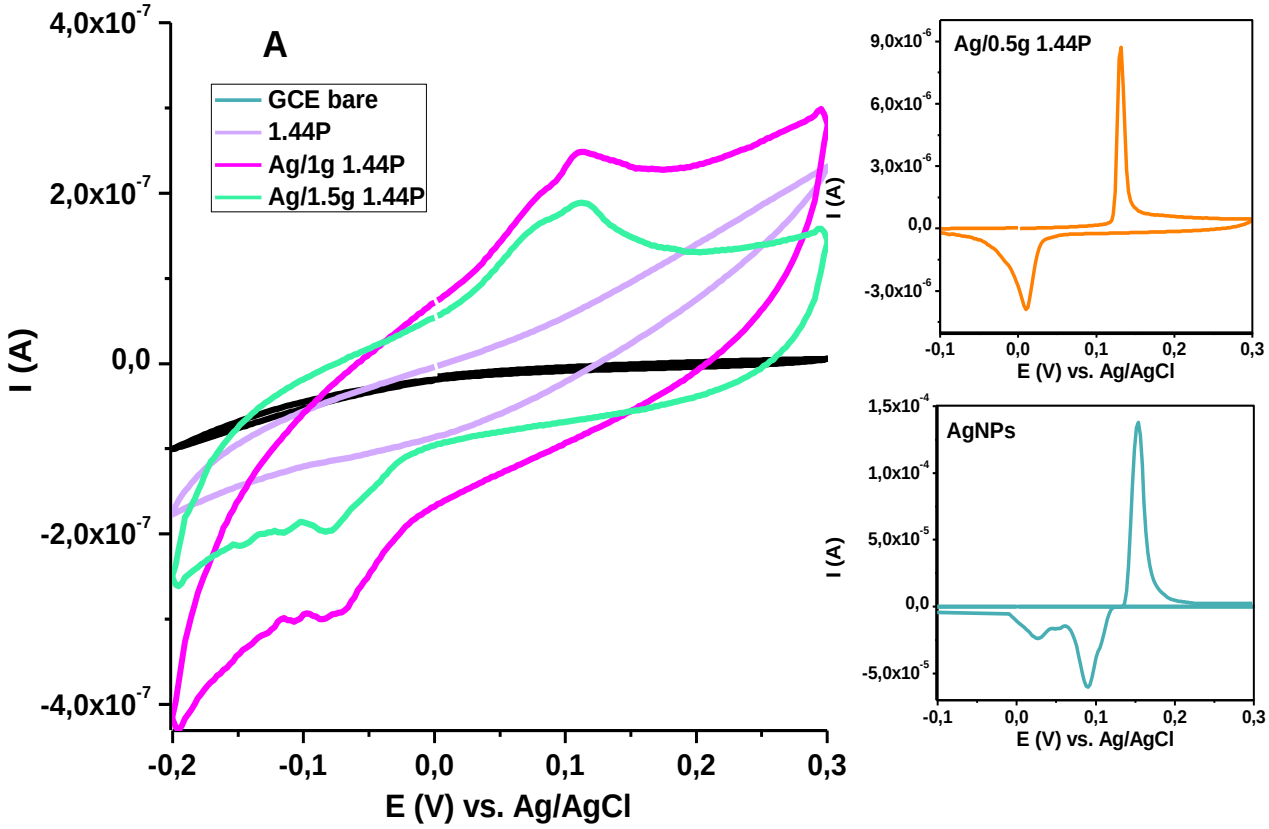

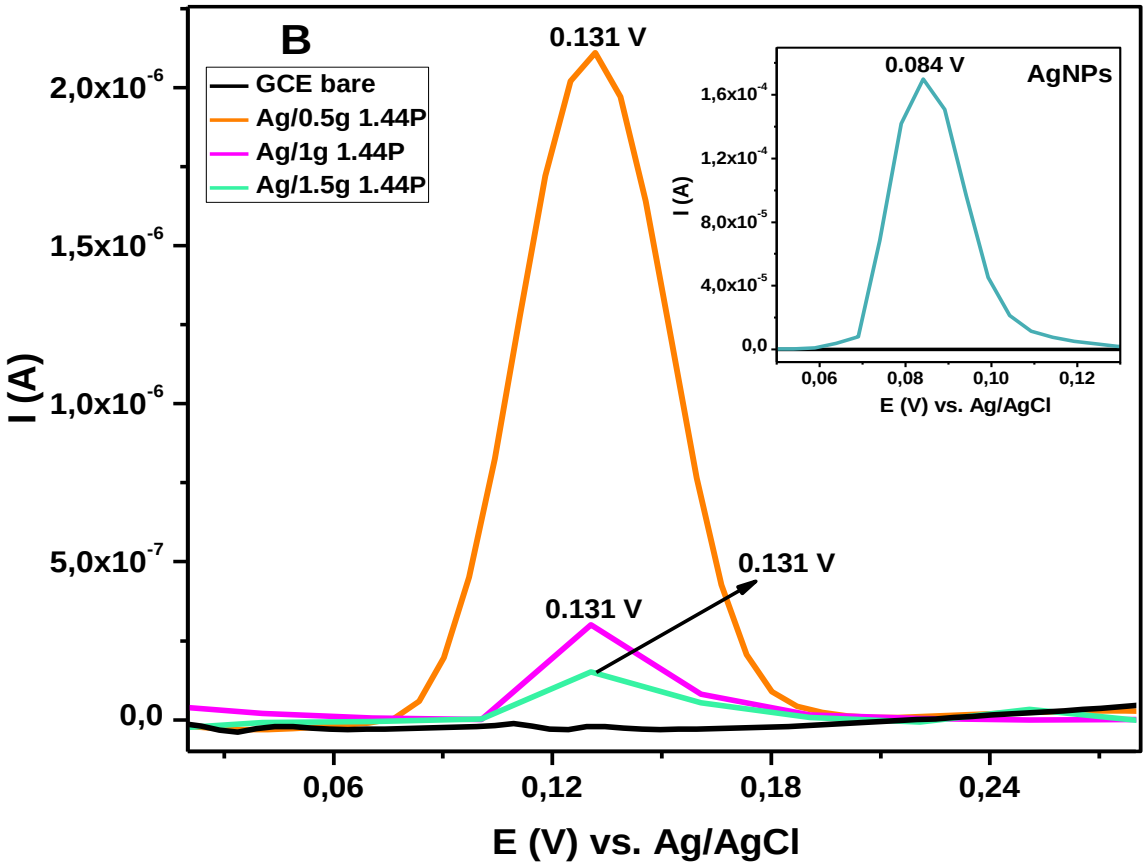

Figure 3.12: (A) Cyclic voltammograms of 1.44P nanoclay, Ag/1g 1.44P, Ag/1.5g 1.44P composites at 0.08 V/s. *Insert*: Ag/0.5g 1.44P, AgNPs. (B) Differential pulse voltammograms of Ag/ 1.44P composites at potential step 8 mV at GCE in 0.1 M HCl. *Insert:* AgNPs.

These were compared with the cyclic scan of 100 mM AgNPs as shown in figure 3.12 (A) which was found to be a good choice based on the spectroscopic studies and DPV as discussed previously, to examine the effect of silver on nanoclay. Based on the representation in figure 3.12 (A), the effect of silver on the nanoclay composites can be observed where the silver peak is present within the potential range of silver, which cannot be observed in pure nanoclay voltammogram. This is due to its non-conductivity which is enhanced by the presence of silver (Nazir *et al.*, 2016), hence the peak observed in silver nanoclay composites. In comparison with CV for AgNPs, there is a shift in peak potentials observed cathodically for composites as the concentration of the nanoclay increases as represented in table 3.5, with Ag/1g 1.44P having the less positive potential compared to other nanoclay composites indicating smaller sized nanoparticles.

Table 3.5: Silver nanoclay composites potential with changes in concentration of nanoclay using anodic peak data.

Ag/1.44P composites	E_{pa} (V) x10^{-1}	E_{pc} (V) x10^{-3}	ΔE_p (V) x10^{-1}	n	I_{pa} (A) x10^{-8}	I_{pc} (A) x10^{-7}
0.50 g	1.32	7.00	1.25	0.85	87.00	-37.00
1.00 g	1.12	-87.00	1.99	1.00	2.70	-2.90
1.50 g	1.19	-73.00	1.92	0.94	1.80	-2.10

The smaller sized particles revealed by CV with less positive potential is due to the decrease in silver nanoparticle concentration allowing the composites to highly cover the electrode surface. In contrast, Ag/0.5g 1.44P has more positive potential which is due to more silver present that showed aggregation as discussed earlier which agrees with SEM. However, with DPV in figure 3.12 (B), more positive potentials for Ag/1g and Ag/1.5g 1.44P composites were depicted. The potential for Ag/0.5g 1.44P however, is 0.001 V lesser in DPV from that of CV. In addition, the conductivity of nanoclay composites seem to increase with reduced nanoclay concentration which is no surprise because lesser nanoclay concentration implies more silver concentration in the composite solution, hence greater conductivity which is a good indication. Subsequent to this, Ag/0.5g 1.44P is found suitable for sensor fabrication which will be elaborated further in chapter five.

3.4 Conclusion

To routinely and reliable use AgNPs for therapeutically and sensor application, a study of the effect of varying reducing agent concentrations on nanoparticle synthesis was carried out, together with the corresponding nanoclay composites with different concentrations of nanoclays. The produced materials were confirmed by spectroscopic, microscopic, and electrochemical techniques. However, UV-Visible spectroscopy was not applied in nanoclay composites since it only considers liquid samples. The CV was used in comparison to UV-Visible spectroscopy for AgNPs to extract information on the size and aggregation of the nanoparticles and corroborated these results with SEM. The results indicate the mixture of various shapes and larger sizes of the synthesized AgNPs at lower concentrations while higher concentrations produced small aggregated spherical shape nanoparticles. UV-Vis spectra of AgNP showed 100 mM TSC as the best option for nanoclay functionalisation hence it was used. However, CV and DPV methods were able to uncover details about aggregation at both 50 and 100 mM concentrations in agreement with SEM, which proved 10 mM TSC as a good concentration in comparison to other concentrations. A correlation was found in FWHM of all

the methods. 10 mM gave FWHM with narrowest particles size distribution which indicates good concentration in comparison to other concentrations thus its consideration for sensor fabrication which will be detailed in chapter five. This proves that the voltammetry is more sensitive for identifying of aggregates than the UV-Vis method. Also, a combination of these methods with careful interpretation of the data is usually the best option. All X-ray data of the composites showed four diffraction peaks within the silver spectrum range, with intensity of silver decreasing with increasing concentration of 1.44P, depicting successful functionalisation of nanoclay. SEM represented well dispersed particles of different shapes and particle sizes which were confirmed with CV displaying Ag/0.5g 1.44P composites as bigger sized particles which are highly conductive compared to other composites. However, DPV depicted more potentials for all composites with higher conductivity of Ag/0.5g 1.44P and its slight decrease in DPV potential of Ag/0.5g 1.44P from the CV potential. Due to these reasons, Ag/0.5g 1.44P is considered for sensor fabrication which will be elaborated further in chapter five. This study is a useful guideline helping the researchers to consider including electrochemistry as a complementary technique in monitoring the behaviour of nanoparticles/nanocomposites.

3.5 References

Acharya, D., Mohanta, B., Deb, S. & Sen, A. K. 2018. Theoretical prediction of absorbance spectra considering the particle size distribution using Mie theory and their comparison with the experimental UV–vis spectra of synthesized nanoparticles. *Spectrosc. Lett.* Vol.51. pg 139–143.

Ahmadi, E., Eyvani, M.R., Riahifar, V., Momeneh, H. & Karami, C. 2019. Amperometric determination of nevirapine by GCE modified with c-MWCNTs and synthesized 11-mercaptundecanoyl hydrazinecarbothioamide coated silver nanoparticles. *Microchemical Journal*. Elsevier B.V. Online [https://doi.org/10.1016/j.microc.2019.02.054].

Ali, M.S., Al-Lohedan, H.A., Atta, M.A., Ezzat, A.O. & Al-Hussain, S.A.A. 2015. Interaction of human serum albumin with silver nanoparticles functionalized with polyvinylthiol. *Journal of Molecular Lipids*. Elsevier B.V. Online [www.elsevier.com/locate/molliq].

Aziz, B.S., Abdullah, O.G., Saber, D.R., Rasheed, M.A. & Ahmed, H.M. 2017. Investigation of metallic siver nanoparticles through UV-Vis and optical micrograph techniques. *International journal of electrochemical science*. Vol.12. Online [doi:10.20964/2017.01.22].

Brainina, K.Z., Galperin, L.G., Vikulova, E.V., Stozhko, N.Y., Murzakaev, A.M., Timoshenkova, O.R. & Kotov, Y.A. 2011. Gold nanoparticles electrooxidation: Comparison of theory and experiment. *Journal of Solid-State Electrochemistry*. Vol.15(5). Springer-Verlag. Online [DOI 10.1007/s10008-010-1133-6].

Chen, J.E., Wang, Q., Shull, K.R. & Richards, J.J. 2020. Control over electroless plating of silver on silica nanoparticles with sodium citrate. *Journal of Colloid and Interface Science*. Vol.576. Elsevier. Online [https://doi.org/10.1016/j.jcis.2020.05.024].

Edvinsson, T. 2018. Optical quantum confinement and photocatalytic properties in two-, one- and zerodimensional nanostructures. *R. Soc. Open Sci.* Vol.5.

Eksin, E., Erdem, A., Fafal, T. & Kıvçak, B. 2019. Eco-friendly Sensors Developed by Herbal Based Silver Nanoparticles for Electrochemical Detection of Mercury (II) Ion. *Electroanalysis.* Vol. 31(6). Online [https://doi.org/10.1002/elan.201800776].

Elgrishi, ́N., Rountree, K.J., McCarthy, B.D., Rountree, E.S., Eisenhart, T.T. & Dempsey, J.L. 2018. A Practical Beginner's Guide to Cyclic Voltammetry. *Journal of Chemical Education.* Vol.95(2). American Chemical Society Division of Chemical Education. Online [DOI: 10.1021/acs.jchemed.7b00361].

Goulart, L.A., Gonçalves, R., Correa, A.A., Pereira, E.C. & Mascaro, L.H. 2018. Synergic effect of silver nanoparticles and carbon nanotubes on the simultaneous voltammetric determination of hydroquinone, catechol, bisphenol A and phenol. *Microchimica Acta.* Vol.185(1). Online [https://doi.org/10.1007/s00604-017-2540-5].

Gurunathan, S., Kalishwaralal, K., Vaidyanathan, V., Deepak, V., Pandian, S.R.K., Muniyandi., J., Hariharan, N. & Eom, H.S. 2009. Biosynthesis, purification, and characterization of silver nanoparticles using Escherichia Coli. *Journal of colloids and surface B*. Vol.74. Elsevier B.V. Online [www.elsevier.com/locate/colsurfb].

Hassan, M.M., Zareef, M., Jiao, T., Liu, S., Xu, Y., Viswadevarayalu, A., Li, H. and Chen, Q. 2021. Signal optimized rough silver nanoparticle for rapid SERS sensing of pesticide residues in tea. *Food chemistry.* Vol.338. Elsevier. Online [https://doi.org/10.1016/j.foodchem.2020.127796].

Huang, M., Du, L. & Feng, J. 2016. Photochemical synthesis of silver nanoparticles/ eggshell membrane composite, its characterization and antibaterial activity. *Science of advanced materials*. Vol.8(8). American Scientific Publishers: USA. Online [www.aspbs.com/sam].

Kim, D., Jeong, S. & Moon, J. 2006. Synthesis of silver nanoparticles using the polyol process and the influence of precursor injection. *Journal of nanotechnology*. Institute of physics publishing: Korea. Vol.17. Online [stacks.10p.org/Nano/17/4019].

Mainali, B.P., Pattadar, D.K. & Zamborini, F.P. 2021. Reverse Size-Dependent Electrooxidation of Gold Nanoparticles Coated with Alkanethiol Self-Assembled Monolayers. *The Journal of Physical Chemistry C*. Vol.*125*(4). American Chemical Society. Online [https://dx.doi.org/10.1021/acs.jpcc.0c10173?ref=pdf].

Movlarooy, T. 2018. Study of quantum confinement effects in ZnO nanostructures. *Mater. Res.* Express. Vol.5.

Narasimha, G., Alzohairy, M., Khadri, H. & Mallikarjuna, K. 2013. Extracellular synthesis, characterization, and antibacterial activity of silver nanoparticles by Actinomycetes isolative. *International journal of Nano Dimension*. Vol. 4(1). Online [www.IJND.ir].

Nazir, M.S., Haafiz, M., Kassim, M., Mohapatra, L., Gilani, M.A., Raza, M.R. & Majeed, K. 2016. Characteristic properties of nanoclays and characterization of nanoparticulates and nanocomposites. Springer Science & Business Media. Singapore. Pg 36-52.

Okumu, F. O., Silwana, B. & Matoetoe, M. C. 2020. Application of MWCNT/Ag-Pt Nanocomposite Modified GCE for the Detection of Nevirapine in Pharmaceutical Formulation and Biological Samples. *Electroanalysis*. Vol.32. Wiley-VCH Online [doi:10.1002/elan.202060374].

Piella, J., Bastús, N.G. and Puntes, V., 2017. Modeling the optical responses of noble metal nanoparticles subjected to physicochemical transformations in physiological environments: Aggregation, dissolution and oxidation. *Zeitschrift für Physikalische Chemie*. Vol.231(1). Oldenbourg Wissenschaftsverlag. Online [https://doi.org/10.1515/zpch-2016-0874].

Pillai. Z. S. & Kamat, P.V. 2004. What factors control the size and shape of silver nanoparticles in the citrate ion reduction method. *Journal of physical chemistry*. Vol. 108(3). American Chemical Society. Online [10.1021/jp037018r].

Rashid, M.U., Buiyan, K.H. & Quayum, M.E. 2013. Synthesis of silver nanoparticles and their uses for quantitative analysis of vitamin C tablets. *Journal of pharmaceautical sciences*. Vol.12(1).

Saba, N., Jawaid, M. and Asim, M., 2016. Recent advances in nanoclay/natural fibers hybrid composites. *Nanoclay reinforced polymer composites.* Online [https://link.springer.com/chapter/10.1007/978-981-10-0950-1_1].

Sileikaite, A., Prosycevas, I., Puiso, J., Juraitis, A. & Guobiene, A. 2006. Analysis of silver nanoparticles produced by chemical reduction of silver salt solution. *Journal of material science*. Vol.12 (4).

Sohrabnezhad, S., Pourahmad, A., Mehdipour Moghaddam, M. J. & Sadeghi, A. 2015. Study of antibacterial activity of Ag and Ag2CO3 nanoparticles stabilized over montmorillonite. *Spectrochim. Acta - Part A Mol. Biomol. Spectrosc*. Vol.136.

Soliwoda, R.K., Tomaszewska, E., Socha, E., Krzyczmonik, P., Ignaczak, A., Orlowsk, P., Krzyzowska, M., Celichowski, G. & Grobelny, J. 2017. The role of tannic acid and sodium

citrate in the synthesis of silver nanoparticles. *Journal of nanoparticles research*. Vol.19. Springer. Online [doi:10.1007/s11051-017-3973-9].

Van der Horst, C., Silwana, B., Iwuoha, E. and Somerset, V. 2015. Synthesis and characterization of bismuth-silver nanoparticles for electrochemical sensor applications. *Analytical Letters*. Vol.48(8). Taylor & Francis. Online [https://doi.org/10.1080/00032719.2014.979357].

Viani, V., Oktaviani, V., Hidayat, H. & Fatimah, I. 2021. Green synthesis of silver nanoparticles using Ocimum citriodorum leaf extract for antibacterial soap application.*AIP Conference Proceedings.* Vol. 2370(1). AIP Publishing. Online [https://doi.org/10.1063/5.0062196].

Wade, L.G. 2006. Measurement of IR spectrum. *Organic Chemistry*. 6th edition. Pearson Education: Upper Saddle River. pg514-51.

Xu, P., Zeng, G.M., Huang, D.L., Feng, C.L., Hu, S., Zhao, M.H., Lai, C., Wei, Z., Huang, C., Xie, G.X. & Liu, Z.F. 2012. Use of iron oxide nanomaterials in wastewater treatment: a review. *Science of the Total Environment*. Vol. 424. Elsevier. Online [doi: 10.1016/j.scitotenv.2012.02.023].

Yin, H., Yamamoto, T., Wada, Y. & Yanagida, S. 2003. Large-scale and size-controlled synthesis of silver nanoparticles under microwave irradiation. *Materials chemistry and physics*. Elsevier B.V. Online [www.elsevier.com/locate/matchemphys].

Zhang, X., Xu, R., Wu, Z. & Zhou, C. 2003. The synthesis and characterization of polyurethane/clay nanocomposites. *Journal of polymer international society if chemical industry*. Online [DOI: 10.1002/pi.1152].

Zhao, X., Li, N., Jing, M., Zhang, Y., Wang, W., Liu, L., Xu, Z., Liu, L., Li, F. & Wu, N. 2019. Monodispersed and spherical silver nanoparticles/graphene nanocomposites from gamma-ray assisted in-situ synthesis for nitrite electrochemical sensing. *Electrochimica Acta.* Vol.295*.* Elsevier. Online [https://doi.org/10.1016/j.electacta.2018.10.039].

CHAPTER 4

ELECTROCHEMICAL PARAMETERS

A brief background on parameter used in electrochemistry with appropriate equations and their significance are found in the chapter. This elaborates on electrochemical parameters of silver nanoparticles and their nanoclay composites which were synthesised in chapter three, as well as their electrochemical behaviour on the surface modified glassy carbon electrode. The discussion will extend to the summary of the most important findings, to obtain a general picture of the redox behaviour and changes in cyclic voltammogram at lower and higher scan rates.

4.1 Background

Electrochemical parameters determine the electrochemical behaviour of the species (Habekost *et al.*, 2015). They are important in determining the size of the material and how it affects the performance of the material on an electrode surface. Electrochemical parameters are mostly applied as a guide to assess the efficiency of a mediator because their values define the electron transfer kinetics among electrode and the mediator, the nature of limitations of current examined whether diffusion limited or kinetics, the adsorbed or packed status of the immobilized material and possible connections between the immobilized material (Prodromidis *et al.*, 2000). The electron transfer process together with mass transport, control the electrochemical process through the scan rate obtained from cyclic voltammogram (CV). The mass transport for quasi-reversible process is comparable to the electron transfer rate where the peak potential increases with increasing scan rate (Brownson *et al*., 2014). The implementation of CV is to obtain qualitative information about electrochemical reactions which supplies identification of redox potential particular to the electroactive species under question, giving information about redox process thermodynamic kinetics of heterogeneous electron-transfer reaction, coupled electrochemical reaction analysis or adsorption processes (Brownson *et al*., 2014).

One of the important parameters is ΔE_p which is the difference between the two peak potentials that reveals information about the reversibility of the species in question. For a reversible electrode reaction, ΔE_p is expected to be 0.0592 (Skoog *et al*., 2013) and is given by the equation (4.1), and equation 4.2 is used to deduce the number of electrons involved. If the current function is constant for all scan rates, the electron transfer is quick enough to keep the equilibrium ration between the reduced and oxidised forms of redox couple, hence reversible electron transfer system (Brownson *et al*., 2014). A reversible electron transfer system is indicated by the value of the current function through Randles plot of current against square root of scan rate, Ip vs. $v^{1/2}$. For an irreversible or quasi-reversible behaviour, the

equilibrium ration keeps changing at the electrode surface resulting to wider potential range of voltammetric peaks, reduced current peaks, and enhanced ΔE_p values (Brownson *et al*., 2014).

The diffusion coefficient is another important parameter that describes the mobility of specific molecules of a substance from higher to lower concentration region, through a semipermeable hindrance (Pal *et al*., 2013). It depends on the properties of the interaction of solvent polymer and polymeric network. The rate of diffusion relies on the type of phase, that is, quicker in gases, slowest in liquids and slowest in solids (Pal *et al*., 2013). It can be calculated using Randles-Sevcik equation (4.3), the greater the diffusion coefficient, the smaller the nanoparticle and the higher mobility of ions (Munir *et al.*, 2012; Elgrishi *et al*., 2018). For a freely diffusing species, the linear plot of the peak current (Ip) with the square root of scan rate ($v^{1/2}$) is considered whereas linear plot Ip versus scan rate (v) is considered for the freely adsorbing species (Elgrishi *et al*., 2018). The current response for an adsorbed species is said to vary linearly with scan rate (Elgrishi *et al*., 2018).

Another crucial parameter is the surface coverage which is deduced using equation 4.4 with the slope of Randles-Sevcik plot of Ip vs $v^{1/2}$, where the diffusion is controlled. The current limitations and sensor stability are ultimately or precisely influenced by the degree of the surface coverage, with morphology of the nanoparticles directly affecting the surface coverage (Prodromidis *et al*., 2000). Smaller sized nanoparticles have high mobility on the electrode surface resulting to enhanced values of surface coverage compared to larger molecules and hence good conductivity (Prodromidis *et al*., 2000; Elgrishi *et al*., 2018).

The charge released reflects the extent of the surface oxidation so revealing the extent to which internal surfaces are electroactive. The greater the charge coefficient, the more electroactive the species, and is given by equation 4.5. Lastly, heterogeneous rate constant (Ks) is the other important diagnostic criterion for anticipating the nature of a redox process and can be calculated using equation 4.6 (Rupar *et al.*, 2018; Vassiliev *et al.*, 2019). These values are of importance in this study which helps in identifying the size of nanoparticles. The higher Ks values is an indicative that the oxidized and reduced species reaches equilibrium rapidly thus representing smaller nanoparticles, compared to lesser values of Ks representing slower kinetics and therefore requires longer time to reach equilibrium which suggests larger sized nanoparticles (Rupar *et al.*, 2018). Therefore, smaller Ks values are indicative of sensitivity of the species under investigation.

$$\Delta E_p = E_{pa} - E_{pc} = \frac{0.0592}{n} \quad \text{.....eq 4.1}$$

$$\left| E_{pa} - \frac{E_{pa}}{2} \right| = 2.20 \frac{R.T}{nF} \quad \text{eq 4.2}$$

$$I_p = 2.69 \times 10^5 . n^{3/2} . A . D_{ox}^{1/2} . C_{ox} . V^{1/2} \quad \text{eq 4.3}$$

$$\text{Slope} = \frac{n^2 . F^2 . A . \Gamma}{4RT} \quad \text{eq 4.4}$$

$$\Gamma = \frac{Q}{nFA} \quad \text{eq 4.5}$$

$$Ks = \frac{Ip}{nFAC} \quad \text{eq 4.6}$$

Where E_{pa} and E_{pc} are anodic and cathodic peak potentials (V), n is the number of electrons involved, R is the gas constant ($J.K^{-1}.mol^{-1}$), T is the absolute temperature (kelvin), F is Faraday's constant (C/mol), Ip is the anodic peak current (A), *A* is the glassy carbon electrode surface area (0.0707 cm^2), C is the concentration of electrolyte (mol/cm^3), D is the diffusion current ($cm^2.s^{-1}$), v is the scan rate (V/s). Γ is the surface coverage of the adsorbed species ($mol.cm^{-2}$), Q is the charge (C/cm^2).

4.2 Experimental

The experimental procedures detailed in chapter three for the synthesis of silver nanoparticles and composites were followed for the study electrochemical properties of silver nanoparticles and silver nanoclay composites.

4.3 Results and discussion

4.3.1 Silver nanoparticles

A redox response of silver nanoparticles at potential 0.04 V to 0.2 V in figure 4.1 show an increase in anodic and cathodic peak current with increasing scan rate. This may be ascribed to the charge-transfer kinetic limitations which may be caused by the interaction of the ions of electrolyte with the modifier film, non-equivalent sites existing in the film, electrostatic factors dominance or due to the lateral interaction of redox couple existing on the surface (Nezhad *et al.*, 2009). An increase in current as a function of scan rate could also be due to the diffusion layer which gets thicker as the material gets closer to the surface of the electrode. The oxidation and reduction peak potential between scan rates 0.04 and 0.16 V/s tends to be stable at 5 mM TSC reducing agent. However, for 10, 50, and 100 mM TSC only the oxidation peaks which remain stable between 0.04 and 0.16 V/s, while the reduction peak at a higher scan rate shifts toward a less positive potential.

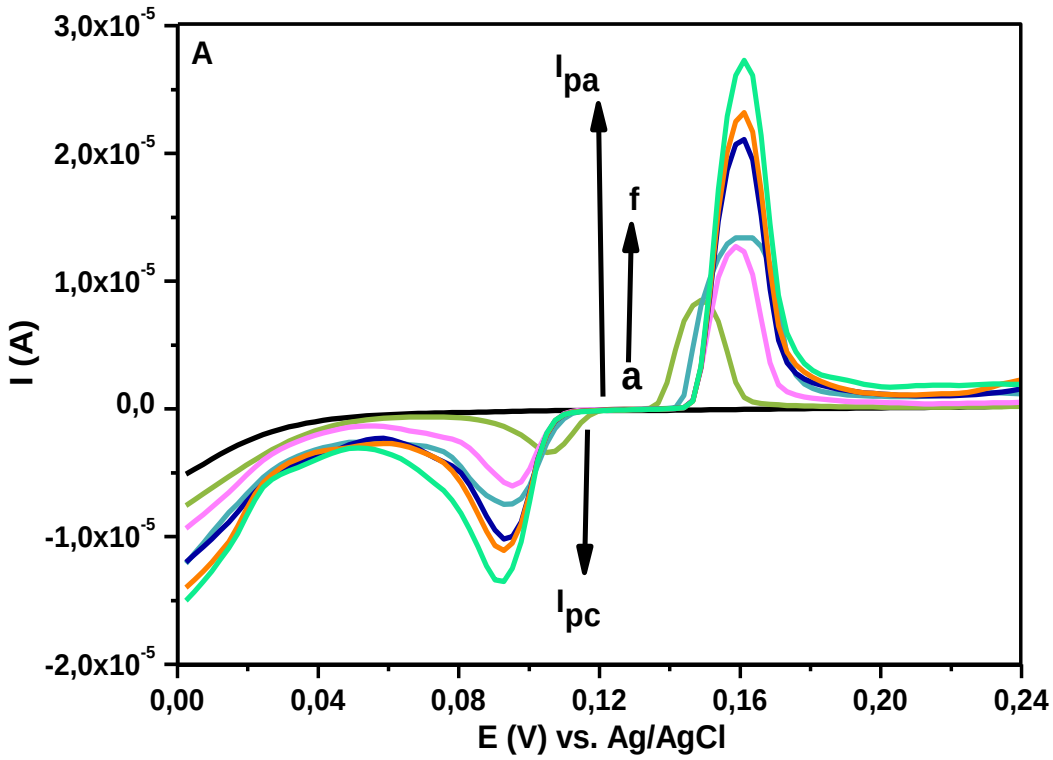
A
I_{pa}
f
a
I_{pc}
3,0x10-5
2,0x10-5
1,0x10-5
0,0
-1,0x10-5
-2,0x10-5
I (A)
0,00
0,04
0,08
0,12
0,16
0,20
0,24
E (V) vs. Ag/AgCl

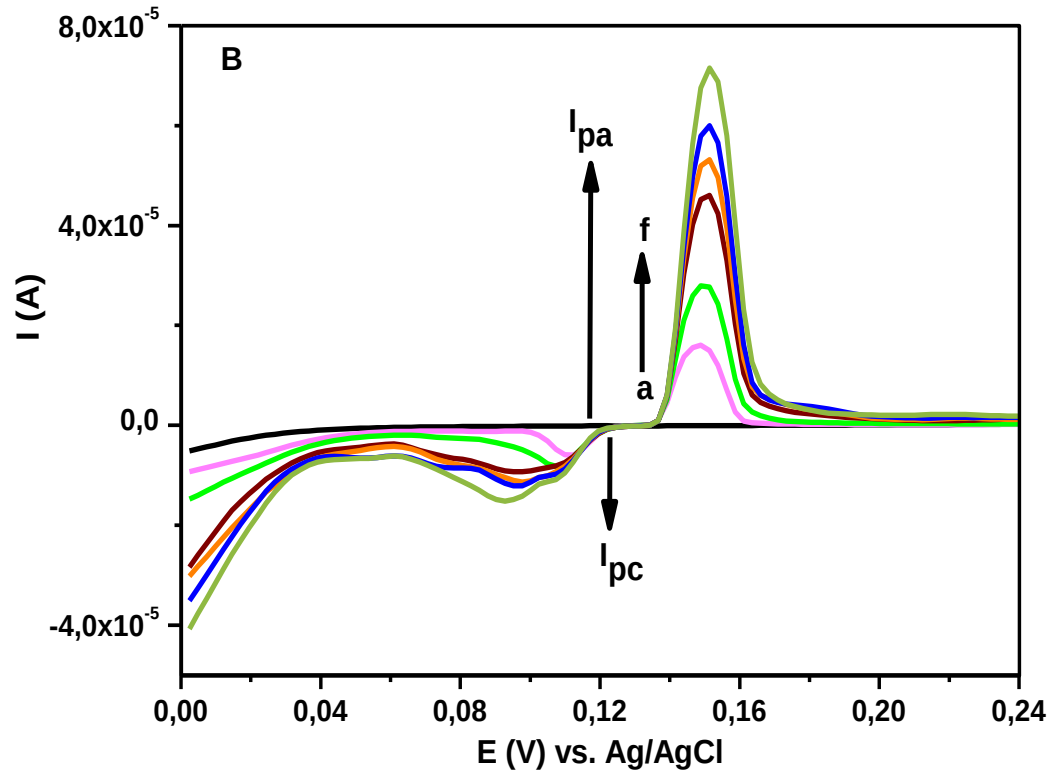
B
I_{pa}
f
a
I_{pc}
8,0x10-5
4,0x10-5
0,0
-4,0x10-5
I (A)
0,00
0,04
0,08
0,12
0,16
0,20
0,24
E (V) vs. Ag/AgCl

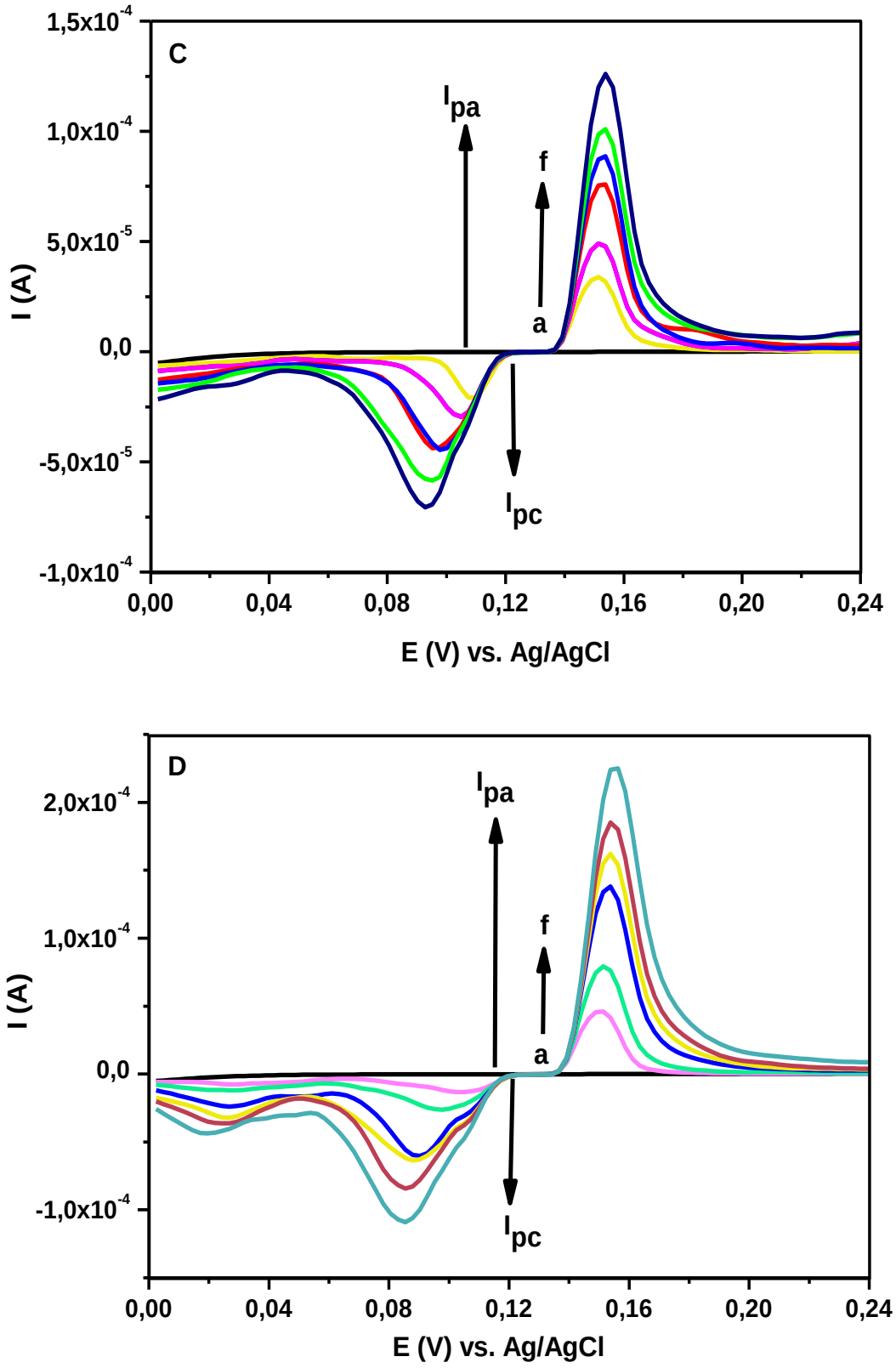

Figure 4.1: Cyclic voltammograms of AgNPs with (A) 5 (B) 10 (C) 50 & (D) 100 mM TSC at bare, (a) 20 (b) 40 (c) 80 (d) 100 (e) 120 (f) 160 mV/s at GCE in 0.1 M HCl.

A linear relationship between the Ipa vs. v (figure 4.2 A) and Ipa vs. $v^{1/2}$ (figure 4.2 B) was observed for oxidation process, where the linearity for concentration 5, 10 and 50 mM TSC was observed in plot of Ipa vs vs. $v^{1/2}$, while there was a lack of linearity for 100 mM TSC reducing agent. The change from linearity serves as proof of complications in the observed

kinetics which could be due to the chemical changes that occur because of electron transfer (Brownson *et al*., 2014).

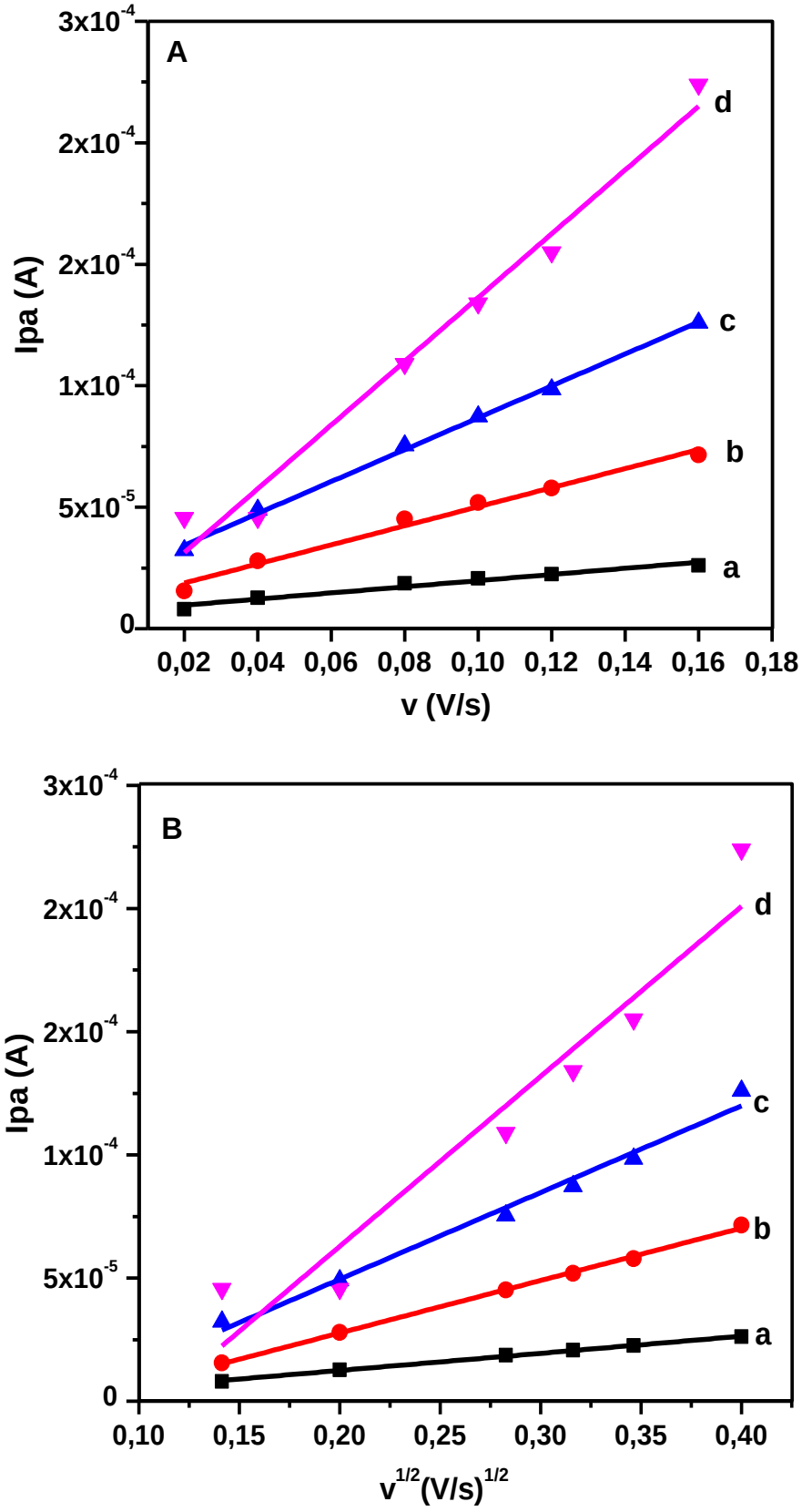

Figure 4.2: Plots of anodic peak current against (A) scan rates and (B) square root of scan rates for (a) 5 (b) 10 (c) 50 (d) 100 mM TSC AgNPs.

Generally, the current (Ipa) is proportional to the square root of scan rate, where charge transfer is the diffusion limit. All the systems show linear diffusion conditions (Bard *et al.*, 2001), and the apparent diffusion coefficient was deduced using equation 4.3. The values obtained are tabulated in table 4.1 showing bigger diffusion coefficient value at 10 mM TSC reducing agent, implying smaller molecule and faster rate of diffusion irons than comparatively larger molecule as supported by the literature (Munir *et al.*, 2012; Nosheen *et al.*, 2012; Elgrishi *et al*., 2018). This was then confirmed by the calculated values of rate constant, Ks where AgNPs with 10 mM TSC had the largest Ks value depicting smaller sized AgNPs which causes them to travel faster in the solution. In contrast, large nanoparticles travel slowly in solution due to the mass resulting in small Ks values (Vassiliev *et al.*, 2019). The calculated values also fall in the range of a quasi-reversible redox system offer evidence to support our attribution of quasi-reversible system. Remarkably noted that charge, Q increases as the reducing agent concentration increases. By observing the Q values in table 4.1, that increases with TSC concentration gave the idea of 50 and 100 mM TSC on GCE with more silver atoms exposed to HCl solution, but only nanoparticles that are oxidized into Ag^{+} are the ones that are in contact with the electrode. The types of reaction taking place at the electrode surface is a mixture of both diffusion (5 & 10 mM) and adsorption-controlled (50 & 100 mM) processes which is based on the better correlation coefficient values observed from Randles –Sevcik linear plots in figure 4.2 (A & B) and tabulated in table 4.1.

Table 4.1: Electrochemical parameters of the modified GCE with AgNPs calculated using equation 4.2 to 4.6.

[TSC] mM	Slope x10^{-5}	D (cm^2 s^{-1}) x10^{-12}	Ks ($cm.s^{-1}$) x10^{-3}	Q ($C.cm^{-2}$) x10^{-6}	R^2 x10^{-1}	
	Ipa vs. $v^{1/2}$				Ipa vs. v	Ipa vs. $v^{1/2}$
5	6.90	8.65	4.50	17.67	9.64	9.97
10	21.30	9.31	16.00	42.56	9.83	9.98
50	35.20	9.13	7.80	52.84	9.97	9.84
100	68.90	9.12	4.50	104.44	9.74	9.51

4.3.2 Silver nanoclay composites

The silver nanoclay composites with varying concentration of surface modified nanoclay (1.44P) were prepared as per the procedure in chapter 3 (3.2.3), and the cyclic voltammograms were recorded in figure 4.3.

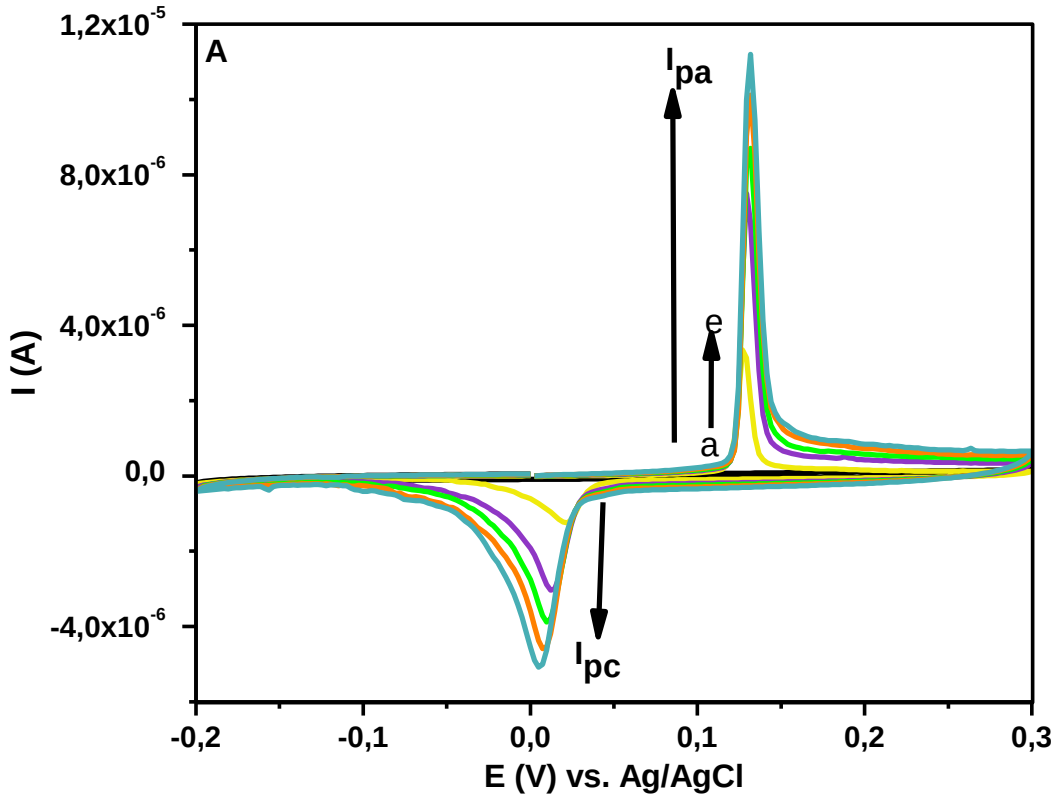
A
I_{pa}
e
a
I_{pc}
1,2x10-5
8,0x10-6
4,0x10-6
0,0
-4,0x10-6
I (A)
-0,2
-0,1
0,0
0,1
0,2
0,3
E (V) vs. Ag/AgCl

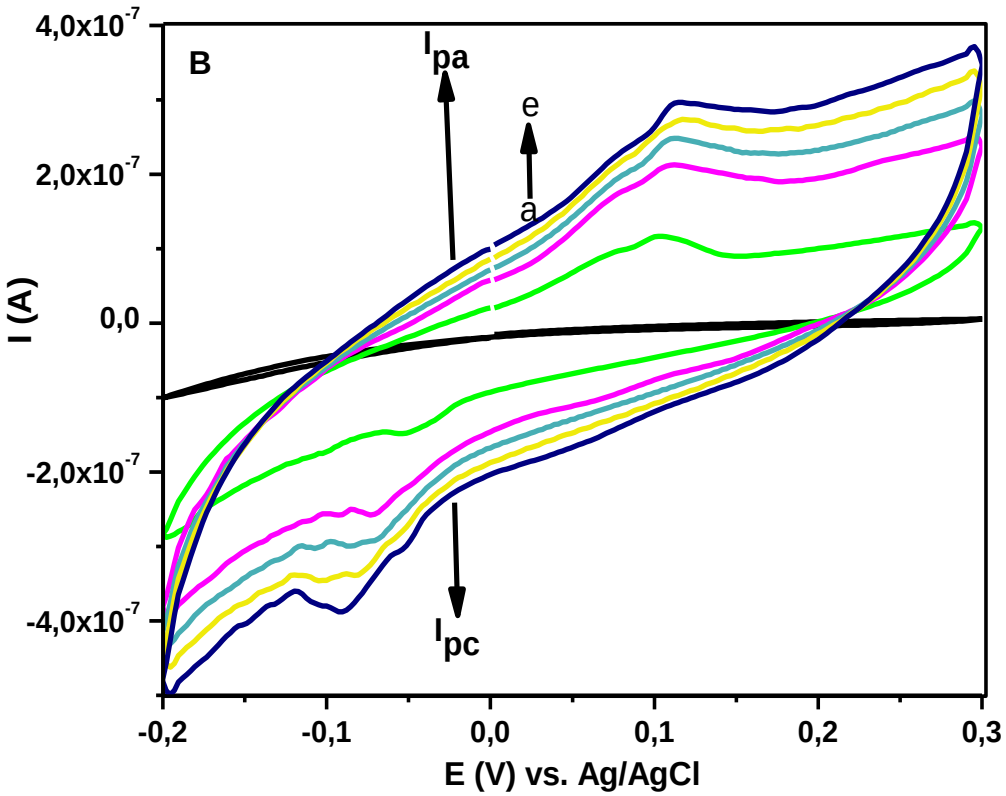
B
I_{pa}
e
a
I_{pc}
4,0x10-7
2,0x10-7
0,0
-2,0x10-7
-4,0x10-7
I (A)
-0,2
-0,1
0,0
0,1
0,2
0,3
E (V) vs. Ag/AgCl

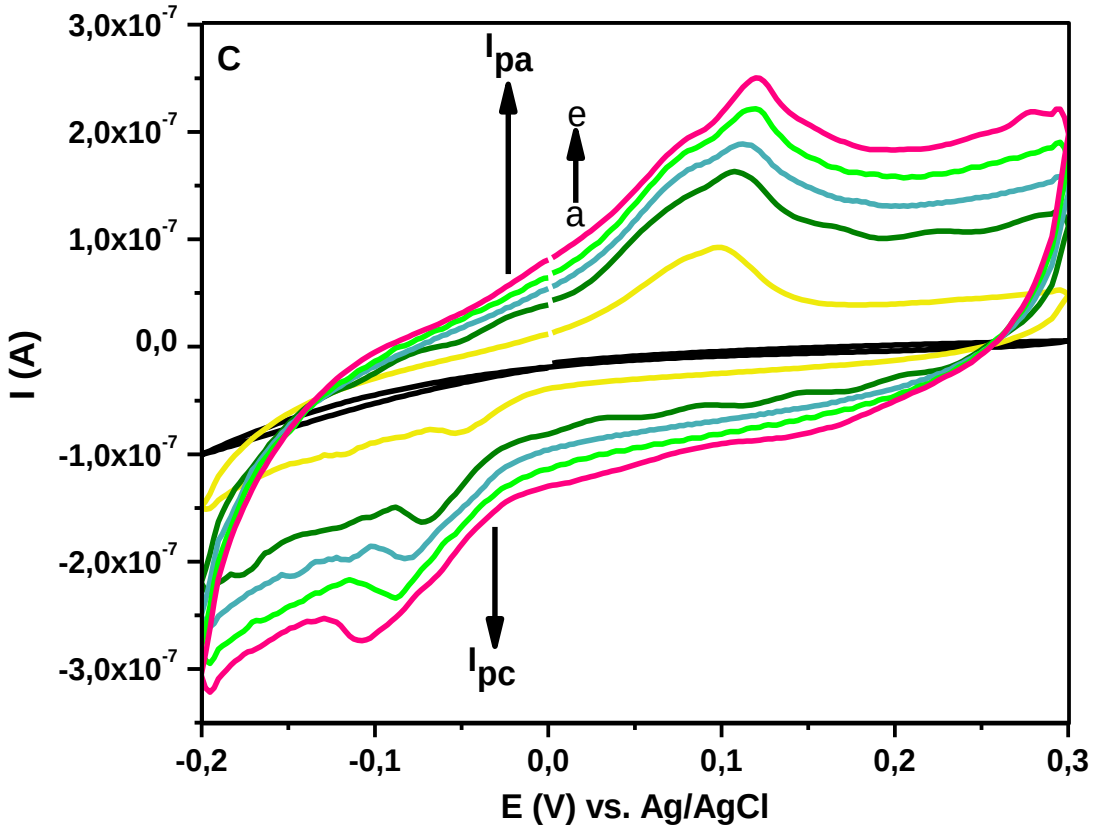

Figure 4.3: Cyclic voltammograms of silver nanoclay composites of (A) 0.5 (B) 1 (C) 1.5 g 1.44 P nanoclay at bare, (a) 20 (b) 60 (c) 80 (d) 100 (e) 120 mV/s at GCE in 0.1 M HCl.

As previously stated in chapter 3 that AgNPs with 100 mM TSC were used in the synthesis of silver nanoclay composites, and the presence of silver was discovered in the CV of silver nanoclay composites in the potential range of -0.2 to 0.3 V. An increase in current peaks is observed, which slides apart as the function of scan rate depicting quasi-reversible system (Habekost *et al*., 2015; Elgrishi *et al*., 2018). The shift in reduction and oxidation peaks both cathodically and anodically with enhanced scan rate is an indication of a controlled by mass transport processes (Rupar *et al.*, 2018). The impact of silver on nanoclay was investigated, where the electrochemical properties of silver through determination of electrochemical parameters which are related to particle size determination were calculated and compared with that of composites to confirm whether the properties improved or not. This was done using Randles-Sevcik equations (4.2 - 4.6), and the slope of Randles-Sevcik's plot (figure 4.4B) constructed from oxidation peak currents of CVs. Through the values obtained, the behaviour of the nanoparticles was revealed.

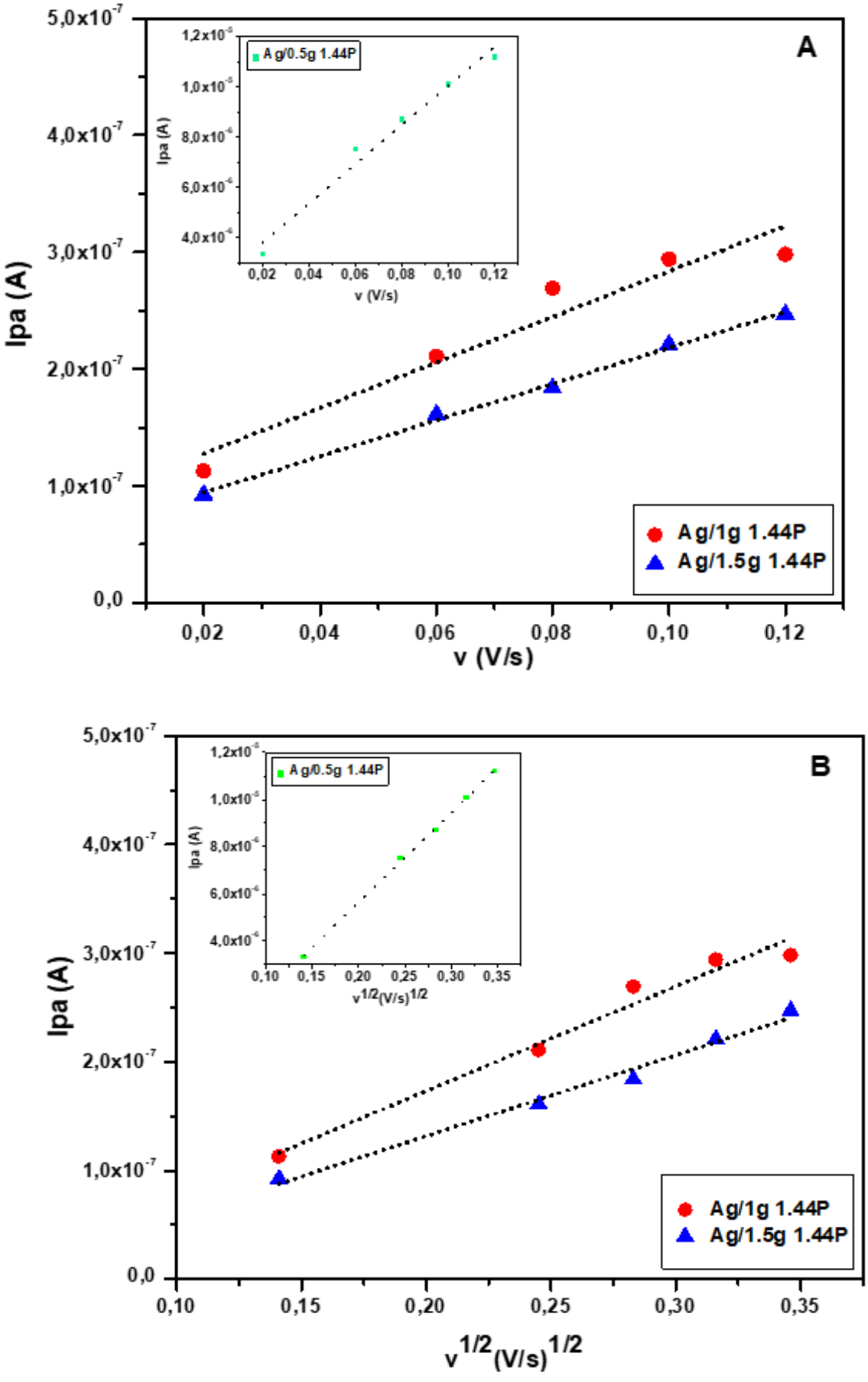

Figure 4.4: Plots of anodic peak current against (A) scan rates and (B) square root of scan rates for (b) Ag/1g 1.44P (c) Ag/1.5 g 1.44P, inserts: Ag/0.5g 1.44P.

Referring to figure 4.4, the plots for composites show poor linearity, especially for Ag/1g 1.44P. However, the linearity improved where current peaks are plotted against square root of scan rate (figure 4.4 B), suggesting diffusion-controlled processes for both Ag/0.5g 1.44P and Ag/1g 1.44P. In the case of Ag/1g 1.44P, better linearity was discovered in the plot of peak current against scan rate (figure 4.4A) which is attributed to adsorption-controlled process.

As per the representation of electrochemical parameters in table 4.2, the parameters such as diffusion coefficient (D), heterogeneous constant (Ks), surface coverage (ɾ) and charge were calculated and recorded.

Table 4.2: Electrochemical parameters of the modified GCE with Ag/1.44P composites calculated using equation 4.2 to 4.6.

Ag/1.44P composites	Slope $x10^{-7}$	D ($cm^2.s^{-1}$) $x10^{-13}$	Ks ($cm.s^{-1}$) $x10^{-7}$	Γ ($mol.cm^{-2}$) $x10^{-13}$	Q ($C.cm^{-2}$) $x10^{-10}$	R^2 $x10^{-1}$	
	I_{pa} vs. $v^{1/2}$					I_{pa} vs. v	I_{pa} vs. $v^{1/2}$
0.50 g	381	4260	150	79.40	46 000	9.72	9.99
1.00 g	9.63	2.50	4.00	1.45	9.89	9.50	9.69
1.50 g	7.45	1.40	3.00	1.27	8.14	9.95	9.83

It can be observed that the values of these parameters were high at low nanoclay concentration due to more concentration of silver present which decreases with increasing concentration of nanoclay leading to less conductivity, thus smaller values depicted. The enhanced values of D and Ks for Ag/0.5g 1.44P suggests smaller sized nanoparticles which travel faster leading to increased surface coverage or area compared to larger nanoparticles which in this case are Ag/1g 1.44P and Ag/1.5g 1.44P produced at higher nanoclay concentrations. Previous studies predicted that the smaller sized nanoparticles have enhanced D values in comparison with bigger sized molecules (Elgrishi *et al*., 2018; Rupar *et al.*, 2018), with arrangement 0.5> 1> 1.5g 1.44P as shown in the table. The literature also states that smaller nanoparticles travel faster in the solution, thus greater Ks value compared to larger nanoparticles which travel most slowly in solution due to the mass, hence smaller Ks value (Vassiliev *et al.*, 2019). The smaller nanoparticles are associated with good sensitivity, hence increased charge for Ag/0.5g 1.44P. However, the latter was observed for Ag/1g and Ag/1.5g 1.44P which result from improved amount of nanoclay. In comparison with silver alone, the electrochemical parameters decreased with increasing concentration of nanoclay resulting to less conductivity, except for D value for Ag/0.5g 1.44P which seemed to improve indicating smaller sized nanoparticles.

4.4 Conclusion

The electrochemical properties of silver nanoparticles with different concentrations of reducing agent and silver nanoclay composites with different concentrations of nanoclay were successfully studied. The results revealed quasi-reversibility for a one electron transfer reaction. The nature of the reaction taking place at the electrode surface was confirmed to be a mixture of both adsorption and diffusion-controlled processes for both silver nanoparticles and nanoclay composites. The electrochemical parameters examined revealed that the best concentration of the reducing agents for AgNPs is 10 mM TSC and that of nanoclay at 0.5 g for a target application. Thus, their consideration in fabrication of a sensor detailed in the next chapter. These findings suggest the usefulness of voltammetry as a complementary method that can be used as a qualitative guide to identify the size of nanoparticles.

4.5 References

Bard, A. J., Faulkner, L. R., Swain, E. & Robey, C. 2001. Electrochemical methods. *Fundamentals and Applications*. 2nd edition. John Wiley & Sons.

Brownson, D.A.C. & Banks, C.E. 2014. Interpreting electrochemistry. *The handbook of graphene electrochemistry.* Springer-Verlag: London. Online [DOI:10.1007/978-1-4471-6428-9_2].

Elgrishi, N., Rountree, K.J., McCarthy, B.D., Rountree, E.S., Eisenhart, T.T. & Dempsey, J.L. 2018. A Practical Beginner's Guide to Cyclic Voltammetry. *Journal of Chemical Education.* Vol. 95(2). American Chemical Society Division of Chemical Education. Online [DOI: 10.1021/acs.jchemed.7b00361].

Farshchi, F., Hasanzadeh, M. & Solhi, E. 2019. Immunosensing of prostate cancer in human plasma samples using immobilization of antibody on the surface of mesoporous silica-modified silver nanoparticles and its immunocomplex with prostate-specific antigen. *Analytical Methods.* Vol.11(48). The Royal Society of Chemistry. Online [https://doi.org/10.1039/C9AY02058F].

Fotouhi, L., Fatollahzadeh, M. & Heravi, M.H. 2012. Electrochemical Behavior and Voltammetric Determination of Sulfaguanidine at a Glassy Carbon Electrode Modified with a Multi-Walled Carbon Nanotube. *International journal of electrochemical science.* Vol.7. Online [www.electrochemsci.org].

Habekost, A. & Aristov, N. 2015. Cyclic voltammetry- a versatile electrochemical method investigating electron transfer processes. *World journal of chemical education*. Science and education publishing. Online[http://pubs.sciepub.com/wjce/3/5/2].

Li, X., Lenhart, J.J. & Walker. H.W. 2010. Dissolution-accompanied aggregation kinetics of silver nanoparticles. *Langmuir*. Vol.26 (22). American Chemical Society. Online [https://doi.org/10.1021/la101768n].

Munir, S., Shah, A., Zafar, F., Badshah, A., Wang, X., Rehman, Z.U., Hussain, H.& Lunsford, S.K. 2012. Redox behavior of a derivative of vitamin K at a glassy carbon electrode. *Journal of The Electrochemical Society.* Vol.159(10). The Electrochemical Society. Online[https://doi.org/10.1149/2.032210jes].

Nezhad, K, G., Hasanzadeh, M., Saghatforoush, L., Shadjou, N., Earshad, S. & Khalilzadeh, B. 2009. Kinetic study of electrocatalytic oxidation of carbohydrates on cobalt hydroxide modified glassy carbon electrode. *Journal of the Brazilian Chemical Society*. Vol 20(1).

Nosheen, E., Shah, A., Badshah, A., Hussain, H., Qureshi, R., Ali, S., Siddiq, M. & Khan, A.M., 2012. Electrochemical oxidation of hydantoins at glassy carbon electrode. *Electrochimica Acta*.Vol.80. Elsevier. Online [https://doi.org/10.1016/j.electacta.2012.06.116].

Pal, K., Paulson, A.T. & Rousseau, D. 2013. Biopolymers in controlled-release delivery systems. In *Handbook of biopolymers and biodegradable plastics*. Elsevier. Online [https://doi.org/10.1016/B978-1-4557-2834-3.00014-8].

Piella, J., Bastús, N.G. and Puntes, V., 2017. Modeling the optical responses of noble metal nanoparticles subjected to physicochemical transformations in physiological environments: Aggregation, dissolution, and oxidation. *Zeitschrift für Physikalische Chemie*. Vol.231(1). Oldenbourg Wissenschaftsverlag. Online [https://doi.org/10.1515/zpch-2016-0874].

Prodromidis, M.I., Florou, A.B., Tzouwara-Karayanni, S.M. & Karayannis, M.I. 2000. The importance of surface coverage in the electrochemical study of chemically modified electrodes. *Electroanalysis: An International Journal Devoted to Fundamental and Practical Aspects of Electroanalysis.* Vol*12*(18). WILEY-VCH Verlag GmbH. Online [http://dx.doi.org/10.1002/1521-4109(200012)12:183.0.CO;2-Y].

Rupar, J., Aleksić, M.M., Nikolić, K. & Popović-Nikolić, M.R. 2018. Comparative electrochemical studies of kinetic and thermodynamic parameters of Quinoxaline and Brimonidine redox process. *Electrochimica Acta.* Vol.271. Elsevier Ltd. Online [https://doi.org/10.1016/j.electacta.2018.03.114].

Skoog, D.A., West, D.M., Holler, F.J. and Crouch, S.R., 2013. *Fundamentals of analytical chemistry*. Cengage learning.

Vassiliev, S.Y., Sentyurin, V.V., Levin, E.E. & Nikitina, V.A., 2019. Diagnostics of lithium-ion intercalation rate-determining step: Distinguishing between slow desolvation and slow charge transfer. *Electrochimica Acta.* Vol.302. Elsevier Ltd. Online [https://doi.org/10.1016/j.electacta.2019.02.043].

CHAPTER 5

FABRICATION OF SENSOR FOR DETECTION OF ZIDOVUDINE

This chapter is about the application of the selected material synthesised previously discussed for sensor fabrication, including the application of human serum albumin for the detection of zidovudine. The modification methods of the electrode will be discussed as well as the techniques used for detection. This discussion elaborates on the methods of fabrication including the criteria for sensor performance. The data on the validation of the sensor developed and its implementation in real samples will also be provided with discussion, as well as the summary on the data accumulated.

5.1 Background

The process of fabricating an electrochemical sensor involves conducting modifiers such as redox pairs, metallic nanomaterials, carbon nanostructure for electron transfer efficiency, and the use of biological recognition elements including DNA, enzymes, RNA, antibodies, aptamers which produces a sensor that follows the criteria stated in figure 5.1, including an increase in sensitivity and selectivity of the fabricated sensor (Khanmohammadi *et al.*, 2020).

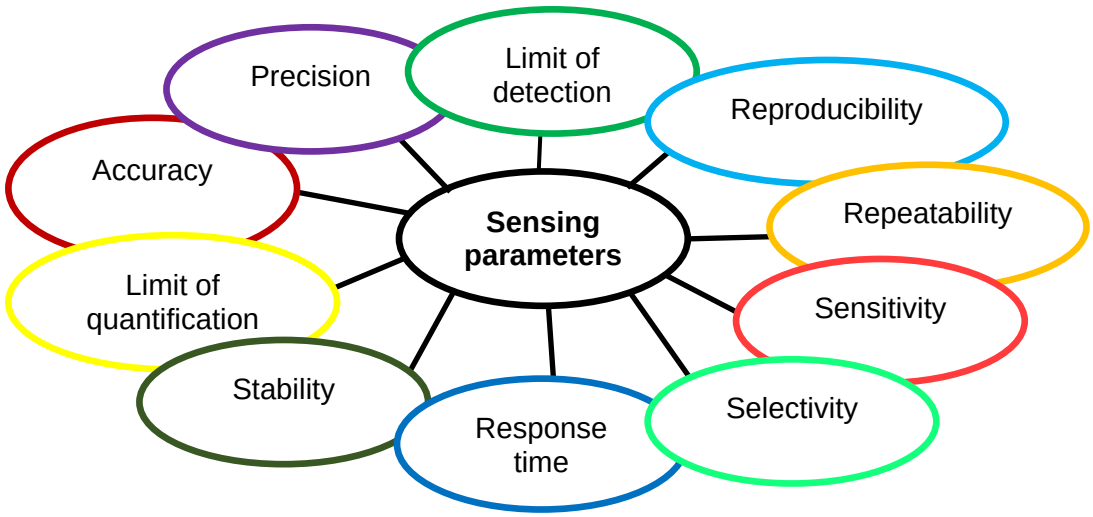

Figure 5.1: Electrochemical sensor performance criteria.

This increase in selectivity is due to the interaction of the analyte with the biological recognition element through electrostatic, intercalation and groove binding, forming a measurable signal (Ahmad *et al*., 2018; Maleh *et al*., 2020). The sensor response is dependent on factors such as geometry, type of transducer, fabrication method, biorecognition reaction and conditions of operation, which are affected by the level of pH, buffer composition, temperature, organic solvents present, sensing area which is in contact with the analyte solution, bioreceptor degradation and complex sample composition (Ahmad *et al*., 2018). To acquire a desirable sensor stability, proper tuning of transducers and electronics is required. This is achieved through modification of electrodes with nanomaterials resulting to high mobility of analyte, good biocompatibility, increased chemical stability and good adsorption capacity (Shetti *et al.*, 2019;

Barry *et al*., 2016). The electrochemical modified sensors have an advantage of determining drugs, food additives and environmental compounds simultaneously with one electrochemical sensor (Maleh *et al.*, 2020). The electrochemical response measurement of electrochemical biosensors is done through addition of known concentration of analyte which is then applied in calibration curve plots for linear detection range and sensitivity evaluation (Ahmad *et al.*, 2018). The linear detection is related to properties of sensitive biorecognition elements which are electrochemical and biocatalytic properties.

The different fabrication methods are represented in figure 5.2, including direct deposition and growth method which are mostly considered due to proper attachment of nanomaterials resulting to fast electron transfer, providing good stability.

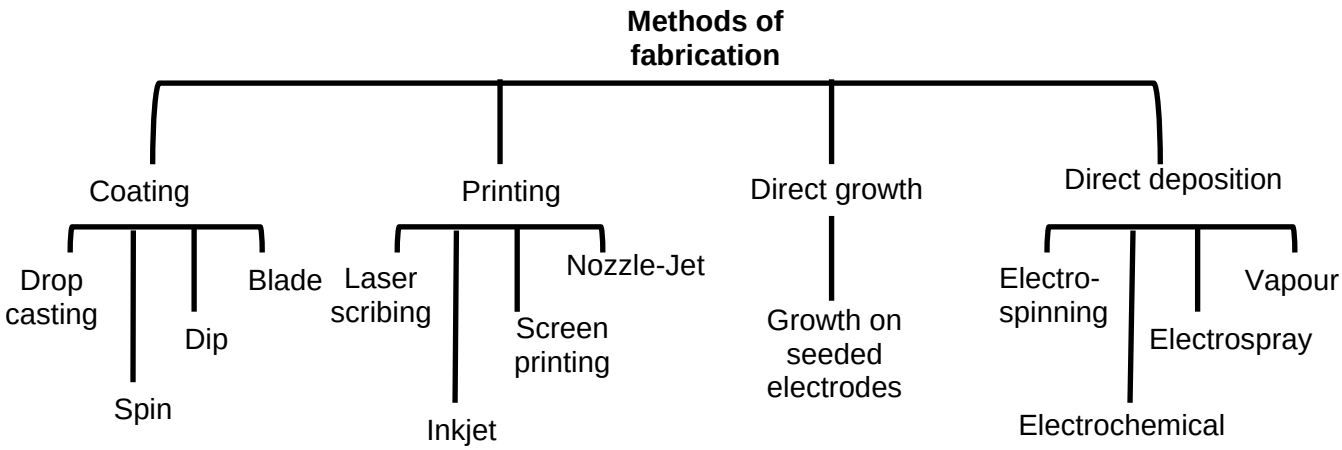

Figure 5. 2: Fabrication methods of a sensor

Furthermore, these methods have many advantages and follows the performance criteria of a sensor shown previously in figure 5.1. However, screen printing and coating methods result to inhomogeneous and dense films which reduces electrocatalytic activity and surface area for enzyme immobilisation (Ahmad *et al.*, 2018). The immobilisation of biorecognition elements directly on the surface of the electrode reduces sensing response and stability of sensors. Hence, the use of nanomaterials as modifiers of the working electrode which increases surface area and immobilisation efficiency, and contains the catalytic activity of proteins and enzymes, increasing the lifespan of the sensor (Ahmad *et al.*, 2018). In the process of material electrodeposition, the negative charge on the electrode is applied, dipping the electrode in a salt solution of the deposition material causing an attraction between positively charged salt ions and the cathode which leads to a reduction process (Lokhande *et al.*, 2019).

The surface modified electrodes were previously characterised with electrochemical techniques such cyclic voltammetry (CV), square-wave voltammetry (SWV) and differential pulse voltammetry (DPV) (Ahmadi *et al.*, 2019). However, CV and SWV were employed in the determination of acyclovir with carbon paste electrode modified with nanoclay (Shetti *et al*., 2017). This includes DPV which was used to detect parathion-ethyl pesticide at glassy carbon

electrode (GCE) modified with mixture of laponite clay and zirconium oxide gel nanocomposites (Bui *et al*., 2015), as well as detection of paracetamol with organoclay modified GCE (Gomdje *et al.*, 2017). The amperometric technique was implemented in nevirapine determination with carboxylated multi-walled carbon nanotubes and synthesized 11-mercaptoundecanol hydrazinecarbothioamide coated silver nanoparticles modified at GCE (Ahmadi *et al.*, 2019). In this chapter, the detection of zidovudine was carried out with electrochemical techniques such as CV, DPV and SWV as implemented in the previous studied, to produce unique properties of the substance or material. The representation of GCE modified with silver nanoclay and Human Serum Albumin (HSA) for ZDV detection is shown in scheme 5.1.

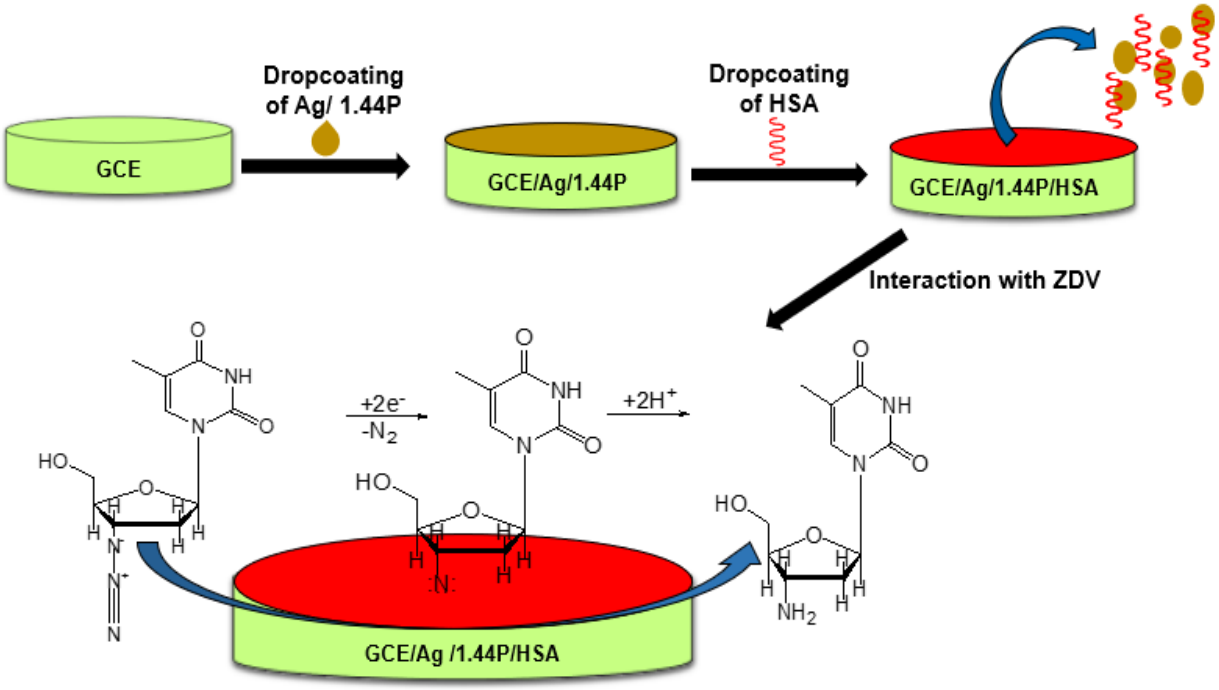

Scheme 5.1: Glassy carbon electrode modification for the detection of ZDV.

HSA has high affinity number of binding sites with domains I, II & III, each of which contains double sub-domains A & B and has 17 stabilizing disulphide bridges. The binding of ZDV to HSA changes the properties of the protein such as biochemical and biophysical (Tajmir, 2007). The study of ZDV binded to HSA, with ZDV situated in III A protein domain displayed two binding sites for ZDV on HSA with association constants that are weak and strong (Tajmir, 2007). The HSA protein act as a biological sensing element due to its high sensitivity leading to more specific and sensitive biosensors (Barry *et al.*, 2016).

5.2 Experimental

5.2.1 Material and reagents

Zidovudine (ZDV) and human serum albumin (HSA) were purchased from Sigma Aldrich (USA), including potassium dihydrogen phosphate (KH_2PO_4), disodium hydrogen phosphate (Na_2HPO_4), Dextrose Glucose, citric acid and ascorbic acid.

5.2.2 Preparation of phosphate buffer saline (pH 7.04)

An amount of 0.06804 g, 0.6804 g, 6.804 g KH_2PO_4 and 0.07098 g, 0.7098 g, 7.098 g Na_2HPO_4 was dissolved separately in 50 mℓ Milli-Q water. Each solution of KH_2PO_4 and Na_2HPO_4 was mixed in 100 mℓ volumetric flask to make up 0.01 M, 0.1 M and 1 M PBS. The solutions were adjusted to pH 7.04 with 1 M NaOH and 1 M HCl and store at room temperature.

5.2.3 Synthesis of silver nanoparticles and composites

The procedure followed for synthesis of silver nanoparticles and composites is detailed in chapter 3.

5.2.4 Zidovudine solution preparation

A solution of 1.869 mM ZDV was prepared in 10 mℓ Milli-Q water and stored in brown bottle and kept refrigerated. A solution of 0.1869 mM ZDV was prepared from the original solution and used for measurements.

5.2.5 Preparation of Human Serum Albumin solution

An amount of 1 mg/mℓ HSA was dissolved in 5 mℓ of 0.1 M PBS (pH 7.04) and kept refrigerated at 2℃ as per the packaging instructions.

5.2.6 Instrumentation

The Autolab and three-electrode system were used for electrochemical measurements using DPV as highlighted in the previous chapter. The HANNA HI2210 pH metre was used to adjust buffer pH.

5.2.7 Optimisation of sensor fabrication method

Dropcoating HSA:
Ag/1.44P was dropcoated onto the electrode and left to dry, followed by dropcoating of HSA onto the modified electrode and left to dry. A volume of ZDV solution was added in 3 mℓ of 0.1 M PBS electrolyte and detected with GCE/Ag/1.44P/HSA.
Immersed HSA method:

Ag/1.44P was dropcoated onto the electrode and left to dry. The modified electrode was left in HSA solution for 15 minutes and ZDV solution was added in 3 mℓ of 0.1 M PBS electrolyte and detected with GCE/Ag/1.44P/HSA after each time.

5.2.8 Detection of zidovudine at different concentrations of PBS electrolyte

The modified GCE was prepared as per the procedure 3.2.4.5 detailed in chapter 3. The bare GCE, GCE/Ag, GCE/Ag/1.44P and GCE/Ag/1.44P/HSA were used to detect ZDV in 0.01 M, 0.1 M and 1 M PBS electrolytes.

5.2.9 Optimisation of procedures for zidovudine detection

The best method for detecting ZDV with the developed GCE/Ag/1.44P/HSA sensor was determined by varying one parameter at a time, while keeping others constant. These parameters include drying time of HSA, effect of electrolyte stirring time and technique optimisation such as step potential, modulation amplitude, modulation time and Interval time.

5.2.10 Validation

5.2.10.1 Reproducibility, repeatability, stability

The reproducibility of GCE/Ag/1.44P/HSA sensor was assessed in 1 M PBS, pH 7.04 with 3.24 μM zidovudine using DPV. Three replicates of the ZDV current response were measured for repeatability purposes. To monitor the stability of the sensor, the GCE/Ag/1.44P/HSA sensor was prepared and used to detect ZDV at day zero. The sensor was then stored in PBS solution, monitoring the current response of zidovudine after every two days for a period of ten days i.e 0, 2, 4, 6, 8 and 10 days.

5.2.10.2 Interference studies

The food supplements such as D-Glucose, ascorbic, and citric acid were used as interferants. Their solutions were prepared by weighing 0.0336, 0.0329, and 0.0392 g of D-Glucose, ascorbic acid, and citric acid respectively. Each mass was separately diluted in 10 mℓ Milli-Q water to make solutions of 18.69 mM. The developed GCE/Ag/1.44P/HSA sensor was used to measure the signal of zidovudine in the presence of these interferants with ratios 1:1, 1:10 and 10:1 (ZDV: Interferant) in 3 mℓ 1 M PBS, pH 7.04.

5.2.10.3 Spiked urine samples

The three ratios of Urine:1 M PBS (i.e 1:4, 1:9 and 1:14) were prepared as spike to measure ZDV response at GCE/Ag/1.44P/HSA. The electrode was cleaned constantly prior to each measurement.

5.2.11 Application of sensor in real samples

5.2.11.1 Preparation of commercial tablet (300 mg) solution

Two zidovudine commercial tablets were weighed and dissolved in Milli-Q water separately. The solutions were allowed to stand for 15 hours for complete dissolution. About 100 µL of each solution was pipetted into 3 mℓ 1 M PBS electrolyte, pH 7.04 and the zidovudine current was generated at GCE/Ag/1.44P/HSA.

5.3 Results and discussion

5.3.2 Optimisation of fabrication method

The voltammograms comparing dropcoating and immersion method of HSA are represented in figure 5.3.

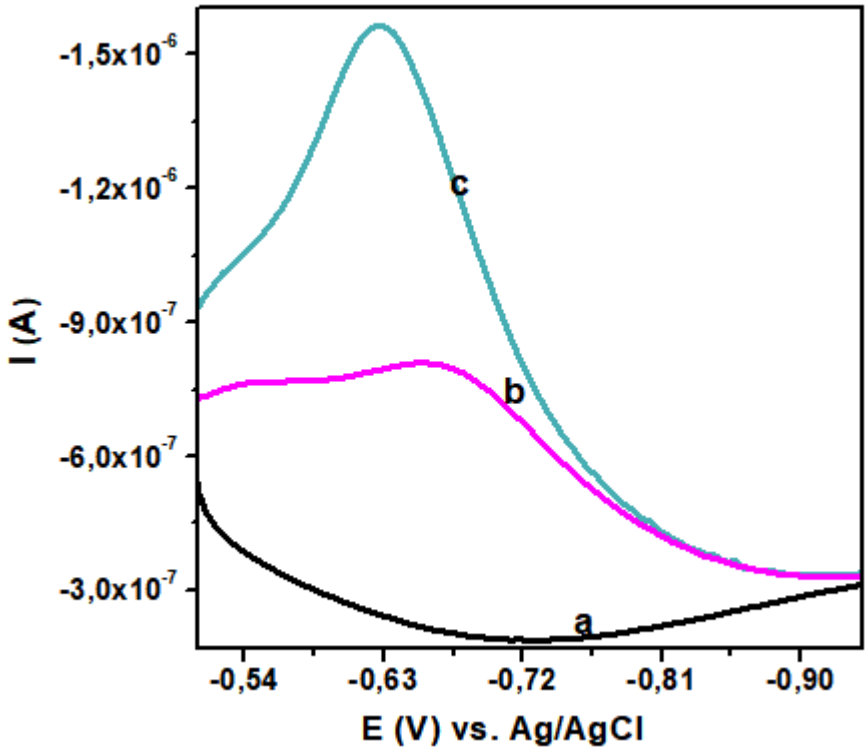

Figure 5.3: DPV of 2.5 µM ZDV detection at (a) blank (b) HSA immersed (c) HSA dropcoated in 0.1 M PBS, pH 7.04 at GCE.

Based on the results obtained, both methods show evidence of zidovudine (ZDV) at -0.65 V (c) for dropcoating method and -0.69 V (b) for immersion method when 2.5 µM ZDV was added. The literature has shown presence of ZDV within that potential range (Rafati *et al.*, 2014). However, enhanced signal with well-defined voltammogram was obtained when HSA was dropcoated compared when it was immersed. Hence, dropcoating method was considered for the study. It can also be observed in table 5.1 that the experimental conditions influence the zidovudine potential. These include the type of electrolyte and working electrode.

Table 5.1: The effect of working electrode and electrolyte on the zidovudine potential.

Potential of zidovudine	Working electrode	Type of electrolyte	References
-0.68 V	Thin film mercury	NaOH	Castro *et al*., 2011
-0.96 V	HMDE	PBS	Leandro *et al.*, 2010
-0.65 V	GCE	PBS	Rafati *et al.*, 2014
0.08 V	Modified graphite paste electrode	Tris-HCl	Mohan *et al.*, 2010

5.3.3 Detection of zidovudine at different concentrations of PBS electrolyte

The detection of ZDV was assessed in three different concentrations of PBS at pH 7.04 with HSA dropcoating method based on the choice discussed earlier. The voltammograms are represented in figure 5.4. The ZDV signal produced by GCE/Ag/1.44P/HSA sensor with voltammograms represented by “e”, was seen to increase with increasing concentration of PBS from 0.01 (A), 0.1 (B) and 1 M PBS (C), This has resulted to 1 M as the best choice PBS concentration for detection of ZDV in the study. The presence of the peak observed between potential range of -0.4 to -0.5 V might have been due to the presence of oxygen.

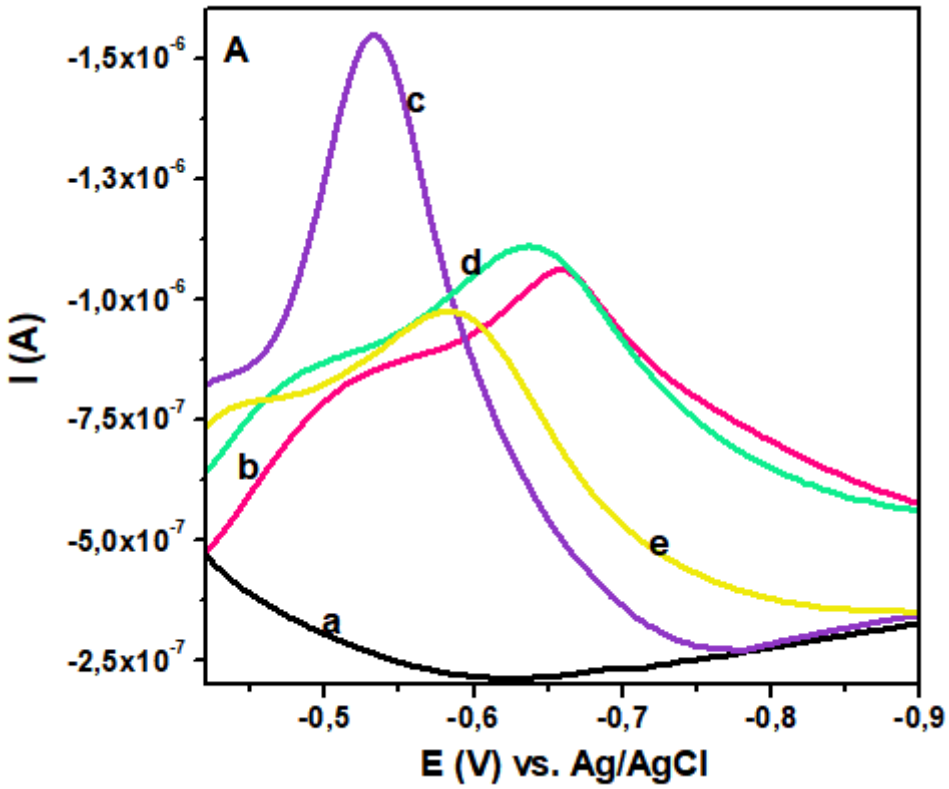

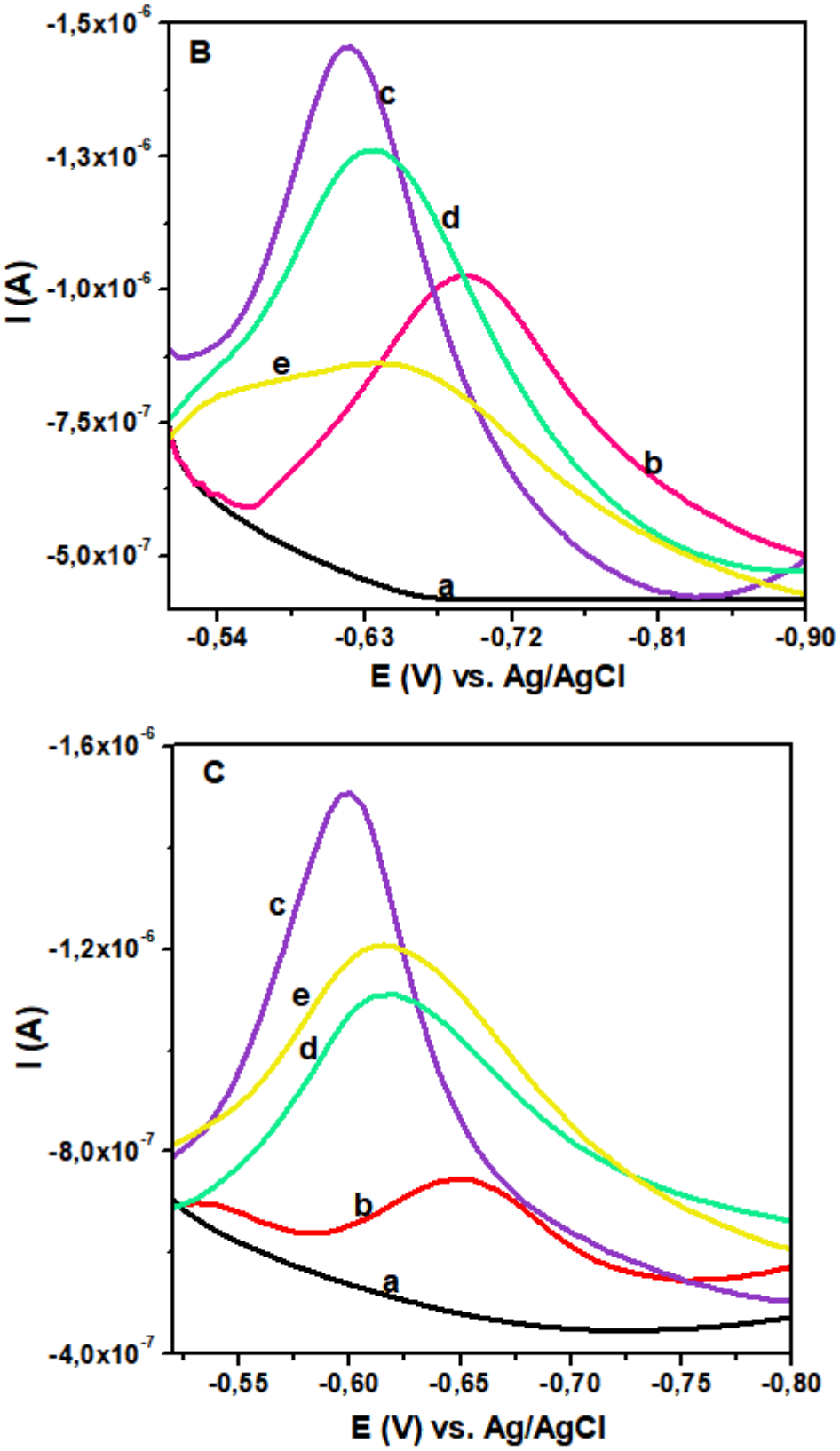

Figure 5. 4: DPV of 2.5 μM ZDV at (a) blank (b) bare (c) Ag (d) Ag/1.44P (e) Ag/1.44P/HSA in (A) 0.01 (B) 0.1 (C) 1 M PBS, pH 7.04 at GCE.

5.3.4 Effect of HSA drying time

The HSA drying time on ZDV signal was monitored and the resulting findings are represented in figure 5.5. There was a sharp increase in the ZDV peak signal after drying for 15 minutes which decreased with enhanced drying time. Therefore, 15 minutes was chosen as the drying time for HSA.

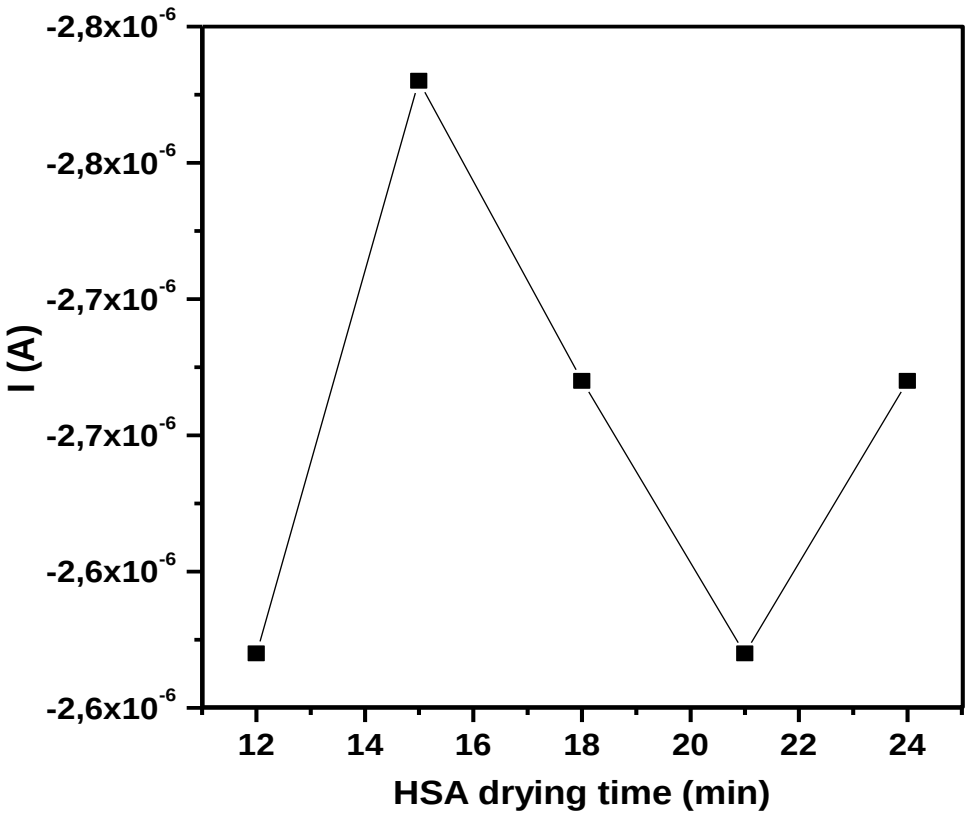

Figure 5.5: Effect of HSA drying time on 2.5 μM ZDV detection at 1 M PBS, pH 7.04 at GCE/Ag/1.44P/HSA.

5.3.5 Effect of stirring

The 1 M PBS electrolyte was stirred multiple times to assess its effect on the ZDV peak detection. The electrolyte was stirred from 0.5 to 4 minutes as shown in figure 5.6. The results depicted an increase in ZDV signal with increased stirring time. However, after 2,5 minutes, the signal decreased leading to consideration of 2.5 minutes going forward.

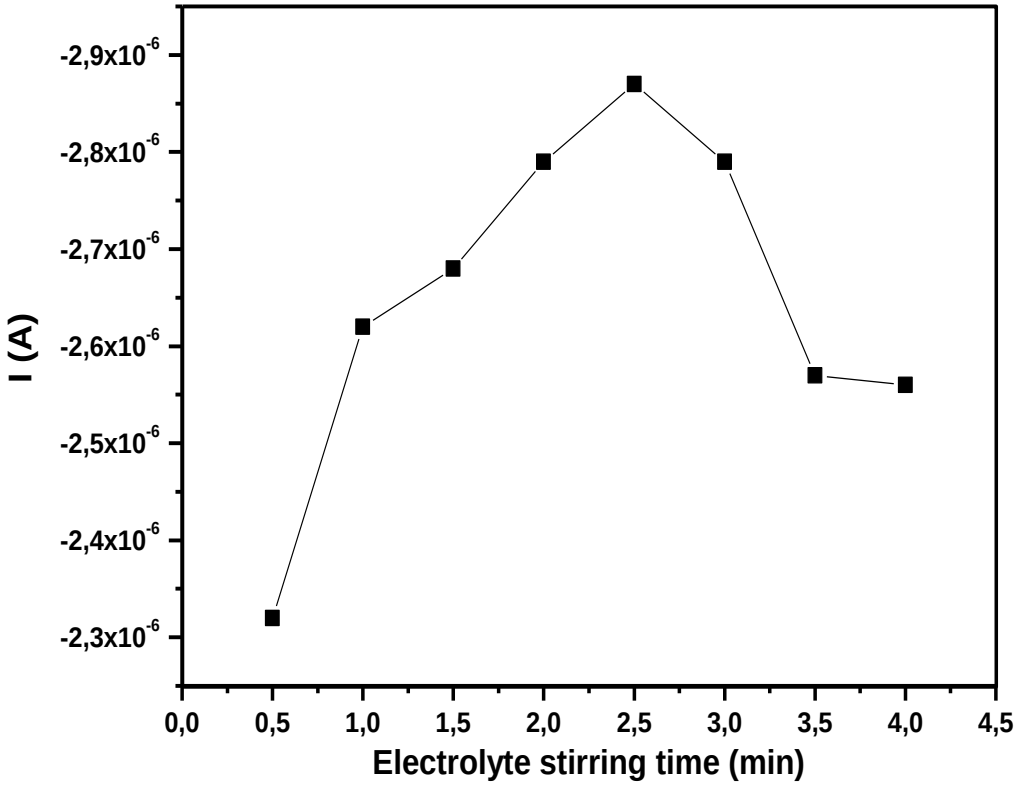

=

Figure 5. 6: Effect of stirring time for 2.5 μM ZDV detection in 1 M PBS, pH 7.04 at GCE/Ag/1.44P/HSA.

5.3.6 Optimisation of procedures for zidovudine detection

The DPV technique parameters were optimised and represented in figure 5.7.

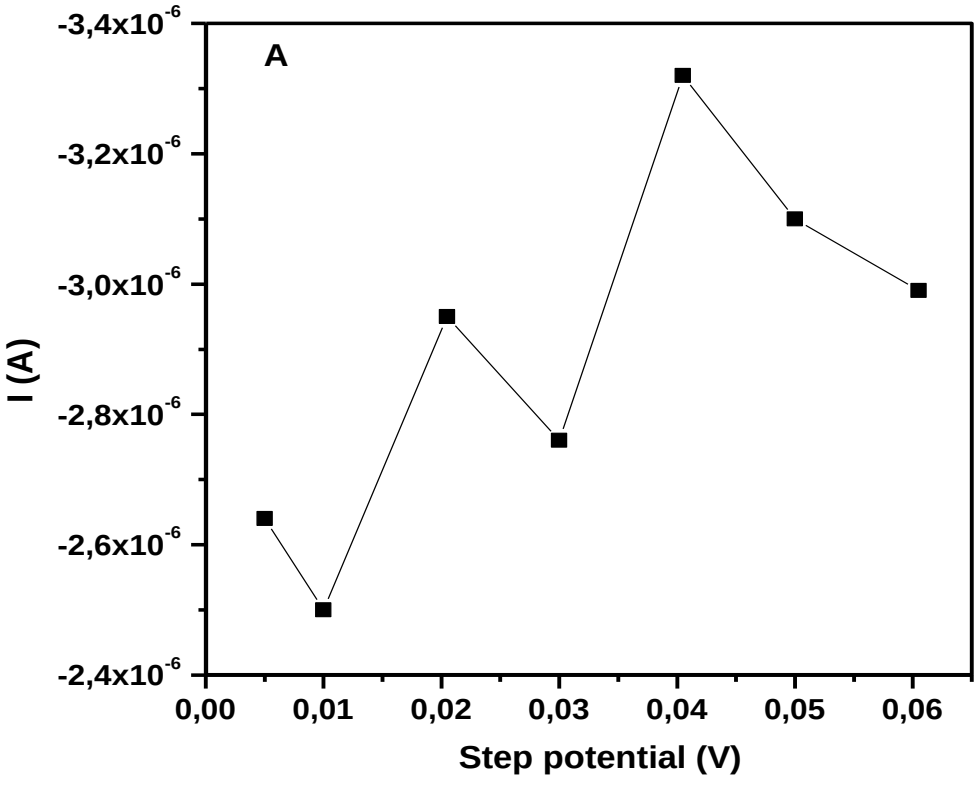

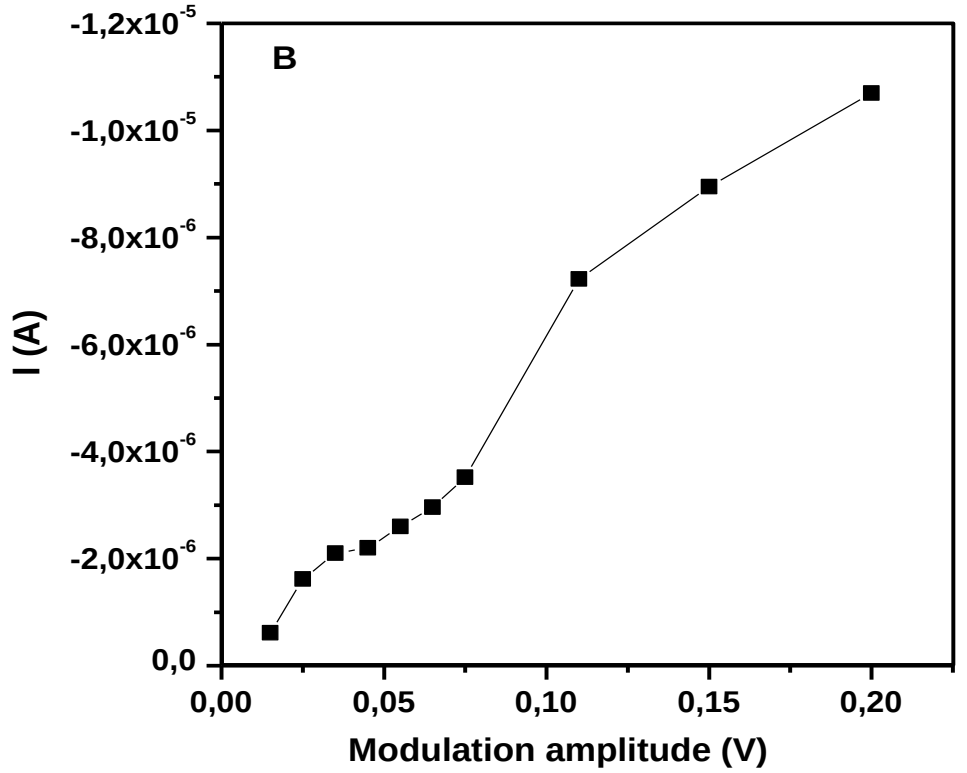
B
-1,2x10-5
-1,0x10-5
-8,0x10-6
-6,0x10-6
-4,0x10-6
-2,0x10-6
0,0
I (A)
0,00
0,05
0,10
0,15
0,20
Modulation amplitude (V)

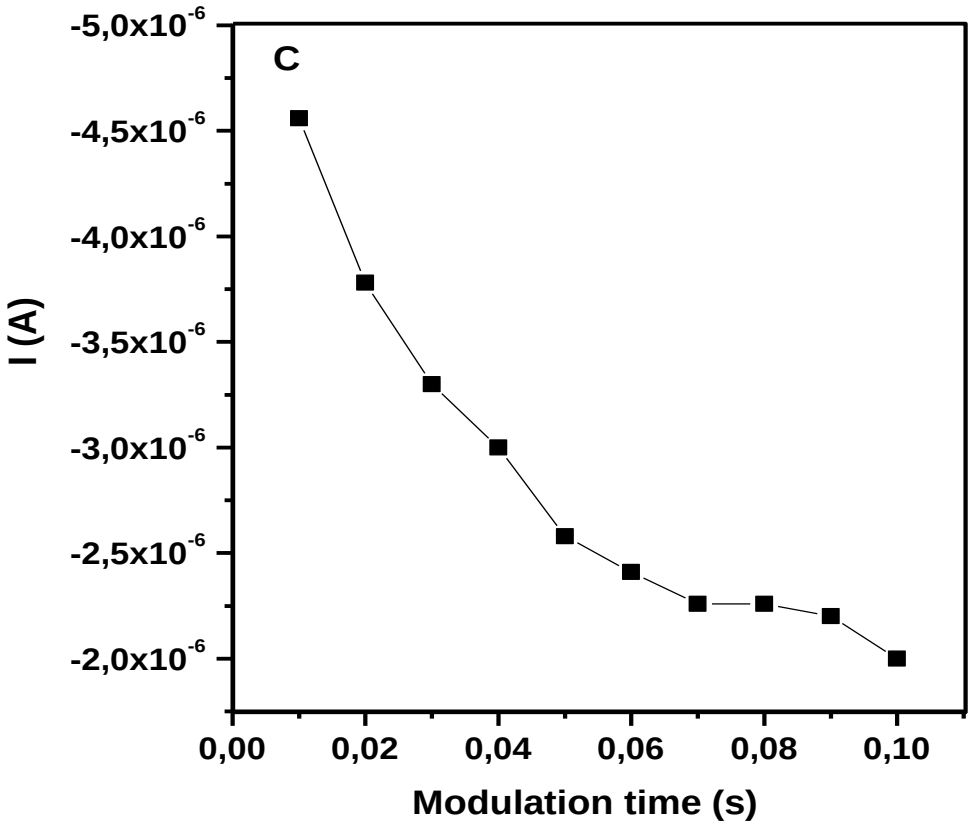
C
-5,0x10-6
-4,5x10-6
-4,0x10-6
-3,5x10-6
-3,0x10-6
-2,5x10-6
-2,0x10-6
I (A)
0,00
0,02
0,04
0,06
0,08
0,10
Modulation time (s)

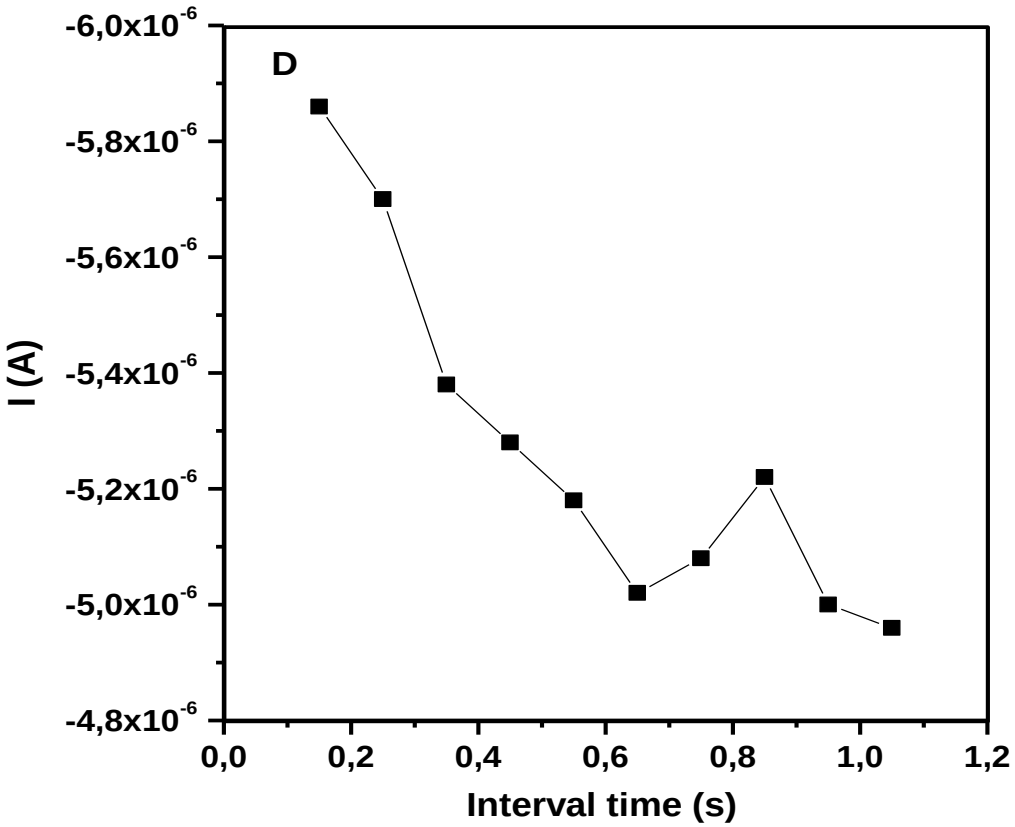

Figure 5. 7: Optimisation of (a) step potential (b) modulation amplitude (c) modulation time (d) interval time for 2.5 μM ZDV in 1 M PBS, pH 7.04 at GCE/Ag/1.44P/HSA.

The effect of varying step potential (figure 5.7 A) show fluctuation of ZDV signal. However, 0.0405 V was chosen based on its greater signal. The choice of step potential was used to monitor ZDV response with changes in modulation amplitude (figure 5.7 B) where the signal of ZDV was increasing with increasing modulation amplitude. Nevertheless, after 0.075 V, the ZDV peak started losing its shape and was becoming broader which is associated with less sensitivity. Therefore, 0.075 V was implemented in monitoring ZDV response in modulation time variations (figure 5.7 C). The results depicted an inverse proportionality between the modulation time and the current response of ZDV with reduced sensitivity. Hence, 0.01 second was considered. The last parameter investigated was interval time (figure 5.7 D) which was monitored from 0.05 to 1.05 sec. An increase in interval time affected the sensitivity of the sensor. However, at 0.25 sec, the peak depicted was well defined hence it was implemented. All these chosen parameters were used for calibration which will be discussed in the chapter.

5.3.7 Determination of electrochemical parameters of zidovudine

The electrochemical parameters of 0.03 mM zidovudine were determined through different scan rates of cyclic voltammetry in 1 M PBS, pH 7.04. Figure 5.8 shows an increase in cathodic peak current between the potential range of -0.8 V to -1 V which slides apart cathodically with increasing scan rate.

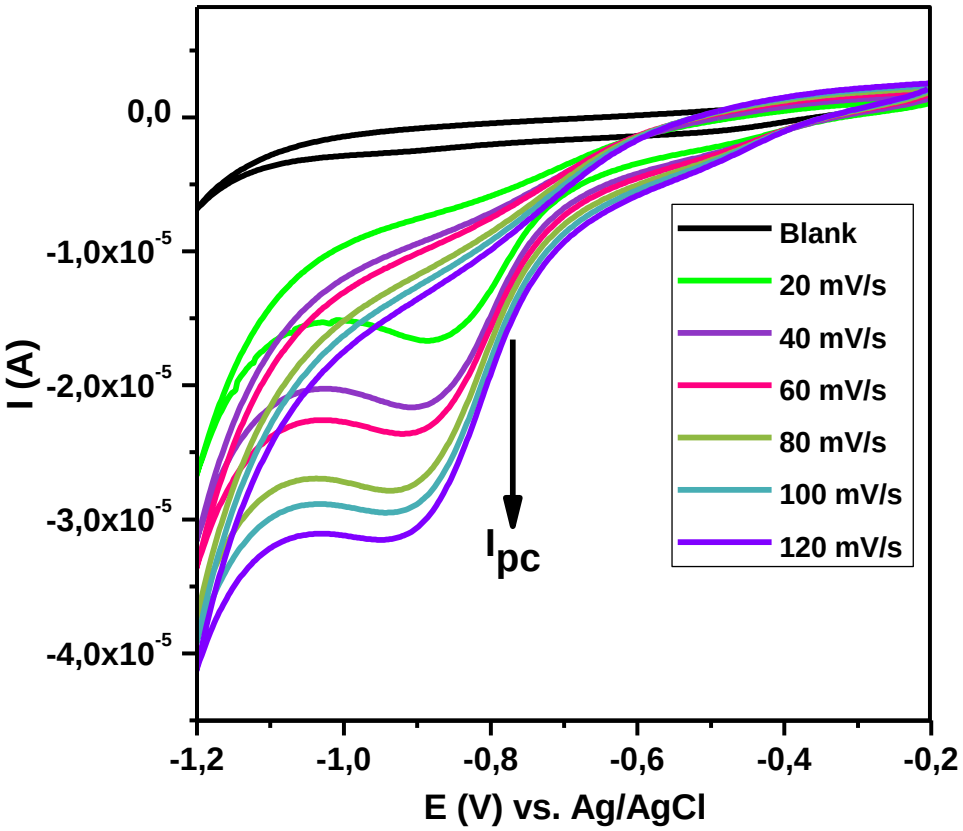

Figure 5.8: CVs of reduction of 0.03 mM ZDV at different scan rates in 1 M PBS at GCE/Ag/1.44P/HSA.

This ZDV peak shifting cathodically with proportional scan rate suggests irreversible chemical reduction of azido group in zidovudine (Rafati *et al.,* 2014), and is attributed to involvement of proton in the zidovudine reduction reaction as represented in scheme 5.2.

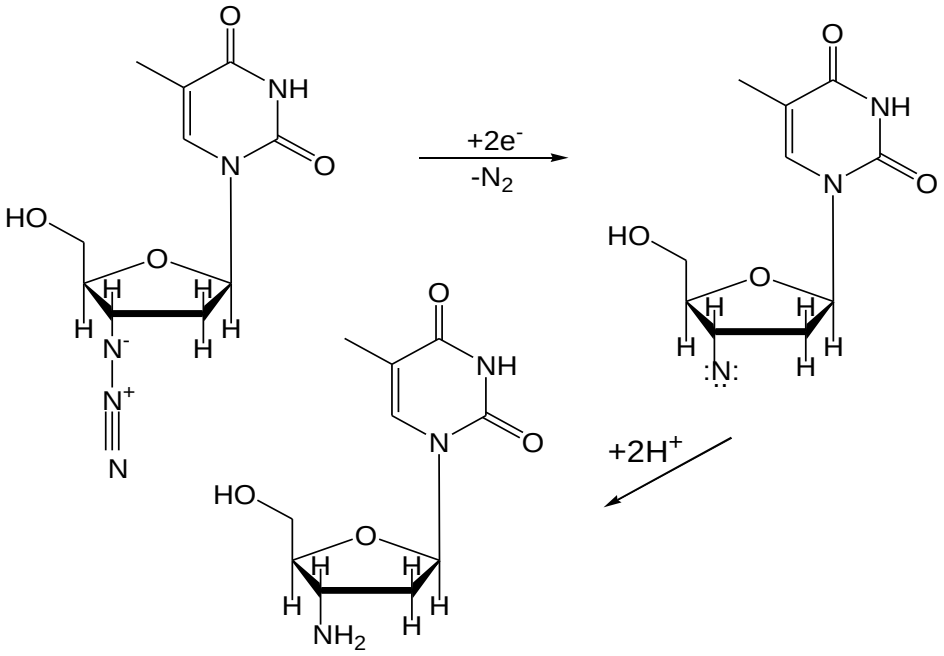

Scheme 5.2: Zidovudine reduction reaction.

The Randles plot for current vs square root of scan rate with a correlation value of 0.9881 (figure 5.9 B) confirms that the electroreduction of zidovudine is diffusion controlled as previously reported (Rafati *et al.*,2014), comparing with plot of current vs scan rate (figure 5.9 A) with a correlation value of 0.9629, and is represented in table 5.2.

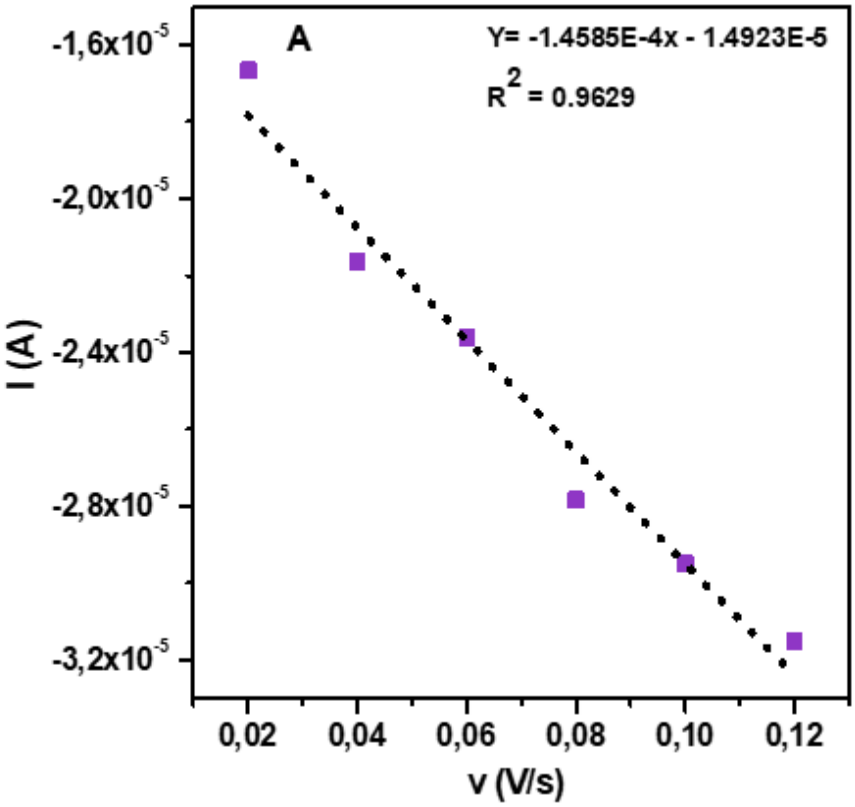

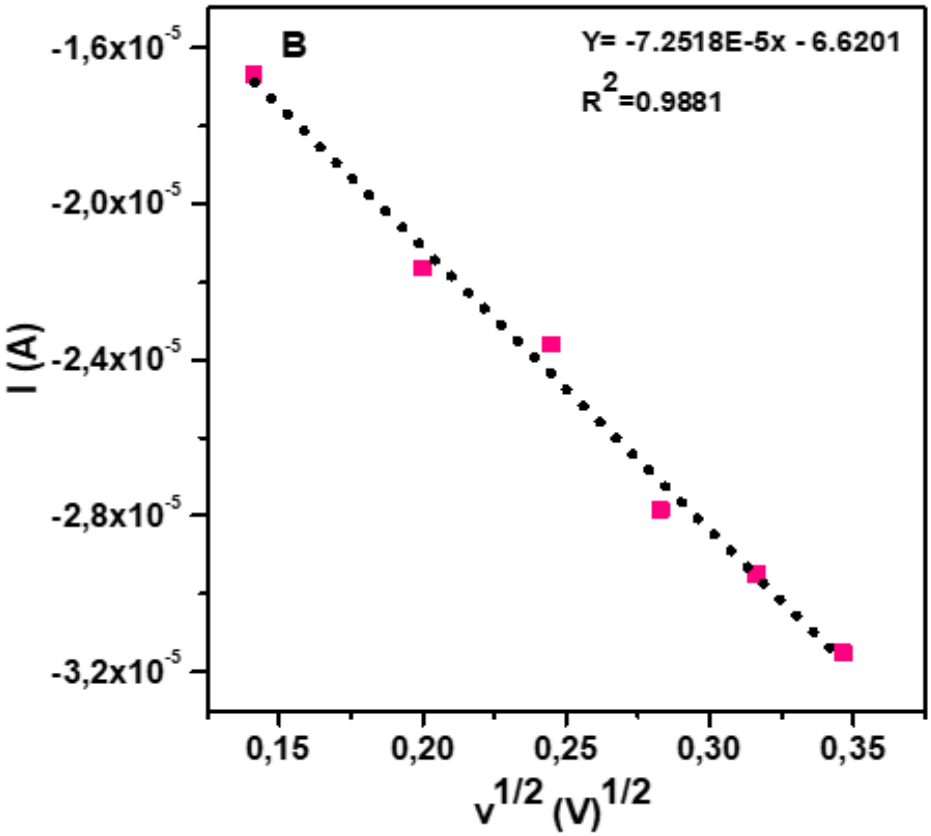

Figure 5.9: Plots of cathodic peak current of 0.03 mM ZDV versus (A) scan rates and (B) square root of scan rates.

Table 5.2: Electrochemical parameters of ZDV from Randles plot.

Parameters	**GCE/Ag/1.44P/HSA**
N	1.2
D ($cm^2\ s^{-1}$)	$1.55x10^{-11}$
Ks (s^{-1})	$3.40x10^{-6}$
Ip vs v (R^2)	0.9629
Ip vs $v^{1/2}$	0.9881

5.3.8 Calibration

The calibration plot in figure 5.10 resulted from the voltammograms *(Insert*) showing an increase in ZDV response with standard addition of ZDV from 0.12 μM to 8.22 μM in 1 M PBS, pH 7.04.

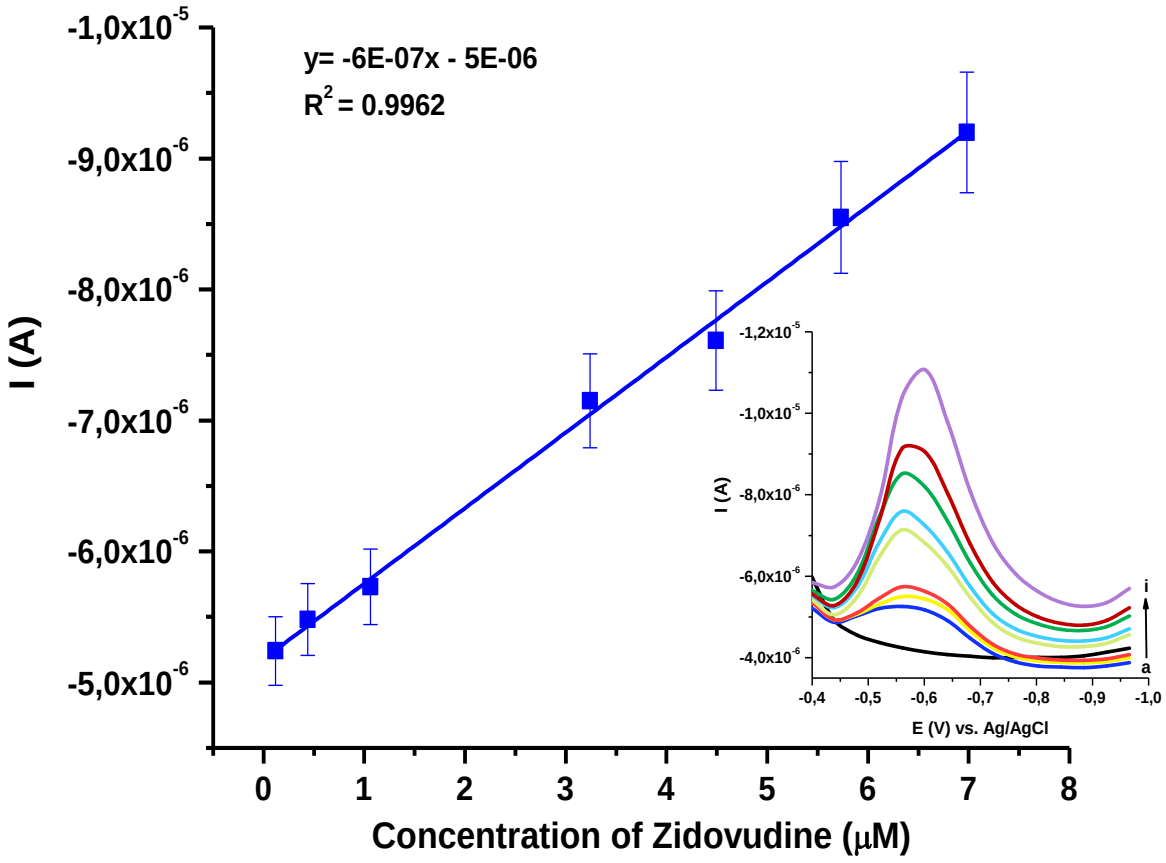

Figure 5.10: Calibration curve from addition of 0.12 to 6.98 μM ZDV. Insert: DPV at (a) blank (b) 0.12 (c) 0.44 (d) 1.06 (e) 3.24 (f) 4.49 (g) 5.73 (h) 6.98 (I) 8.22 μM ZDV at 1 M PBS at GCE/Ag/1.44P/HSA (parameters: 0.0405 V step potential, 0.075 V modulation amplitude, 0.01 second modulation time, 0.25 second interval time).

The calibration plot was used to determine the Limit of detection (LOD) and Limit of quantification (LOQ) with equation, LOD = 3σ/m and LOQ = 10σ/m, where σ is the standard error of y-intercept, m is the slope of the graph. The results obtained are tabulated in table 5.3 and were compared with the previous studies in table 5.4. The LOD for the developed sensor might be a bit higher than the one for other electrochemical methods reported previously. However, due to the toxicity of mercury, the developed sensor can be used as an alternative.

Table 5.3: Parameters of the sensor of ZDV from the calibration measured at GCE.

Parameters	**Zidovudine reduction**
Regression coefficient (n=7)	0.9962
Limit of detection (LOD) (μM)	0.3
Limit of quantification (LOQ) (μM)	1.0
Linear range (μM)	0.12-6.98
Peak potential (V) vs. Ag/AgCl at step 0.0405 V	-0.561

Table 5.4: Detection methods for zidovudine.

Technique	Method of detection	Working electrode	LOD	LOQ	References
Chromatography	RP-HPLC	-	0.003 mg/mℓ	0.009 mg/mℓ	Djurdjevic *et al.*, 2004
Spectroscopy	LC-MS	-	0.1 μM	0.5 μM	Duy *et al.*, 2009
	UV-Vis	-	42 μM	-	Gerayeli *et al.*, 2020
Electrochemical	DPV	HMDE	0.0025 mg/ℓ	0.025 mg/ℓ	Leandro *et al.*, 2010
	ASV	Thin film mercury	0.0025 μM	-	Castro *et al*., 2011
	DPV	Modified graphite paste electrode	1 μM	-	Mohan *et al.*, 2010
	DPV	GCE/Ag/1.44P/ HSA	0.3 μM	1 μM	This work

***See glossary for abbreviation**

5.3.9 Validation

5.3.9.1 Reproducibility, repeatability, stability

The reproducibility of the developed sensor was assessed in 1 M PBS, pH 7.04 for detection of 3.24 μM ZDV using DPV. This resulted to a relative standard deviation (RSD) of 5.3% upon five measurements with the same modified electrode (GCE/Ag/1.44P/HSA). The repeatability of the sensor on the other hand resulted to an RSD value of 1.59% which was obtained from three successive measurements of 3.24 μM ZDV. These RSD values are acceptable for the developed GCE/Ag/1.44P/HAS sensor (Ferrer *et al.,* 2005; Maleh *et al.*, 2021). Moreover, the sensor measured current response of ZDV as per the procedure stated in the chapter (5.2.10.1), maintained stability of the current signal to HSA for 10 days as shown in figure 5.11.

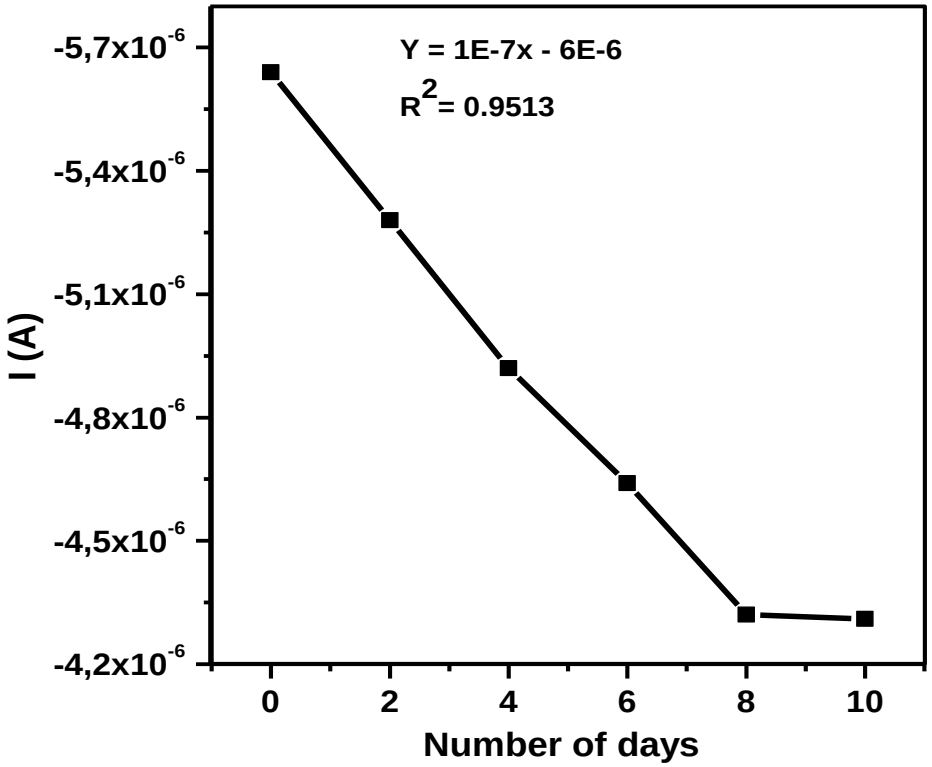

Figure 5.11: Developed sensor stability over 10 days.

5.3.9.2 Interference studies

The Interference study of zidovudine was assessed in the presence of food supplements including ascorbic acid (AA), citric acid (CA), and D-glucose (D-G). These were chosen due to their necessity especially for patients with HIV virus. The impact of these interferants on the zidovudine response is evident from the voltammograms shown in figure 5.12, where a decrease in signal of pure zidovudine was observed when the interferants were introduced. This could be due to the presence of the interferants in the electrolyte solution, leading to a decline in zidovudine concentration. However, when zidovudine was present in high concentration in the electrolyte, with less concentration of the interferants, greater signal was detected.

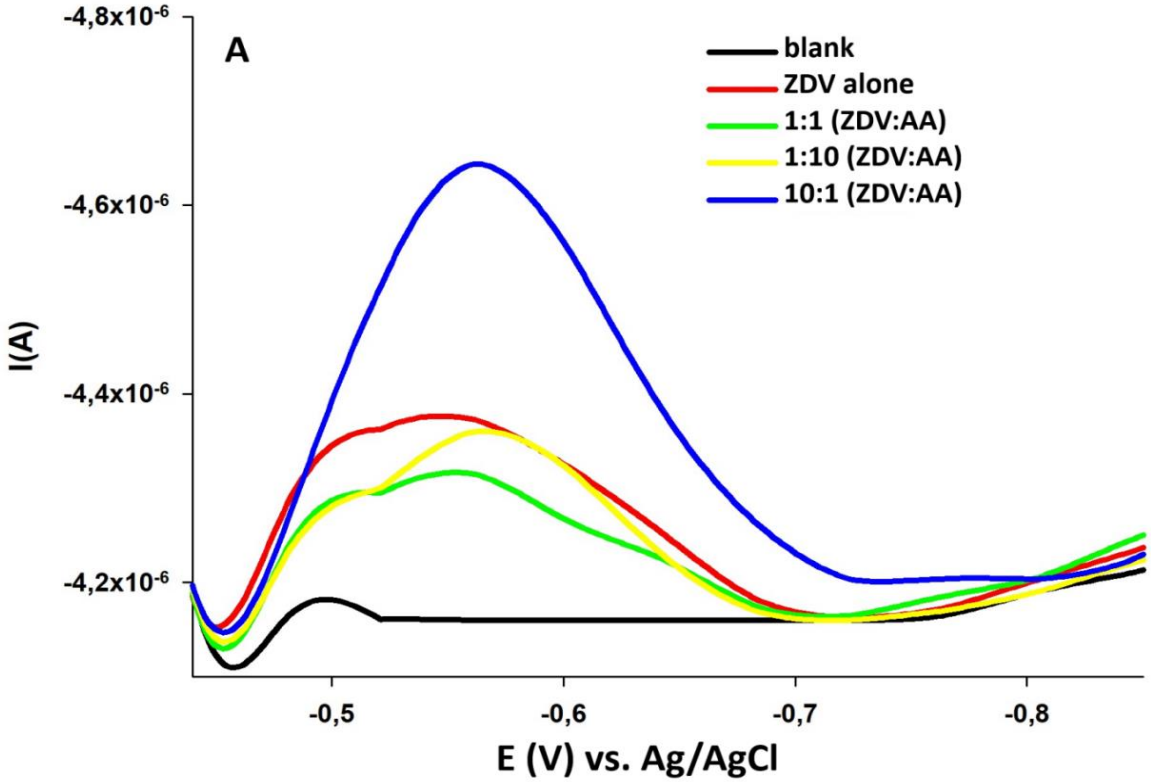
A
blank
ZDV alone
1:1 (ZDV:AA)
1:10 (ZDV:AA)
10:1 (ZDV:AA)
-4,8x10-6
-4,6x10-6
-4,4x10-6
-4,2x10-6
I(A)
-0,5
-0,6
-0,7
-0,8
E (V) vs. Ag/AgCl

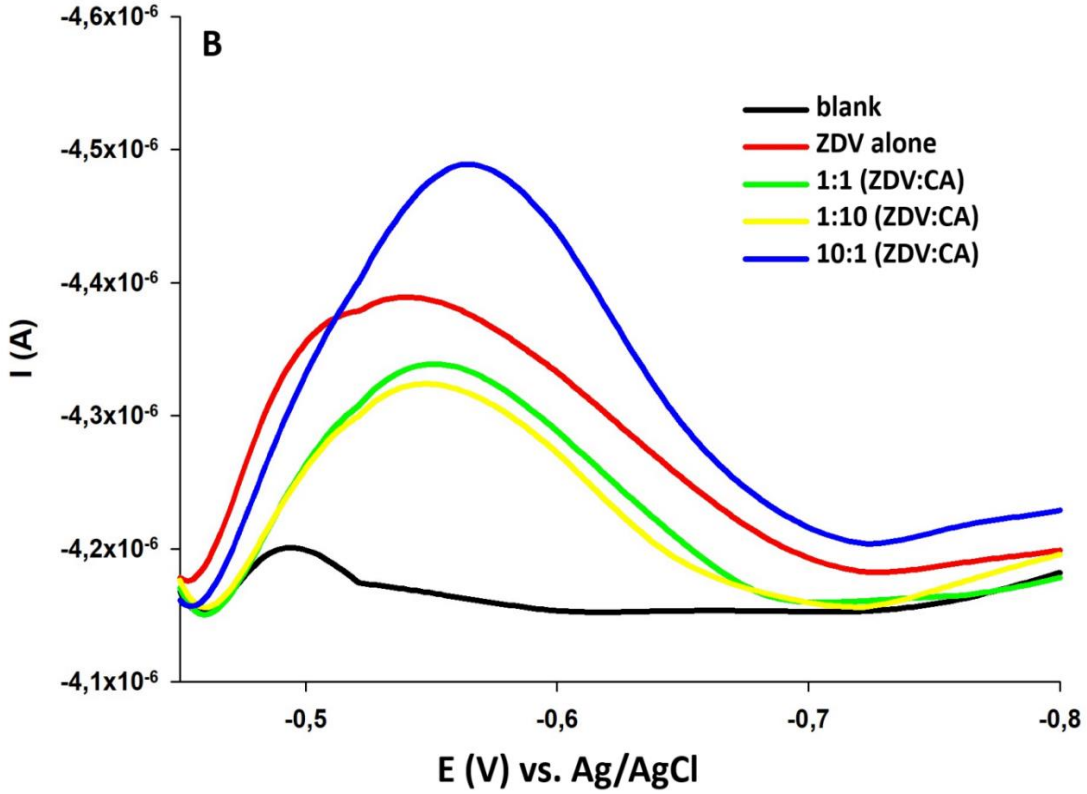
B
blank
ZDV alone
1:1 (ZDV:CA)
1:10 (ZDV:CA)
10:1 (ZDV:CA)
-4,6x10-6
-4,5x10-6
-4,4x10-6
-4,3x10-6
-4,2x10-6
-4,1x10-6
I (A)
-0,5
-0,6
-0,7
-0,8
E (V) vs. Ag/AgCl

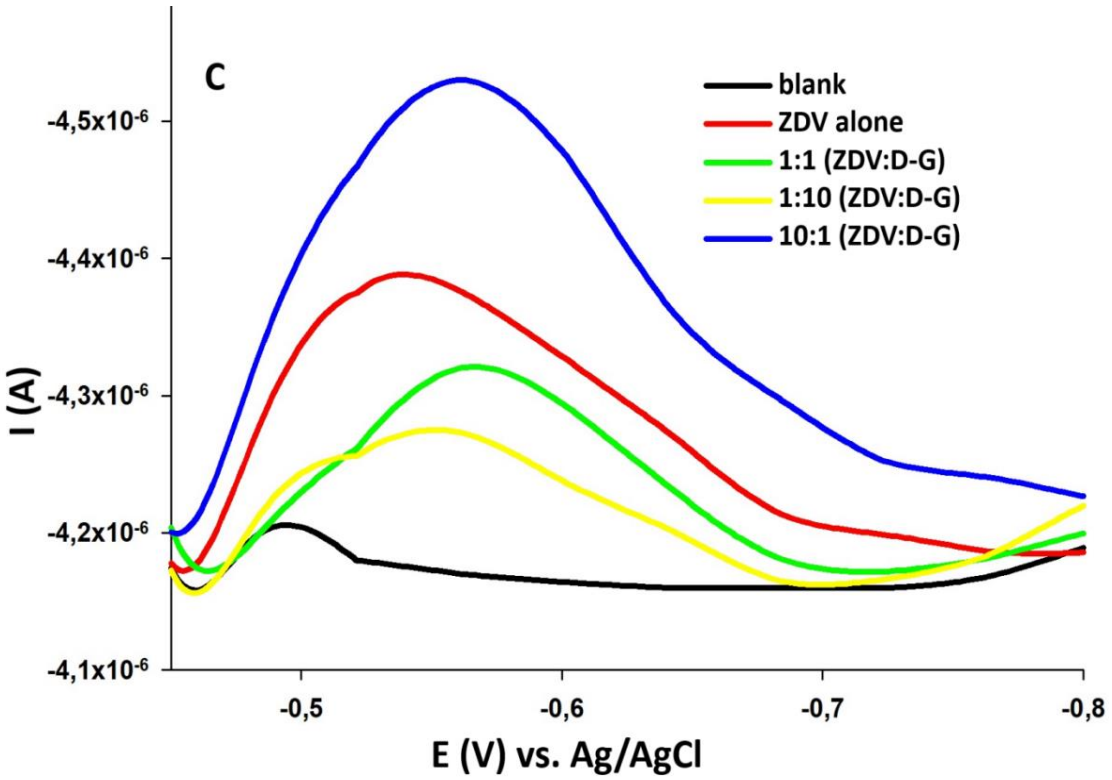

Figure 5.12: DPV of 0.24 μM ZDV in the presence of ascorbic acid (A), citric acid (B), D-glucose (C).

It is visible that the interferants did have an effect on the signal of zidovudine, even when the interferants were present in 10-folds in the solution, and the resulting %recoveries are represented in table 5.5. The response observed in blank scans around -0.5 V potential, which is also visible in ZDV scans with or without interferants, could be due to the presence of oxygen in PBS electrolyte during measurements.

Table 5.5: Zidovudine drug recovery in the presence of interferences (%recovery in brackets).

Interferant	**I_{ZDV} (A) x10^{-6}**	**$I_{ZDV: Interferant}$ (A) x10^{-6}**		
		1:1	1:10	10:1
Ascorbic acid (AA)	-4.37	-4.31 (98.63)	-4.36 (99.77)	-4.64 (106.18)
Citric acid (CA)	-4.38	-4.34 (99.09)	-4.32 (98.63)	-4.49 (102.51)
Dextrose glucose (D-G)	-4.38	-4.32 (98.63)	-4.27 (97.49)	-4.53 (103.42)

5.3.9.3 Detection of zidovudine in spiked urine samples

The urine was spiked with zidovudine for drug recovery purposes. Firstly, the urine was diluted with different volumes of PBS and spiked with different concentrations of zidovudine solution as shown in the table 5.6.

Table 5.6: Zidovudine drug spiking/recovery studies.

Urine: PBS	**1:4**			**1:9**			**1:14**		
Conc. of ZDV (μM)	0.12	1.06	3.24	0.12	1.06	3.24	0.12	1.06	3.24
I_{ZDV} (A) in PBS x10^{-6}	-5.24	-5.73	-7.15	-5.24	-5.73	-7.15	-5.24	-5.73	-7.15
I_{ZDV} (A) in Urine: PBS x10^{-6}	-4.80	-4.22	-4.69	-4.36	-4.28	-4.50	-4.29	-4.24	-4.56
%Recovery	91.60	73.60	65.60	83.20	74.70	62.90	81.90	73.90	63.80

The results shows that in spiked urine, the sensor is highly efficient at low concentrations of ZDV and with low volumes of PBS because in the ratios of dilutions prepared, the recoveries of 91.6%, 83.6% and 81.9% for 1:4, 1:9 and 1:14 Urine:PBS were determined respectively for a concentration of 0.12 μM ZDV and their voltammograms are shown in figure 5.13. However, the %recovered decreased with increasing drug concentration and with increase in PBS volume used for diluting constant volume of urine. Therefore, 1:4 ratio of Urine:PBS spiked with the lowest concentration of zidovudine solution resulted to highest %recovery.

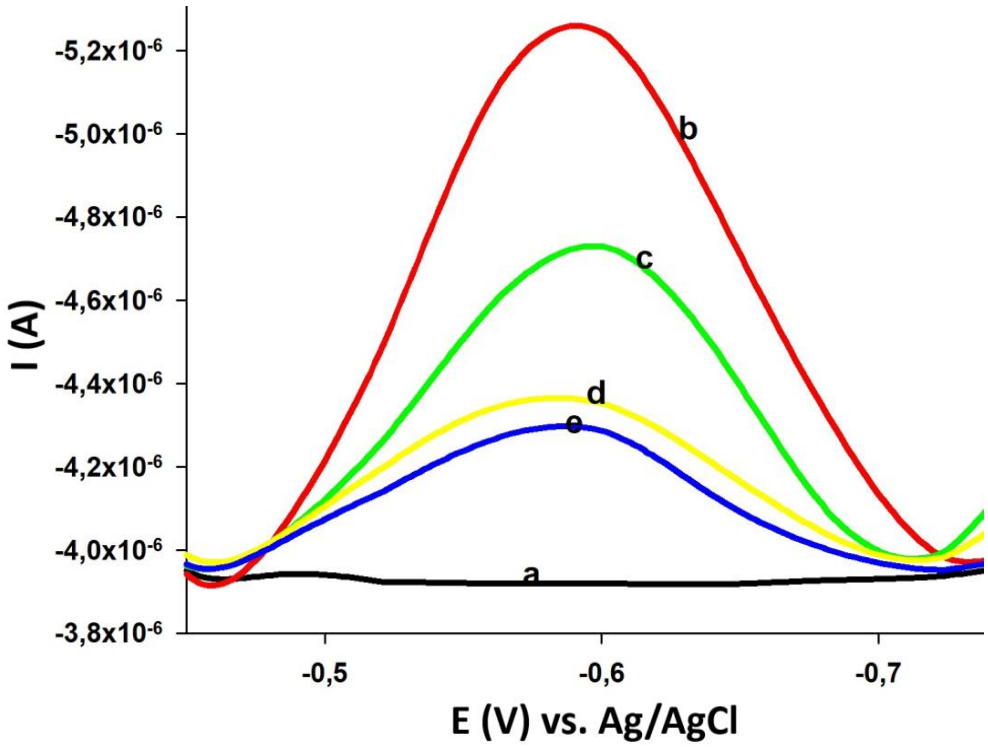

Figure 5.13: DPV of (a) blank and 0.12 μM ZDV at different ratios of Urine:1 M PBS (b) 1:4 (c) 1:9 (d) 1:14 at GCE (parameters: 0.0405 V step potential, 0.075 V modulation amplitude, 0.01 second modulation time, 0.25 second interval time).

5.3.10 Application of the sensor in real samples

5.3.10.1 Detection of zidovudine in commercial tablets

The detection of ZDV in commercial tablets (300 mg ZDV) was done as per the procedure 5.2.11.2 highlighted in this chapter. The resulting voltammograms are represented in figure 5.14.

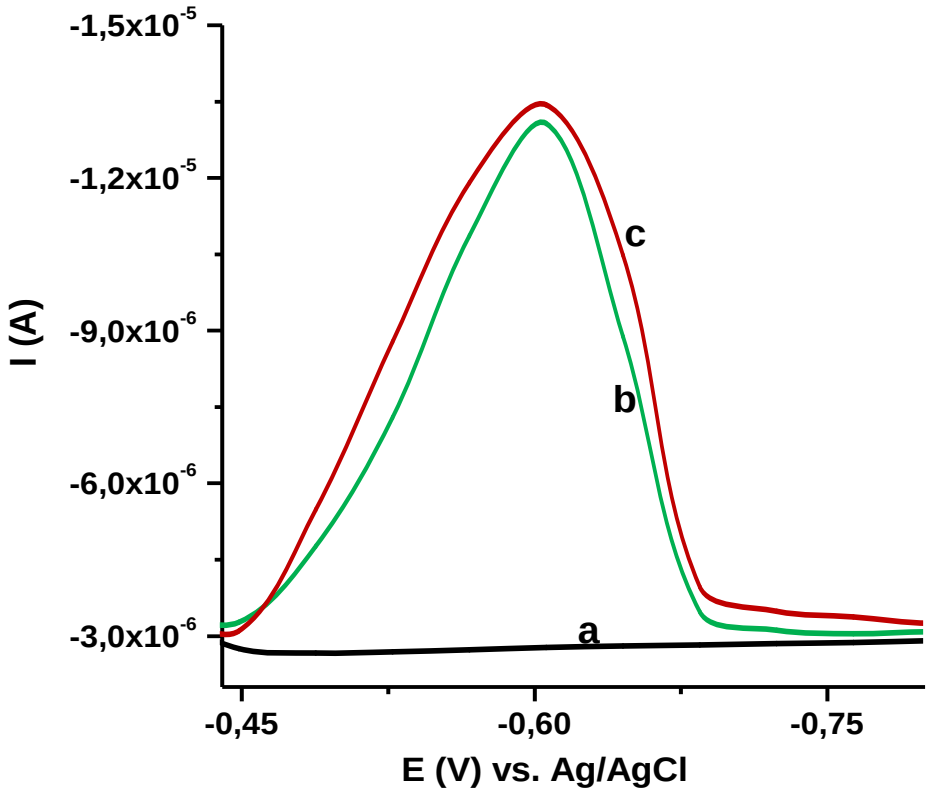

Figure 5.14: DPV of (a) blank, (b) tablet 1, (c) tablet 2 in 1 M PBS, pH 7.04 at GCE (parameters: 0.0405 V step potential, 0.075 V modulation amplitude, 0.01 second modulation time, 0.25 second interval time).

The currents generated together with the calibration equation (y = -0.5761x - 5E-06) were used to calculate the unknown concentration of ZDV in each solution, where x is the unknown concentration of the tablet and y is the current measured. Using the molar mass of ZDV and the concentrations calculated, the content of ZDV in each tablet was obtained and the average mean accumulated for was 313 mg which is comparative to the commercial tablet stated amount (300 mg), with 2.03% RSD less than 5% which indicates that the data measured is precise.

5.4 Conclusion

The development of GCE/Ag/1.44P/HSA sensor for the detection of zidovudine was carried out successfully. It produced good electrochemical properties such as low limit of detection (0.3 μM), with good repeatability and reproducibility, and was not affected by the presence of interferences. These were possible determined with DPV in 1 M PBS, pH 7.04 under optimum conditions. Furthermore, the sensor maintained the stability of ZDV current signal to HSA for 10 days. The detection of the amount of ZDV (313.5 mg) close to the stated amount in commercial tablet (300 mg) is proof that the sensor can be used as an alternative for the detection of zidovudine and can be applied in pharmaceutical industry, observing the mechanism of the ARV drugs.

5.5 References

Ahmad, R., Wolfbeis, O.S., Hahn, Y.B., Alshareef, H.N., Torsi, L. & Salama, K.N. 2018. Deposition of nanomaterials: A crucial step in biosensor fabrication. *Materials Today Communications*. Online [http:// dx.doi.org/10.1016/j.mtcomm.2018.09.024].

Ahmadi, E., Eyvani, M.R., Riahifar, V., Momeneh, H. & Karami, C. 2019. Amperometric determination of nevirapine by GCE modified with c-MWCNTs and synthesized 11-mercaptundecanoyl hydrazinecarbothioamide coated silver nanoparticles. *Microchemical Journal*. Elsevier B.V. Online [https://doi.org/10.1016/j.microc.2019.02.054].

Bui, N.M. & Seo, S.S. 2015. Electrochemical analysis of parathion-ethyl using zirconium oxide-laponite nanocomposites modified glassy carborn electrode. *Journal of applied electrochem*. Vol.45. Springer science & business media. Online [DOI 10.1007/s10800-0015-0789-0].

Ferrer, I., Thurman, E.M. & Fernández-Alba, A.R. 2005. Quantitation and accurate mass analysis of pesticides in vegetables by LC/TOF-MS. *Analytical Chemistry*. Vol. 77(9). American Chemical Society. Online [https://doi.org/10.1021/ac048458x].

Gomdje, H.V., Rahman, N.A., Wahabou, A., Laura, B. & Chtaini, A. 2017. Synthesis of organoclay and its applications in electrochemical detection of paracetamol. *Palagia research library*. Vol.8(1). Der Chemica Sinica: USA. Online [www.pelagiaresearchlibrary.com].

Khanmohammadi, A., Ghazizadeh, A.J., Hashemi, P., Afkhami, A., Arduini, F. & Bagheri, H. 2020. An overview to electrochemical biosensors and sensors for the detection of the environmental contaminants. *Journal of Iranian Chemical Society*. Springer. Online [https://doi.org/10.1007/s13738-020-01940-z].

Lokhande, P.E., Chava, U.S. & Pandey, A. 2019. Materials and fabrication methods for electrochemical supercapacitors: overview. *Electrochemical energy reviews*. Shanghai University and periodicals Agency of Shanghai: Springer. Online [https://doi.org/10.1007/s41918-019-00057-z].

Maleh, K.H., Karimi, F., Alizadeh, M. & Sanati, L.A. 2020. Electrochemical sensors, a bright future in the fabrication of portable kits in analytical systems. *The Chemical Record.* The Chemical Society of Japan & Wiley-VCH, GmbH & Co. KGaA: Weinheim. Online [DOI:10.1002/tcr.201900092].

Maleh, K. H., Alizadeh, M., Orooji, Y., Karimi, F., Baghayeri, M., Rouhi, J., Tajik, S., Beitollahi, H., Agarwal, S., Gupta, V.K. & Rajendran, S., 2021. Guanine-based DNA biosensor amplified with Pt/SWCNTs nanocomposite as analytical tool for nanomolar determination of daunorubicin as an anticancer drug: a docking/experimental investigation. *Industrial &*

Engineering Chemistry Research. Vol. 60(2). American Chemical Society. Online[https://doi.org/10.1021/acs.iecr.0c04698].

Mohan, S. & Prakash, R. 2010. Novel conducting polymer functionalized with metal–cyclam complex and its sensor application: Development of azidothymidine drug sensor. *Talanta.* Vol 81(1-2). Elsevier. Online [https://doi.org/10.1016/j.talanta.2009.12.023].

Rafati, A.A. & Afraz, A. 2014. Amperometric sensing of anti-HIV drug zidovudine on Ag nanofilm-multiwalled carbon nanotubes modified glassy carbon electrode. *Materials Science and Engineering C*. Vol.39. Elsevier B.V. Online [http://dx.doi.org/10.1016/j.msec.2014.02.037].

Shetti, N.P., Nayak, D.S., Malode, S.J. & Kulkarni, R.M. 2017. nano molar detection of acyclovir, an antiretroviral drug at nanoclay modified carbon paste electrode. *Journal of sensing and biosensing research*. Vol.14. Elsevier B.V. Online [http://dx.doi.org/10.1016/j.sbsr.2017.04.004].

Shetti, N.P., Nayak, D.S., Reddy,K.R. & Aminabhvi, T.A. 2019. Graphene–Clay-Based Hybrid Nanostructures for Electrochemical Sensors and Biosensors. Elsevier B.V. Online [https://doi.org/10.1016/B978-0-12-815394-9.00010-8].

Tajmir, R.H. 2007. An overview of drug binding to human serum albumin: protein folding and unfolding. Scientifia Iranica. Vol. 14(2). Sharif University of Technology.

CHAPTER SIX

CONCLUSION AND RECOMMENDATIONS

The conclusion of the study based on the findings acquired will be highlighted, including future recommendations for the determination of zidovudine.

6.1 Conclusion

The synthesis of silver nanoparticles was successfully conducted with chemical reduction method. These were approved with spectroscopic, morphological, and electrochemical techniques. The AgNPs were further used to functionalise the nanoclay forming silver nanoclay composites which were confirmed with FTIR, XRD, SEM, CV and DPV showing successful functionalisation of the nanoclay. Furthermore, Ag/0.5g 1.44P composites were applied in modification of glassy carbon working electrode with HSA protein resulting to GCE/Ag/1.44P/HSA sensor. For optimisation of sensor fabrication, a choice between immersion and dropcoating of HSA method was made. The detection of ZDV was done under optimum conditions of GCE/Ag/1.44P/HSA sensor with DPV at 1 M PBS, pH 7.04, step potential 0.0405 V, modulation amplitude 0.075 V, modulation time 0.01 second, and 0.25 second interval time. Subsequently, low limit of detection of 0.3 μM and 1.0 μM limit of quantification was obtained, with redox properties confirming one electron transfer process by Randles-Sevcik equation using CV. The developed sensor was validated through reference standard analysis and was found to possess good reproducibility, repeatability, and stability.
In real sample analysis, the sensor was tested in the commercial tablet successfully, and was able to detect about 104.5 % of the tablet in relation to the theoretical value. This proved to be a good alternative for the detection of zidovudine and can be applied in pharmaceutical industry for ARV drug monitoring.

6.2 Recommendations

For future work purposes, one should consider using optical, morphology methods in combination with electrochemical methods which helps to fully understand the behaviour of the material in question. For example, the morphology revealed aggregates of the nanoparticles which were further confirmed with electrochemical methods. This information discovered, however, was not possible with only optical methods, hence the combination of methods. Upon the use of electrochemical methods, the electrochemical parameters should be determined as they play a significant role in confirming the size of the nanoparticle which is critical for sensitivity of the sensor. The HSA protein needs to be thoroughly investigated first with other methods first before being applied. When applying the sensor in commercial tablets, the tablets should be completely dissolved in order to accurately detect the commercially stated amount. The developed sensor can be evaluated with other previously approved methods. It

can also be used in pharmaceutical industry, and in water treatment to detect the traces of drug in wastewater and river water.

APPENDICES

Appendix A 1: Antiretroviral drugs from each drug class (AIDSinfo, 2019).

Drug Class	Generic Names and their acronyms	Brand Name	Date of approval by FDA
Nucleoside Reverse Transcriptase Inhibitors (NRTIs)	abacavir (abacavir sulfate, ABC)	Ziagen	17 December 1998
	emtricitabine (FTC)	Emtriva	02 July 2003
	lamivudine (3TC)	Epivir	17 November 1995
	tenofovir disoproxil fumarate (tenofovir DF, TDF)	Viread	26 October 2001
	zidovudine (azidothymidine, AZT, ZDV)	Retrovir	19 March 1987
Non-Nucleoside Reverse Transcriptase Inhibitors (NNRTIs)	doravirine (DOR)	Pifeltro	30 August 2018
	efavirenz (EFV)	Sustiva	17 September 1998
	etravirine (ETR)	Intelence	18 January 2008
	nevirapine (extended release nevirapine, NVP)	Viramune	21 June 1996
		Viramune XR (extended release)	25 March 2011
	rilpivirine (rilpivirine hydrochloride, RPV)	Edurant	20 May 2011
Protease Inhibitors (PIs)	atazanavir (atazanavir sulfate, ATV)	Reyataz	20 June 2003
	darunavir (darunavir ethanolate, DRV)	Prezista	23 June 2006
	fosamprenavir (fosamprenavir calcium, FOS-APV, FPV)	Lexiva	20 October 2003
	ritonavir (RTV)	Norvir	01 March 1996
	saquinavir (saquinavir mesylate, SQV)	Invirase	06 December 1995
	tipranavir (TPV)	Aptivus	22 June 2005
Fusion inhibitors	enfuvirtide (T-20)	Fuzeon	13 March 2003
Integrase Inhibitors	dolutegravir (DTG, dolutegravir sodium)	Tivicay	13 August 2013
	raltegravir (raltegravir potassium, RAL)	Isentress	12 October 2007
		Isentress HD	26 May 2017
Post-Attachment Inhibitors	ibalizumab-uiyk (Hu5A8, IBA, Ibalizumab, TMB-355, TNX-355)	Trogarzo	06 March 2018
Pharmacokinetic Enhancers	cobicistat (COBI)	Tybost	24 September 2014

Appendix B 1: Antiretroviral drugs combination (AIDSinfo, 2019).

Combination of HIV drugs	Brand name	Approval date by FDA
Lamivudine and Zidovudine	Combivir	27 September 1997
Abacavir, Lamivudine and Zidovudine	Trizivir	14 November 2000
Lopinavir and Ritonavir	Kaletra	15 September 2000
Emtricitabine and Tenofovir Disoproxil Fumarate	Truvada	02 August 2004
Abacavir and Lamivudine	Epzicom	02 August 2004
Efavirenz, Emtricitabine and Tenofovir Disoproxil Fumarate	Atripla	12 July 2006
Emtricitabine, Rilpivirine and Tenofovir Disoproxil Fumarate	Complera	10 August 2011
Elvitegravir, Cobicistat, Emtricitabine and Tenofovir Disoproxil Fumarate	Stribild	27 August 2012
Abacavir, Dolutegravir and Lamivudine	Triumeq	22 August 2014
Darunavir and Cobicistat	Prezcobix	29 January 2015
Elvitegravir, Cobicistat, Emtricitabine and Tenofovir Alafenamide	Genvoya	05 November 2015
Atazanavir and Cobicistat	Evotaz	29 January 2015
Emtricitabine, Rilpivirine and Tenofovir Alafenamide	Odefsey	01 March 2016
Emtricitabine and Tenofovir Alafenamide	Descovy	04 April 2016
Dolutegravir and Rilpivirine	Juluca	21 November 2017
Bictegravir, Emtricitabine and Tenofovir Alafenamide	Biktarvy	07 February 2018
Darunavir, Cobicistat, Emtricitabine and Tenofovir Alafenamide	Symtuza	17 July 2018
Doravirine, Lamivudine and Tenofovir Disoproxil Fumarate	Delstrigo	30 August 2018
Efavirenz, Lamivudine and Tenofovir Disoproxil Fumarate	Symfi	22 March 2018
Efavirenz, Lamivudine and Tenofovir Disoproxil Fumarate	Symfi Lo	05 February 2018
Lamivudine and Tenofovir Disoproxil Fumarate	Cimduo	28 February 2018
Dolutegravir and Lamivudine	Dovato	08 April 2019